INAUGURAL - DISSERTATION

zur Erlangung der Doktorwürde der

Naturwissenschaftlich-Mathematischen Gesamtfakultät der

Ruprecht-Karls-Universität Heidelberg

Vorgelegt von

Diplom–Geograph Achim Heilig

aus: Hausham

Tag der mündlichen Prüfung: 06.11.2009

The search for and location of inhomogeneities in seasonal snowpacks utilizing ground-penetrating radar technology

Gutachter:

Prof. Dr. Kurt Roth

Dr. Olaf Eisen

Summary

The location of singular objects or layered transitions below the surface and properties thereof in the ground are a pivotal topic in geosciences. In mountainous regions is the investigation of objects and layer transitions specifically of interest for the seasonal snowpack, primarily to reduce the threat to humans and infrastructures by natural hazards. Snow avalanches are a major natural hazard causing numerous fatalities throughout the world and they are a direct consequence of snowpack conditions. The annual fatality numbers of avalanches are fairly constant for the last 30 years, while in other fields such as e.g. road traffic these numbers decreased significantly. It can be assumed that the permanent enhancements in active and passive safety systems in road traffic are the reason for the decrease in victim numbers. In the field of professional search and rescue operations or accident prevention in avalanches such as hazard forecast, enhancements of instrumentations are marginal for the last three decades. The present study describes two different assessments for the use of ground-penetrating radar (GPR) systems to improve the instrumentation for the location of buried avalanche victims and the prediction of avalanches. Consequently, it demonstrates the feasibility of radar systems for the detection of inhomogeneities in seasonal snowpacks.

With regard to the improvement of current methods to search and locate buried avalanche victims, which are not equipped with a location device (e.g. avalanche beacon), the main objective is to shorten search time. The assessment of this thesis was therefore to use helicopter-borne non-invasive location methods. To simulate helicopter flights, test arrangements were designed to perform field tests from above the surface. I developed methods to measure from 6–12 m above the snow cover. To measure non-invasively, the arrangement is based on pulsed radar technology. To shorten search time and to minimize the influence of man-made error possibilities, an automatic location software was developed. The results of the field tests present the answers of the fundamental questions for an airborne location operation and enabled the development of a location algorithm. Measurements showed, that the sidewise detectable range of 3–5 m of an antenna set-up with one transmitter – receiver pair is rather small for the given flight height of 6 to 12 m. Furthermore, the reflection amplitude of the snow surface decreases almost linearly with the flight height. Unfortunately, in wet snow avalanches a buried object in the snowpack does not appear as typical reflection pattern and is therefore not explicitly locatable. The developed software algorithm proved to be sufficient for all applied test arrangements in dry

snow conditions. The algorithm is able to distinguish between buried victims in the snowpack and reflections caused by only air holes within the snow cover. Further implementations on helicopters can be achieved, based on these results, but more field tests are necessary to adapt the software to the rougher flight conditions in helicopters.

Concerning the observation of stratigraphic inhomogeneities within a snowpack, this thesis showed that a record of specific snowpack conditions from beneath the snow cover is feasible with GPR. The assessment of the present work is to provide snowpack information in avalanche endangered slopes and to follow the temporal evolution of the snowpack over a whole season. Two different kinds of field measurements in dry and wet snow conditions were performed to ascertain the GPR set-up, which provides the best trade-off between penetration depth and layer resolution. On the one hand, temporally singular measurements at different locations, concerning altitude, snowpack conditions and climatic regions in the European Alps, enabled the determination of capable test arrangements. On the other hand, a temporal monitoring of the snow cover at a fixed position over several months, facilitated the record of the change of specific parameters in the snowpack. In terms of system parameters, antennas with a center frequency of about 800–900 MHz are able to penetrate and adequately record stratigraphic transitions in dry and wet snow conditions. The radar-measured snow height in dry snow using a mean wave speed value for the conversion of the two-way travel time was in a good agreement to the probed snow depth and arose in an uncertainty slightly higher than of ultrasonic sensors. In terms of snowpack parameters, the recorded signals of the various snow covers were in good agreement with the measured snow properties. For dry snow conditions, the appearance and the manner of reflections recorded in the snow cover corresponded to the size and the algebraic sign of the gradient in snow density. Moisture in the snowpack attenuates the radar signal significantly.

This thesis presents encouraging results of the use of impulse radar technology for the location of inhomogeneities in seasonal snowpacks. Parts of the presented results and methodologies (e.g. the automatic location algorithm) are possibly easily adaptable in related areas of geoscientific research and could also provide advances in other, non-snow related fields.

Zusammenfassung

Die Lokalisierung von einzelnen Objekten oder von Schichtübergängen unterhalb der Oberfläche und die Bestimmung von deren Eigenschaften sind zentrale Themen in den Geowissenschaften. Für Bergregionen ist die Erkundung von Objekten und Schichtübergängen im Speziellen für die saisonale Schneedecke von Interesse. Dieses Interesse besteht vor allem in Hinblick auf die Reduzierung der Bedrohung für Mensch und Infrastruktur durch Naturgefahren. Schneelawinen stellen eine der bedeutensten Naturgefahren in Bergregionen dar, mit jährlich zahlreichen Todesopfern weltweit. Lawinen sind eine direkte Folge der Schneedeckeneigenschaften. Die durchschnittlichen Zahlen von Lawinenopfern pro Jahr sind seit 30 Jahren fast unverändert. Für andere Bereiche hingegen, wie zum Beispiel im Straßenverkehr, haben sich die Zahlen der jährlichen Unfälle mit Todesopfern signifikant verringert. Es ist anzunehmen, dass die ständige Weiterentwicklung von aktiven und passiven Sicherheitssystemen im Straßenverkehr zu dieser deutlichen Verringerung der Opferzahlen geführt hat. Im Bereich der Suche und Rettung von Lawinenverschütteten und der Vorhersage der Lawinengefahr sind die Entwicklungen von Instrumenten zur Unterstützung der Einsatzkräfte im Vergleich eher marginal. Diese Arbeit beschreibt zwei verschiedene Ansätze für den Einsatz von Georadarsystemen, um gegenwärtige Instrumentierungen für die professionelle Lawinensuche und Lawinenvorhersage zu verbessern und zeigt deren Möglichkeiten für die Ortung von Inhomogenitäten in der Schneedecke.

Im Hinblick auf die Verbesserung von momentanen Ortungsmethoden für Lawinenverschüttete, welche kein Ortungssystem (z.B. Lawinenverschütteten-Suchgerät LVS) bei sich tragen, ist das Hauptziel, Suchzeiten zu verringern. Der Ansatz dieser Arbeit ist demzufolge berührungsfreie, helikoptergestützte Lokalisierungsmethoden einzusetzen. Für die Simulation von Helikopterflügen wurden Versuchsaufbauten konstruiert, mit denen Feldtests in einer Höhe von 6–12 m über Grund möglich waren. Für die berührungsfreie Untersuchung der Schneedecke wurden Georadarsysteme ausgewählt. Um Suchzeiten zu verringern und um den Einfluss von menschlichen Fehlermöglichkeiten zu minimieren wurde eine automatische Lokalisierungssoftware entwickelt. Die Ergebnisse der Feldmessungen ergaben Antworten auf die Grundfragen zur luftgestützten Verschüttetenortung und ermöglichten die Entwicklung eines Lokalisierungsalgorithmuses. Die Messungen zeigten, dass die zur Seite gerichtete Detektierungsreichweite einer Antennenkonfiguration mit einem Sender – Empfängerpaar für die gegebenen Flughöhen von 6–12 m sehr schmal ist. Zusätzlich nimmt die Stärke der Reflektionsamplitude der Schneeoberfläche mit der Flughöhe

annähernd linear ab. Für den Fall von Nassschneelawinen erscheint kein typisches Reflexionsmuster von verschütteten Objekten, mit der Folge, dass eine eindeutige Lokalisierung nicht möglich ist. Der entwickelte Lokalisierungsalgorithmus hingegen hat in allen angewandten Versuchsaufbauten in trockenen Schnee gute Ergebnisse erbracht. Der Algorithmus ist in der Lage zwischen eingegrabenen Objekten, Schnee und Reflexionen, hervorgerufen durch Hohlräume, eindeutig zu unterscheiden. Eine zukünftige Implementierung dieses Systems, basierend auf den hier präsentierten Ergebnissen, ist möglich, jedoch sind weitere Feldarbeiten nötig, um die Software an die schwierigeren Flugbedingungen in Helikoptern anzupassen.

Im Hinblick auf die Beobachtung von stratigraphischen Inhomogenitäten in der Schneedecke zeigt diese Arbeit, dass die Aufnahme von bestimmten Schneeeigenschaften von unterhalb der Schneedecke mittels Georadarsystemen möglich ist. Der Ansatz der präsentierten Arbeit ist, Schneedeckeninformationen in lawinengefährdeten Gebieten bereit zu stellen und die zeitliche Entwicklung der Schneedecke über den gesamten Winter zu beobachten. Zwei verschiedene Arten von Feldmessungen unter trockenen und nassen Schneebedingungen wurden durchgeführt, um die Georadar – Komponenten zu bestimmen, welche den besten Kompromiss zwischen Eindringtiefe und Auflösungsvermögen garantieren. Einzelmessungen mit Versuchsaufbauten an verschiedenen Orten, mit unterschiedlichen Höhenlagen, Schneedeckenbedingungen und Witterungseinflüssen, ermöglichten zum einen die Bestimmung von einsetzbaren Messmethoden. Andererseits war es möglich, mittels einer Langzeituntersuchung der Schneedecke über mehrere Monate an einem gegebenen Ort, die zeitlichen Veränderungen bestimmter Schichten aufzunehmen. Es hat sich herausgestellt, dass Antennen mit einer Nominalfrequenz von 800–900 MHz trockene und nasse Schneedecken ausreichend durchdringen und Schichtübergänge hinreichend detailliert aufnehmen können. Die Schneehöhenbestimmung mittels der angewandten Radarsysteme bei trockenen Schneebedingungen, war in guter Übereinstimmung mit den sondierten Schneehöhen, und die Messungenauigkeit nur knapp höher als bei Ultraschallsensoren, wobei die doppelte Signallaufzeit von Radarwellen im Schnee mit einer mittleren Ausbreitungsgeschwindigkeit in Höhenwerte umgerechnet wurde. Bezüglich aufgenommener Schneeparameter war eine Konkordanz zwischen reflektierten Signalen in der Schneedecke und gemessenen Schneeeigenschaften beobachtbar. Das Auftreten von Reflexionen und die Art der jeweiligen Reflexion entsprachen der Größe und des Vorzeichens von korrespondierenden Dichteübergängen an den jeweiligen Schichtgrenzen im trockenen Schnee. Feuchte in der Schneedecke dämpft das Radarsignal signifikant.

Diese Arbeit präsentiert ermutigende Resultate für den Einsatz von Georadartechnologie für die Detektion von Inhomogenitäten in saisonalen Schneedecken. Teile der präsentierten Resultate und Methoden (z.B. der Lokalisierungsalgorhythmus für die Hyperbeldetektierung) sind unter Umständen leicht in vergleichbare Gebiete der Geowissenschaften implementierbar, wodurch dort ebenfalls Fortschritte erzielt werden können.

Acknowledgements

This thesis is a result of the contribution of many people at various institutes. Without them this work would not have been possible. Specific persons made it a pleasure to work with and guided me towards a scientific approach. I feel deeply grateful to the following persons:

- Martin Schneebeli for his guidance throughout the many years of cooperation, his tremendous support and particular for his encouraging manner to solve problems.
- Olaf Eisen for employing me for the final work on the thesis and supervising the whole project in the right direction. Furthermore, I have to thank for numerous corrections on various manuscripts, his commitment and ideas to finalize this thesis.
- Kurt Roth for accepting me as doctoral student and giving me the space to follow own ideas.
- Christoph Mayer for sharing the office at the Bavarian Academy of Sciences and always having a helping hand, while I was struggling with some kind of a problem.
- Ludwig Braun, Heidi Escher-Vetter and the team at the Commission of Glaciology for the kindness to host me and the support.
- The coauthors Wolfgang Fellin, Florian Frühauf, Hans Peter Marshall, Ottmar Scherzer and Michael Schober.
- HP Marshall for valuable discussions and comments.
- Annette, Catherine and Leah for several "inlingua" courses.
- Many colleagues at all the institutes: Cathi, Christian, Coen, Lena, Matthias, Michi, Pascal, Paul M., Paul R., Reinhard, Stephan S. and Stephan J. and who ever I may have forgotten.

Financial support for the presented studies was provided by alpS Centre for Natural Hazard and Risk Management, AWI Alfred Wegener Institute for Polar and Marine Research, IUP Institute of Environmental Physics, WSL Institute for Snow and Avalanche Research SLF and Pieps GmbH.

A thesis consisting of field work is always a contribution of several people. It is not possible to perform field measurements, especially in snow-related topics all alone. Therefore, I have to thank numerous people, who helped to gather the data for the here presented work. These people

are named at the end of each publication. Thank you all for your support.

Finally, I would like to thank you:

- My mum & dad, my family and all the friends who believed in me and gave me the strength to finalize this work.
- Stephan J. for the friendship, even though it was too short.
- Sonja, for being close and sharing the love of mountains.

Contents

List of Figures

List of Tables

1. Introduction

Nature does not reveal its secrets. It only responds to our method of questioning.

- Werner Heisenberg

1.1. Motivation

In mountainous regions natural hazards such as landslides, mudflows, floods, rock falls, ice avalanches, glacier floods and snow avalanches are a threat to humans and infrastructures (e.g. Haeberli et al., 1989). Only snow avalanches cause about 250 fatalities on average per year worldwide (Meister, 2002). In Switzerland for example the longtime annual mean is at about 25 avalanche victims (Tschirky et al., 2000). Harvey and Zweifel (2008) investigated the number of fatalities of backcountry recreationalists (mountaineer, skier, snowboarder, snowshoeer, hiker) for the last 30 years (1977–2006). The mortality rate for these recreationalists on average was 24 people per year in Switzerland. They recognized a slight trend in decreasing annual fatalities, but the numbers are oscillating and are still above 20 fatalities per year in 2006. In comparison thereto, the annual fatality rate in Switzerland caused by road traffic decreased by about two-third, from 1'800 in 1970 to about 600 in 2001 (Basler et al., 2002). The risk[1] of death concerning these accident cases (avalanche accident and traffic accident) cannot be determined as the total number of participants (basic population data) for the probability calculation is not known. Nevertheless, an increase of both persons recreating in avalanche terrain and people participating in road traffic for the last 30 years can be assumed (Gilgen, 2005; Marshall, 2005; Harvey and Zweifel, 2008). It is likely not the case that people have changed their way of driving or their behavior in avalanche terrain but rather that technical support systems were improved or newly introduced. In road traffic rescue and accident prevention, an enormous effort on active and passive safety systems has been conducted to reduce the annual fatality numbers. However, in snow and avalanche rescue and hazard prediction, similar techniques as in the 1970's are employed. Concerning a professional operation with organized rescue teams, the search and location techniques for completely buried people have not been improved since decades (Heilig et al., 2008; Frühauf et al., 2009 – Paper 1, 2). Dogs and snow-probing teams consisting of large

[1] Definition of risk: Combination of the probability of an event and its consequences - www.iso.org

man-power, continue to be mobilized in case of an accident, while a successful search operation is not guaranteed. However, the introduction of modern avalanche transceivers (digital transceiver with up to three antennas) in companion rescue and better training with these instruments reduced the mortality rate in the last 10 years significantly from 59% fatalities recovered by transceivers in the years 1987–1996 to 29% fatalities in the years 1997–2006 (Harvey and Zweifel, 2008). This improvement is based on the reduction of search time for the location of the buried victim. After 18 min of burial time the survival probability decreases from 91% to 34% for completely-buried victims (Brugger et al., 2001).

In avalanche prediction, the basic system of the current methods to determine the snow height remotely were already published in 1981 (Gubler, 1981). This technique is feasible to measure the snow height in flat fields. On the contrary, the sensor systems are insufficient to determine the snow stratigraphy and to measure in slopes, where a predominant avalanche hazard exists (Heilig et al., in press; Heilig et al., submitted – Paper 3, 4). Both, the record of internal stratigraphy and the snow height determination in slope areas, are a significant gain of knowledge for avalanche hazard prediction and will enable to improve the spatial coverage of data of the snowpack.

The aim of the present study is to determine the potential of radar systems in the non-destructive detection of inhomogeneities within various seasonal snowpacks. Impulse radar systems, in specific ground-penetrating radar (GPR) technology, was applied to clarify the fundamentals for the development of sensor systems for either, the automatic airborne detection of avalanche victims (point shaped inhomogeneities with completely different dielectric properties than the host material) as well as for the improvement in recording snow height and snowpack stratigraphy (horizontally coherent linear inhomogeneities with almost equal dielectric properties than the neighboring material). The fundamental questions, for which the present study provides answers are: (i) how pulsed electromagnetic waves interact with snowpack properties with regard to the improvement of current professional avalanche rescue and forecast instruments; (ii) how detailed can internal microstructures be recorded in the snowpack; (iii) to what extent disturb microstructures in the snowpack the record of macrostructures as point-shaped impurities. The results of this thesis of both analyzed cases, have the ability to contribute to improving the current status quo of professional avalanche rescue and forecast technology.

1.2. Background in radar waves

The following section introduces to the theoretical background of radar technology and demonstrates the advantages of electromagnetic wave systems for remote snow measurements. Additionally, I explain the reason for the employment of complex test arrangements with moved antennas.

1.2.1. Motivation for radar based studies

The application of radar technology in cryospheric research started after discovering the reason of tremendous mismeasurements of radar-based aircraft altimeters over ice sheets (Waite and Schmidt, 1961). This awareness led to various applications of radar soundings in polar regions and on glaciers in the following decade (Bailey et al., 1964; Bentley, 1964; Walford, 1964). Ice and snow are very "radar friendly" materials (Daniels, 2004, p. 455). In comparison to the surrounding and underlaying materials such as bedrocks, soil or talus, the electrical and dielectric parameters of ice are rather constant (only slightly depending on the temperature and density) and thereto the influence on radar waves low, which enables a good reflection response at material transitions. Thereby the characterization of ice bodies or layer thicknesses is possible in a fast and non-invasive way.

In this study, only pulsed radar antennas are applied. Other techniques, such as frequency modulated continuous wave (FMCW) systems are very common in snow and avalanche research as well (Marshall and Koh, 2008). FMCW systems do not emit a single impulse, but a periodic signal whose frequency varies linearly with time. One advantage of this system is the layer resolution or the ability to distinguish two nearby targets, which is determined by the bandwidth. In continuous wave systems, the bandwidth can be enlarged up to 8 GHz and more (Marshall, 2005), which enables one to distinguish layer boundaries only a few cm apart. Disadvantages are the restricted availability of normed FMCW-antennas. To date, no commercial manufacturer of FMCW-systems in a suitable frequency range exists. Previous studies used custom-made single units, which hamper the implementation as standard tools for the professional rescue and forecast services. Furthermore, the price and the feasibility of a production in higher unit numbers favors pulsed radar systems up to now. A short review of the different radar systems (FMCW and GPR) and their record capabilities is given in appendix C.

The list of potential applications of pulsed radar technology is steadily expanding. A few examples for the successful applications of GPR technology are: building and infrastructure investigations, archeology, road and tunnel quality assessment, mine detection, forensic investigations and pipe and cable locations (Daniels, 2004) as well as preparations for extra-terrestrial applications e.g. the location of ice on Mars (Grant et al., 2003). Various terms for impulse radar systems are commonly used. This study uses impulse radar, ground-penetrating radar (GPR) and georadar as synonyms. Other common terms are e.g. surface-penetrating radar and radio echo sounding.

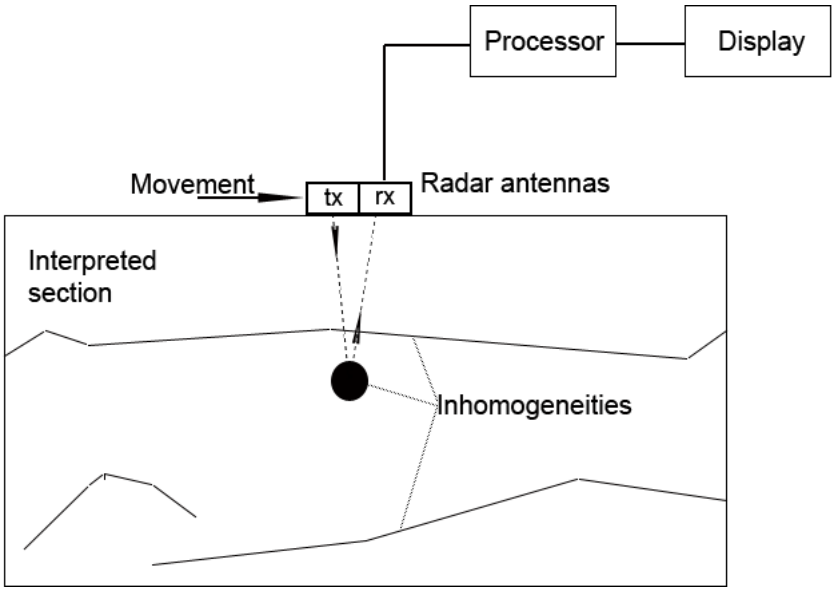

Figure 1.1.: Simplified diagram of the mode of operation of a GPR system. The radar antennas are visualized by the transceiver (tx) and receiver (rx) pair.

1.2.2. GPR theory

In principle, radar systems emit electromagnetic radiation following the propagation as described by Maxwell's equations, where the electric component is orthogonal to the magnetic component (Reynolds, 1997; Daniels, 2004). Ground-penetrating radar is a ultrawide band technique, which emits very short pulses with a typical pulse repetition frequency of 50'000 times per second (50 kHz) (Reynolds, 1997). The transmitted electromagnetic waves are scattered and reflected by layer boundaries and objects and recorded by a receiver (Fig. 1.1). The receiver is set to scan at a fixed time rate, depending upon the used system. The time range of record for the receiver can be adjusted and therefore the possible depth range of the scan determined. Antennas can be used either in monostatic or bistatic mode. Monostatic mode is defined as when one antenna device is used as transmitter and receiver. Bistatic mode describes the record technique with two separated antennas: one serves as a transmitter and the other as a receiver. In the context of this study, I utilized mainly a bistatic mode of antennas, with the transmitter and receiver arranged in a short, fixed distance with a nominal frequency of 400 MHz – 2000 MHz, according to the requirements of the application. These antennas are shielded in one radiation direction, which resulted in a limited emitted radiation pattern and record constraints in the direction of interest (Fig. 1.1). This improves the interpretability of the recorded reflections significantly.

The propagation of radar waves in media is dependent on the properties of the penetrated materials. Some materials such as polar ice are virtually transparent to electromagnetic waves, whereas other materials such as seawater or water-saturated clay degrade the propagation of

the signal to such an extent or reflect the signal at the surface in a way that they are virtually non-transparent. The transparency of radar waves defines the measurement scale for GPR applications in a material. While in polar ice the measurement scale ranges from centimeters to several kilometers, applications in e.g. soil science can be found on scales between a few meters to several tens of meter using standard devices. The possible penetration depth depends on the used frequencies and on the clay, water, iron and salt content of the penetrated medium. High surface salt concentrations can totally prohibit any GPR application. The propagation of electromagnetic waves in one dimension in z-direction can be represented by:

$$\frac{\partial^2 E}{\partial z^2} = \mu\varepsilon \frac{\partial^2 E}{\partial t^2}, \tag{1.1}$$

with E the electrical field. The magnetic permeability μ; $\mu = \mu_0\mu_r$ and the dielectric permittivity ε; $\varepsilon = \varepsilon_0\varepsilon_r$ consist of the relative part according to the penetrated material (with the subscript r) and magnetic susceptibility or electric permittivity constants of free space (subscript 0). The velocity of propagation v is

$$v = \frac{1}{\sqrt{\mu\varepsilon}} \tag{1.2}$$

and the velocity of light in free space c

$$c = \frac{1}{\sqrt{\mu_0\varepsilon_0}}. \tag{1.3}$$

The permeability is a quantity of the magnetization of the penetrated material, which is $\mu_r = 1$ for nonmagnetic materials (Daniels, 2004). The velocity of propagation in a constant nonmagnetic material simplifies therefore to

$$v_r = \frac{c}{\sqrt{\varepsilon_r}}. \tag{1.4}$$

As mentioned above, within snow and ice formations, the parameters influencing the emitted waves are limited, mostly to the three phases of water and the fraction volume of air, which are all nonmagnetic materials. The relative dielectric permittivity values of the respective contributions to snow are the permittivity of air $\varepsilon_a = 1$, the permittivity of ice $\varepsilon_I = 3.1 - 3.2$ (depending on the pureness and density) and the permittivity of water $\varepsilon_w = 81$ (for $T = 20°\text{C}$). The contrast in relative dielectric number or dielectric permittivity between adjacent layers in radiation direction causes reflection. At a boundary between two media, parts of the emitted energy of the radar waves will be reflected and the remaining parts transmitted. The reflected field strength is dependent of the impedances Z_i of the two media (medium 1 and 2) at the boundary and described by the reflection coefficient R.

$$R = \frac{Z_2 - Z_1}{Z_2 + Z_1}, \tag{1.5}$$

while $Z = \sqrt{\frac{\mu}{\varepsilon}}$. As the permeability is set to $\mu_r = 1$ for the here investigated media R simplifies to

$$R = \frac{\sqrt{\varepsilon_1^\star} - \sqrt{\varepsilon_2^\star}}{\sqrt{\varepsilon_1^\star} + \sqrt{\varepsilon_2^\star}}. \tag{1.6}$$

$$\varepsilon^\star = \varepsilon^{'} - i\varepsilon^{''} = \varepsilon^{'} - i\frac{\sigma}{\omega}, \tag{1.7}$$

is the complex permittivity, with $\varepsilon^{'}$ the ordinary permittivity, $\varepsilon^{''}$ the dielectric loss factor, which is equal to the electrical conductivity σ divided by the circular frequency ω and with $i = \sqrt{-1}$. Based on the statement of Eisen (2002) that for the upper parts of an ice body (upper 100 m), the generation of electromagnetic reflections is dominated by discontinuities in the ordinary part of the dielectric permittivity. I disregarded the imaginary part and the dielectric anisotropy of the crystal fabric as sources of reflections. For conditions with a low electrical conductivity σ ($\sigma < 0.1$ S/m; Daniels, 2004), the effect of $\varepsilon^{'}$ is commonly disregarded and it is sufficient to replace $\varepsilon^{'}$ by the relative dielectric permittivity ε_r. Equation (1.6) simplifies for media with low σ values to

$$R = \frac{\sqrt{\varepsilon_{r1}} - \sqrt{\varepsilon_{r2}}}{\sqrt{\varepsilon_{r1}} + \sqrt{\varepsilon_{r2}}}. \tag{1.8}$$

The sign of the reflection coefficient changes depending on whether the waves passes into a medium with higher or lower permittivity. This is apparent in the phase structure of the reflected signal in relation to the transmitted wavelet (Arcone et al., 2005). The analysis of the phase structure of specific reflections is used for interpretation of related layer transitions in the snowpack in chapter 4 and 5. In dry snow conditions, the contributing factors to the reflection coefficient are limited to the fraction volumes of the two contributing materials air and ice. Therefore, a contrast from air to ice will result in the highest amount of reflected radiowave energy. However, liquid water appearances, with a relative dielectric permittivity of more than 20 times the permittivity of ice, dominate the signal reflections in a recorded snowpack and will further increase the reflection coefficient. Additionally, the penetration of the signal will be strongly attenuated due to added absorption as the electrical conductivity cannot be neglected anymore.

In the following, to confirm the disregard of the electrical conductivity in dry snow and to demonstrate the influence of water, I will calculate the theoretic extent of the gradient in conductivity to cause reflections in the snowpack, based on the experiences of the results in chapter 4 and 5. Previously, I describe the maximal extent of conductivity for a dry snow cover. Basically, dry snow consists of a mixture of ice particles and air and therefore, the electrical conductivity is set by the mixture between the fraction of ice and air. The resulting conductivity of snow is approximately located in the range between the conductivity of ice $\sigma_I \approx 10^{-8}\,\mathrm{S/m}$ (Hobbs, 1974), and the conductivity of air $\sigma_a = 2.5 \cdot 10^{-13}\,\mathrm{Sm}^{-1}$ (Lide, 1996), (see Heilig et al., 2008 for

details). In addition, to calculate the theoretical extent for the change in electrical conductivity in snow, I utilize the approximated power reflection coefficient R_p derived from Paren (1981)

$$R_p = (\frac{1}{4}\Delta(\tan\delta))^2 \tag{1.9}$$

with $\Delta\tan\delta = \Delta\frac{\varepsilon''}{\varepsilon'}$, the dielectric loss tangent. The following assumptions shall be given: the relative dielectric permittivity at a layer boundary is constant and a reflection only caused by an effective reflectivity value of about $R_i \simeq -70$ dB (Heilig et al., in press –Paper 3). This results in a change in electrical conductivity of about $\Delta\sigma_I = 10^{-2}$ S/m for a reflection in ice and $\Delta\sigma_s = 1.5 \cdot 10^{-2}$ S/m for a typical permittivity of snow (appendix B). These values are in the range of a change in electrical conductivity from air to tap water (Hobbs, 1974; Daniels, 2004) and far above the given values for ice and air. This theoretical determination confirms the assumption that the electrical conductivity is negligible in dry snow conditions to cause reflections in the snowpack and demonstrates that even if the dielectric permittivity of water would not be different to snow, the change in electrical conductivity can cause remarkable reflections in moist snow conditions.

Regarding the objective of this study, which is the seasonal snow cover, the relative permeability in equation (1.1) is set to $\mu_r = 1$ for snow as a nonmagnetic material and the electrical conductivity is insignificant for dry-snow conditions. Therefore, I conclude that snow and air are low-loss materials for electromagnetic waves, with the consequence, that the one-dimensional propagation of radar signals with time is only dependent on the dielectric relative permittivity of the penetrated material. Hence, and in agreement with previous studies (Kovacs et al., 1995; Mätzler, 1996), I assume for dry snow conditions, that the change in snow density within the snowpack is the sole parameter causing reflections of electromagnetic waves, conditionally on the absence of conducting impurities such as dust layers or buried objects.

1.2.3. Antenna movement

While utilizing pulsed radar transmitters with a constant frequency spectrum, the recorded response of the penetrated media is constant with two-way travel time, when the transmitter and/or the receiver are not moved. This implicates that GPR antennas, which consist of one transmitter – receiver pair in a defined distance (usually about 0.1–0.2 m) must be moved to allow interpretability of the recorded signals or, alternatively, the medium changes over time. Otherwise, it is hardly possible to distinguish between instrumentally caused signals (direct wave, ringing, clutter and noise), signals reflected by the stratigraphy of the investigated medium and reflections caused by internal objects in the medium and to allocate the various recorded amplitudes. In this work, the signal response of moved antennas is utilized in two different ways. On the one hand, this study uses the fact that the antennas radiate a dipole pattern

with a beam width of 45° in the perpendicular direction of the antenna polarization, which is orthogonal to the recommended movement direction. While the antennas are horizontally moved and approaching a buried object, the distance from the antennas to the object is decreasing and by this the two-way travel time of the observed reflection. While the antennas are departing from the object the distance is increasing. The resulting recorded radar pattern is a reflection hyperbola when the antennas are moved with an almost constant speed or radar scans triggered at constant distances. The shape of the hyperbola depends on the beam width of the antennas, the distance between antennas and target, the size of the buried object and the spatial distance of adjacent scans. Heilig et al. (2008) – (Paper 1) and Frühauf et al. (2009) – (Paper 2) describe in detail how this reflection pattern can be used to locate buried objects automatically. The other issue investigated in this study concerns to what extent snow stratigraphy parameters are recordable. Therefore, the antennas are moved vertically, which results in a signal pattern in which instrumentally caused signals appear horizontally constant (in two-way travel time - TWT) in the radargram and reflections generated by stratigraphic parameter correspond to the vertical movement. Heilig et al. (in press) – (Paper 3) and Heilig et al., submitted – (Paper 4) describe processing algorithms, which are applied to attenuate signal responses of the instrument and enhance the visibility of snowpack-stratigraphical reflections.

1.2.4. Penetration depth and resolution limits

Concerning the penetration depth in relation to the frequency, Heilig et al. (in press) – (Paper 3) summarize: "The frequency determines the penetration depth and the bandwidth the vertical resolution (Marshall et al., 2007). A lower frequency enables a deeper penetration into the medium and a higher frequency has higher sensitivity to layer transitions. A larger bandwidth or frequency range results in improved vertical resolution." For the application of GPR-systems with one receiver – transmitter pair, the frequency range, over which a significant amount of power is transmitted, is predetermined. Therefore, the choice of the right antenna frequency is decisive for the performance of the system. Even in dry snow conditions, frequencies above 1'000 MHz can be strongly limited in the penetration of the snow cover (Heilig et al., in press – Paper 3). Theoretically, the vertical resolution limit for small divergence angles, as it is the case in this study (transmitter and receiver in one antenna box) is $\delta z_{min} = \lambda/2 = \frac{v}{2f}$, with λ the wavelength, v the wave speed in the penetrated medium and f the used antenna frequency (Daniels, 2004). The exact limit of detectability of horizontal layers depends on the contrasts in dielectric permittivity between adjacent layers, on the length of the wavelength in the medium and on layer roughness. For thin layers, scattering at boundaries (roughness is neglected in this study) begins to be noticeable at a layer thickness of about 1/10 of the wavelength in the material (Olhoeft, 1998). In practical implementation, a remarkable dielectric permittivity change causes a signal response, even when the layer thickness is much thinner than the vertical resolution

limit. Theoretically, a very thin water layer with a thickness of less than 1 mm embedded in a homogeneous low-loss medium is distinctly recordable as single reflection using antenna systems with frequencies of 250 MHz or more, as the permittivity change from low-loss medium to water is large. However, it becomes very difficult to separate between two nearby water layers situated in a close distance in radar wave direction. This *range resolution* (Marshall, 2005) or the ability to distinguish two nearby layers is determined by the bandwidth, which is rather small for pulsed radar systems in comparison to frequency modulated wave systems. Constructive and destructive interference of the resulting reflections at the layer boundaries prevent the possibility to distinguish if these layers are closer together than the vertical resolution limit.

1.3. Background in snow and avalanche research

The observation of snow in a seasonal aspect has a wide field of relevance, mainly in the subject of hazard management. Local, regional and national avalanche warning centers have the duty to estimate the current avalanche danger level. Water power plant operators are interested in the snow water equivalent (SWE) of the snow masses situated in the catchment area of a reservoir for the correct prediction of run-off amounts. Snow and the related hazards such as snow avalanches and melt water floods, are of wide interest for the society, either in an economical point of view for power plants or insurance companies or directly for the people in regard to safety aspects. Since the beginning of the 20th century, snowpack stratigraphy is regarded as an important contribution to avalanche formation. Paulcke (1938) wrote an early comprehensive publication on practical snow and avalanche science and snow classification, for which he made the first experiments already 40 years before the publishing. Several other publications followed. Pielmeier and Schneebeli (2003) give an extensive overview on the developments in snow stratigraphy research.

Snow is regarded as an aeolian sediment with rapidly changing properties in time and space (Pielmeier, 2003). In research works, studying the microstructure in a very detailed view, snow is closer defined as: "... sintered porous material consisting of a continuous ice network and a continuous pore space in between" (Heggli et al., 2009; p. 631). Schweizer et al. (2003) consider snow to be a cellular solid material. The pore volume in snow ranges from 30–95%. Avalanches are defined as snow masses that rapidly descend steep slopes (Schweizer et al., 2003). In contrast to other granular sediments (e.g. sand), snow grains usually commit bonds to neighboring grains and convert their shape and size due to metamorphism and sublimation within the snowpack as well as at the snow surface (McClung and Schaerer, 2006). While the natural angle of incline for sand accumulations is limited to about $\theta \simeq 34°$ (Parteli and Herrmann, 2008), snow accumulations can reach 90° and more in inclination according to the type of bonds between the snow grains and influences by external factors such as wind and moisture (e.g. cornice, rime; Fig. 1.2). It should be kept in mind that snow is a high temperature material, which exists close to its melting

point (Schweizer et al., 2003). As any material close to its melting point, the constituent parts are susceptible to phase transformation from the solid to the liquid state and vice versa. This results in various changes in the physical properties of the material. The mechanical properties of snow are closely related to temperature as well (McClung, 1996). Temperature and temperature gradients cause metamorphism of the snow structure (Schweizer et al., 2003), which influences failure toughness and shear strength. Low rates in failure toughness and shear strength of a specific layer or at layer transitions result in the ability of the release of a cohesive slab over an extended plane of weakness, so called slab avalanches. Slab avalanches are the most dangerous type of avalanches (McClung and Schaerer, 2006). In literature, two general types of avalanches are defined: loose snow avalanches and slab avalanches (e.g. Schweizer et al., 2003; McClung and Schaerer, 2006). Loose snow avalanches start at or near the surface and usually involve only near-surface snow. They start at a single area or point and spread out in a triangular pattern while moving down the slope. Slab avalanches, however, are usually initiated by a failure in the snowpack and ultimately result in a block, which is entirely cut out by propagating fractures in the snowpack. Slab avalanches occur mostly in a rectangular shape (McClung and Schaerer, 2006). The release of a slab avalanche depends on the existence and also on the horizontal variability of a weak layer within the snow cover (Colbeck, 1991; McClung and Schaerer, 2006). Contributing factors to failure toughness and shear strength and thereby contributing to avalanche formation are (Schweizer et al., 2003):

- terrain; is an essential factor, a slope angle of more than 30° is usually required for dry snow slab avalanches;
- new snow; precipitation is the strongest forecast parameter for the prediction of extreme or catastrophic avalanches. However, even large new snow events do not necessarily increase the release probability in avalanche paths to over 50% (Schaer, 1995), as the time range of the new snow accumulation is of high influence;
- wind; loading by wind-accumulated snow can be fast and produce very irregular deposits, depending on the wind direction and the terrain;
- temperature; the mechanical properties of the snowpack are closely related to the temperature and the constituent parts are prone to phase transformations due to temperatures and gradients thereof;
- snow-cover stratigraphy; for the formation of dry slab avalanches the existence of weak layers or interfaces is the key parameter (see above).

Figure 1.2.: Cornice above a rock face as an example for bonds among snow grains. The width of the overhanging cornice is about 2–3 m.

Not only the existence of a weak layer but also its spatial extension and variability in a slope is decisive for the formation of slab avalanches (e.g. Kronholm and Schweizer, 2003; Marshall, 2005). The spatial variability influences the fracture initiation and the fracture propagation. Kronholm (2004) provides an assessment to quantify spatial snowpack variability in small slopes. In addition, it is important to mention that the segmentation of the snow cover in various layers is in accordance to classification (Colbeck et al., 1990) and not necessarily to physical reality. For example, changes in the mean grain size among adjacent layers in a snowpack are classified as a layer transition, while beside the mean grain size no other parameter is changing.

While moisture infiltrates the snowpack, snow as a two-phase material changes to a three-phase material. The additional liquid state changes the electrical parameters of the material in an enormous way. Radar measurements are strongly influenced by the appearance of liquid water in the snow cover (section 1.2.2). Heilig et al. (2008) and Heilig et al. (in press) describe the changes in the application of wave-speed determination and inhomogeneity-relation in detail.

1.4. Thesis outline

The present study is a composition of four single research works, which are already published in or submitted to peer-reviewed journals. It is structured by two main parts. The first part concerns the capabilities of an airborne detection of avalanche victims with GPR and additionally describes a feasible automatic detection algorithm working in real-time. The second part describes the capabilities of GPR in recording snowpack conditions and observing them tempo-

rally. Furthermore, it gives an overview about feasible radar systems for such an application. The further outline of the thesis is as following:

Chapter 2 is based on an article published in the journal *Cold Regions Science and Technology* (Heilig et al., 2008) – Paper 1. I presented this work at the *International Snow Science Workshop 2006*, in Telluride, Colorado, USA. The study provides an overview on the feasibility of GPR technology in airborne detection of avalanche victims. In this chapter, the following fundamental questions for further developments and applications are raised:

- Is it possible to distinguish between the reflection response of a buried body and the response of unstructured avalanche snow measuring from far above the snow surface?
- What is the maximum horizontal detectable range in flight direction of single GPR antennas? In other words: Which search stripe width has to be flown to detect a buried object in the snowpack on all accounts?
- How does the reflection pattern change if liquid water infiltrated the snowpack?
- To what extent is the influence of the orientation of a victim with respect to the flight direction on the reflection pattern of a buried object?

This chapter represents the results of field work performed to determine the feasibility of airborne GPR application. Antennas are mounted on an aerial railway system to analyze the reflection response generated from "only snow" in comparison to "victim" reflections. The results present the fundamentals for further development, especially in the software evolution for the automatic detection of victim reflection patterns in real-time.

Chapter 3 is based on an article published in the *IEEE Transactions on Geoscience and Remote Sensing* journal (Frühauf et al., 2009) – Paper 2. This chapter represents the constitutive work on chapter 2 including a feasible location algorithm for the automatic detection of buried victims. The following questions are asked in this work:

- How does the reflection pattern change if more realistic test arrangements than in chapter 2 concerning the victims and the flight height are applied?
- How much does the detectable range in flight direction enlarge if a multi-channel antenna array is used?
- Is a matched filter algorithm feasible in nearby realistic scenarios to locate avalanche victims on-the-fly?
- How much does the reflection magnitude decrease with the increase of the distance between the antennas and the target?

This work originated as a collaboration with the Department of Mathematics at the University of Innsbruck, Austria. Florian Frühauf and myself contributed equally to this publication. In

this chapter, I present a feasible software algorithm to detect avalanche victims automatically in real-time. The algorithm is tested on various measurement set-ups covering a large range of realistic scenarios for the helicopter-borne avalanche search. In all tested scenarios, the software shows a clear sign for the case of a victim in the scan-line and no sign if air holes or only snow is scanned.

From chapter 4 on, the topic of investigation changes, the approach and the instrumentation for the research remain the same, however. I start again with a feasibility study in chapter 4 to define the system requirements for the record of snowpack stratigraphy and snow height from beneath the snowpack. This chapter corresponds to an article accepted for publication in the journal *Cold Regions Science and Technology* (Heilig et al., in press) – Paper 3. The material of this study was presented at the *International Snow Science Workshop 2008*, in Whistler, BC, Canada, parts of it were presented as well on the *International Symposium on Radioglaciology and its Applications 2008*, in Madrid, Spain.

To define the system requirements for such an upward-looking sensor system with GPR the following questions are raised:

- Is it feasible to record internal snow stratigraphy using GPR systems?
- What frequency and antenna concept works best?
- Is a wet snowpack still penetrateable by electromagnetic waves in the used frequency ranges and if so, what is the limit under which conditions?
- Is a relation of reflection phase structure and calculated effective reflectivity to snowpack parameters possible?

This work describes the system requirements to enable a feasible record of snowpack stratigraphy and the snow height from beneath the snow cover in various seasonal snow conditions. A GPR system with a specific frequency range is found to penetrate the snowpack either in dry snow conditions with an adequate layer resolution as well as in wet snow conditions. The origin of reflections within the snowpack are allocateable to reflection properties as phase structure or calculated effective reflectivity.

Chapter 5 presents the data set gathered with a buried GPR system over a period of 2 1/2 months beneath the snowpack and is based on an article submitted to the journal *Hydrological Processes* the 23.09.2009 (Heilig et al., submitted) – Paper 4. I presented the data at the *General Assembly of the European Geosciences Union 2009*, in Vienna, Austria. In accordance to the results of chapter 4 the radar system consist of 800 MHz antennas, which are vertically moved. The data of regular measurements of the reflection response above the antennas is related to snowpack conditions measured in a nearby plain area. The results of this long-term observation are analyzed according to:

- How accurate is the radar recorded snow height in comparison to probed snow depth?
- Are internal layers recordable and temporally observable?
- Are moisture infiltrations recordable and can their penetration depth into the snowpack be determined?
- Can the gathered results from individual point measurements in the previous chapter (Paper 3), concerning the physical origin of the reflections, be confirmed by this long-time observation?

The results of this work are very encouraging in respect to further development towards snowpack monitoring with upward-looking GPR. This study shows that the determined snow height with the radar data is in good agreement with the probed snow depth. The accuracy utilizing a standard conversion value of the two-way travel time in dry snow conditions is slightly below than the one for snow height measurements with ultrasonic sensor systems. Several internal layers are traceable over days to weeks and their physical formation origin can be determined. The results of chapter 4, of specific physical properties influencing the manner of reflections, are confirmed with this data set.

In chapter 6, I summarize the results of this thesis and give an outlook on further research towards an operational instrumentation of the mentioned applications.

In the appendix I present non-peer-reviewed publications submitted for the proceedings of the International Snow Science Workshops, ISSW, which I attended or I am going to attend in September/October 2009. The first article in the appendix presents basic work for Paper 3, which was extended to become a peer-reviewed publication. Nevertheless, specific results are presented, which makes it worth for being attached in the appendix. The second article in the appendix presents a short review and comparison of the two different radar technologies (FMCW and GPR systems), which have been used to date for the record of snowpack conditions.

Bibliography

Arcone, S. A., Spikes, V. B., Hamilton, G. S., 2005. Phase structure of radar stratigraphy horizons within Antarctic firn. Annals of Glaciology 41, 10–16.

Bailey, J., Evans, S., Robin, G. d. Q., 1964. Radio echo sounding of polar ice sheets. Nature 204 (4957), 420–421.

Basler, E., Merz, H., Schlatter, H., 2002. Prognose der Strassenverkehrsunfälle 2010. Tech. rep., Eidgenössisches Departement für Umwelt, Verkehr, Energie und Kommunikation UVEK, Bundesamt für Strassen ASTRA.
URL http://www.bfu.ch/German/strassenverkehr/viasicura/Documents/Unfallprognose%202010.pdf

Bentley, C., 1964. The structure of Antarctica and its ice cover. Research in Geophysics 2, 355–389.

Brugger, H., Durrer, B., Adler-Kastner, L., Falk, M., Tschirky, F., 2001. Field management of avalanche victims. Resuscitation 51, 7–15.

Colbeck, S., 1991. The layered character of snow covers. Reviews of Geophysics 29, 81–96.

Colbeck, S., Akitaya, E., Armstrong, R., Gubler, H., Lafeuille, J., Lied, K., McClung, D., Morris, E., 1990. The international classification for seasonal snow on the ground. Tech. rep., International Commission of Snow and Ice of International Association of Scientific Hydrology / prep. by Working group on Snow Classification.

Daniels, D., 2004. Ground Penetrating Radar, 2nd Edition. The Institution of Electrical Engineers, London, UK.

Eisen, O., 2002. On the nature, interpretation, and application of electromagnetic reflections in cold ice. Doctoral thesis, University of Bremen, Bremen, Germany.

Frühauf, F., Heilig, A., Schneebeli, M., Fellin, W., Scherzer, O., 2009. Experiments and Algorithms to Detect Snow Avalanche Victims Using Airborne Ground-Penetrating Radar. IEEE Transactions on Geoscience and Remote Sensing 47 (7), 2240–2251.

Gilgen, K., 2005. Kommunale Raumplanung in der Schweiz. vdf - Lehrbücher und Skripten, Zürich, Switzerland.

Grant, J., Schutz, A., Campell, B., 2003. Ground-penetrating radar as a tool for probing the shallow subsurface of Mars. Journal of Geophysical Research 108 (E4, 8024).

Gubler, H., 1981. An inexpensive remote snow-depth gauge based on ultrasonic wave reflection from the snow surface. Journal of Glaciology 27 (95), 157–163.

Haeberli, W., Alean, J., Müller, P., Funk, M., 1989. Assessing risks from glacier hazards in high mountain regions: some experiences in the Swiss Alps. Annals of Glaciology 37 (3), 289–298.

Harvey, S., Zweifel, B., 2008. New trends of recreational avalanche accidents in Switzerland. In: Campbell, C., Conger, S., Haegeli, P. (Eds.), Proceedings ISSW 2008, International Snow Science Workshop, Whistler, Canada,.

Heggli, M., Frei, E., Schneebeli, M., 2009. Snow replica method for three-dimensional X-ray microtomographic imaging. Journal of Glaciology 55 (192), 631–639.

Heilig, A., Eisen, O., Schneebeli, M., submitted. Temporal Observations of a Seasonal Snowpack using Upward-Looking GPR. Hydrological Processes.

Heilig, A., Schneebeli, M., Eisen, O., in press. Upward-looking Ground-Penetrating Radar for monitoring snowpack stratigraphy. Cold Regions Science and Technology.

Heilig, A., Schneebeli, M., Fellin, W., 2008. Feasibility study of a system for airborne detection of avalanche victims with ground penetrating radar and a possible automatic location algorithm. Cold Regions Science and Technology 51 (2-3), 178–190.

Hobbs, P., 1974. Ice Physics. Oxford University Press, Oxford, UK.

Kovacs, A., Gow, A., Morey, R., 1995. The in-situ dielectric constant of polar firn revisited. Cold Regions Science and Technology 23, 245–256.

Kronholm, K., 2004. Spatial variability of snow mechanical properties with regard to avalanche formation. Doctoral Thesis, University of Zürich, Zürich, Switzerland.

Kronholm, K., Schweizer, J., 2003. Snow stability variation on small slopes. Cold Regions Science and Technology 37, 453–465.

Lide, D., 1996. Handbook of Chemistry and Physics, 76th Edition. CRC Press, USA.

Marshall, H., Koh, G., 2008. FMCW radars for snow research. Cold Regions Science and Technology 52, 118–131.

Marshall, H., Schneebeli, M., Koh, G., 2007. Snow stratigraphy measurements with high-frequency FMCW radar: Comparison with snow micro-penetrometer. Cold Regions Science and Technology 47 (1-2), 108–117.

Marshall, H.-P., 2005. Snowpack spatial variability: towards understanding its effect on remote sensing measurements and snow slope stability. Ph.d. thesis, University of Colorado, Boulder, Colorado, USA.

McClung, D., 1996. Effects of temperature on fracture in dry slab avalanche release. Journal of Geophysical Research 101, 21907–21920.

McClung, D., Schaerer, P., 2006. The Avalanche Handbook, 3rd Edition. The Mountaineers, Seattle, USA.

Meister, R., 2002. Avalanches: Warning, rescue and prevention. Avalanche News 62, 37–44.

Mätzler, C., 1996. Microwave permittivity of dry snow. IEEE Transactions on Geoscience and Remote Sensing 34 (2), 573–581.

Olhoeft, G., 1998. Electrical, Magnetic and Geometric Properties that Determine Ground Penetrating Radar Performance. In: Proceedings of GPR '98. 7th International Conference on Ground Penetrating Radar. pp. 177–182.

Paren, J., 1981. PRC at a dielectric interface. Jounal of Glaciology 27 (95), 203–204.

Parteli, E., Herrmann, H., 2008. Die Entdeckung der Langsamkeit. Physik in unserer Zeit 39 (5), 229–233.

Paulcke, W., 1938. Praktische Schnee- und Lawinenkunde. Julius Springer-Verlag.

Pielmeier, C., 2003. Textural and mechanical variability of mountain snowpacks. Ph.d. Thesis, University of Berne, Berne, Switzerland.

Pielmeier, C., Schneebeli, M., 2003. Developments in the stratigraphy of snow. Surveys in Geophysics 24 (5-6), 389–416.

Reynolds, J., 1997. An Introduction to Applied and Environmental Geophysics. John Wiley and sons.

Schaer, M., 1995. Avalanche activity during major avalanche events – a case study for hydroelectric reservoirs. In: Sivardiere, F. (Ed.), Les apports de la recherche scientifique a la sécurite neige, glace et avalanche, Actes de Colloque. ANENA, Grenoble, France, Chamonix, France, pp. 133–138.

Schweizer, J., Jamieson, B., Schneebeli, M., 2003. Snow avalanche formation. Reviews of Geophysics 41 (4).

Tschirky, F., Brabec, B., Kern, M., 2000. Lawinenunfälle in den Schweizer Alpen – Eine statistische Zusammenstellung mit den Schwerpunkten Verschüttung, Rettungsmethoden und Rettungsgeräte. Ammann, W.J., Davos, Switzerland, Ch. Durch Lawinen verursachte Unfälle im Gebiet der Schweizer Alpen, pp. 125–136.

Waite, A., Schmidt, S., 1961. Gross errors in height indication from pulsed radar altimeters operating over thick ice or snow. Institute of radio engineers. International Convention Record 5, 38–54.

Walford, M., 1964. Radio echo sounding through an ice shelf. Nature 204 (4956), 317–319.

2. Feasibility Study of a System for Airborne Detection of Avalanche Victims with Ground Penetrating Radar and a possible Automatic Location Algorithm [1]

Achim Heilig, Martin Schneebeli and Wolfgang Fellin

[1] published in a similar form as: Heilig, A., Schneebeli, M., Fellin, W., 2008. Feasibility study of a system for airborne detection of avalanche victims with ground penetrating radar and a possible automatic location algorithm. Cold Regions Science and Technology 51 (2-3), 178–190.

Abstract

Slightly more than one third of all buried avalanche victims of the last four years in Austria and Switzerland did not wear any locating device. This is a demanding problem for rescue operations. A fast and reliable method to locate these victims is desired. A ground-penetrating radar (GPR) mounted on a helicopter with an automatic location of buried objects via processing the radar data and GPS referencing is suggested to be a tremendous support for organized rescue teams. To set up the basis of such a system, we performed field experiments in the winter of 2006 to investigate three fundamental topics: (i) the influence of the snow properties on the radar signal, (ii) the maximum horizontal distance of a victim from the flight direction and (iii) the influence of the orientation of the victim with respect to the flight direction. A numerical simulation of radar signals on an inhomogeneous moist snowpack was computed and compared to field measurements. Post processing of the radar data was developed based on statistical evaluation of the reflected radar energy. To simulate a helicopter flight the radar antennas, a 400 MHz GPR system, were mounted on an approximately 6 m high aerial railway system. The victim was substituted by water bags in various depths. In experiments with dry snow, the water bags could easily be detected, independently of the large spatial variation of snow densities in the test arrangement. In moist simulated avalanche snow deposits, however, it was impossible to detect the target. The numerical simulation of this situation gives reason to presume that the variations of electrical conductivity in addition to the various dielectric permittivity changes, due to the vertical alternations of the moisture content, cause this difficulty. The post processing was able to provide a numerically cheap automatic location procedure using a simple threshold value. The maximum transversal distance of a victim from the direction of a flight in 6 m height turned out to be approximately 1.5 m. Victims buried longitudinal to the flight direction are slightly better to detect than orthogonal buried victims.

2.1. Introduction

In the case of a buried avalanche victim not wearing a transmitter or responder system and not being visible on the snow surface (37% of all avalanche fatalities in the winter seasons 02/03 – 05/06 in Austria and Switzerland, Würtl, 2003, 2004; Zweifel, 2004; Würtl, 2005; Zweifel, 2005; Mair, 2006; SLF, 2007) the currently available systems for an organized search operation are dogs or snow probing teams. It is a very time consuming process to organize several dog teams or an adequate amount of man-power to locate a buried person conventionally. Rescue teams have to stay within the hazardous zone from a few minutes to numerous hours with the consequence of a high risk exposure. Additionally, the costs for the usage of several helicopters for the transport of the team often reach up to 100'000 sFr (US$ 70'000) (Tschirky et al., 2000).

Since 1979, radar has been considered for the search of avalanche victims (Coumes, 1983; Fuks, 1983; Osterer, 1983; Paul, 1983). In the past 15 years, a few other research groups were analyzing the possibilities for improving an organized avalanche search operation with GPR systems (Niessen et al., 1994; Jaedicke, 2003; Instanes et al., 2004; Modroo and Olhoeft, 2004). Although GPR was utilized in various airborne applications (e.g. Arcone and Delaney, 2000; Machguth et al., 2006), no rescue activity or research has been conducted with airborne radar so far. Ground-penetrating radar (GPR) in combination with helicopters would be the most efficient solution for a fast and less man-power-intensive search. In addition, the risk of exposure to subsequent avalanches could be reduced. The aims of the present study are: (i) to determine the influence of the snow properties on the radar signal, (ii) to analyze the maximum horizontal distance of a victim from the flight direction and (iii) to investigate the influence of the orientation of the victim with respect to the flight direction. The ultimate goal for further development would be a combined hard- and software system which can be used by rescue teams without expert radar knowledge.

2.2. Methods

2.2.1. Instrumentation

For the fieldwork, a RIS One GPR instrument (IDS Ingegneria dei Sistemi, Pisa, Italy) with two different antennas was used. Measurements were conducted with 400 MHz and 600 MHz antennas. The radar scans were triggered by an odometer wheel with the resolution of one vertical scan per horizontal centimeter and a sampling rate of at least 512 samples per scan. The radar antenna was moved along a steel cable in one direction approximately 6 m above the snow surface.

For the simulation of helicopter flights, we constructed and built an aerial railway system (Fig. 2.1). The railway system was composed of a 6 m high mobile and an 8 m stationary pole for moving the system in a 360° circle around the stationary pylon. The system was installed on the Stubai Glacier in the Austrian Alps, near the station Eisgrat (2865 m a.s.l.). The fixed pylon was mounted on glacier ice, while the mobile pylon had a spread foundation on the snow surface. In case of a snow height of about 2 m (from mid of February – beginning of April 06), the cable of the system was situated about 6 m above the snow surface. The length of the railway system was 20 m but the measuring length was limited to 15 m due to the antenna cable. For the simulation of avalanches, an artificial snow structure, similar to an avalanche deposit, was created. We used a snow grooming machine to scrape up a snow accumulation with one push forward (4 m wide, about 2 m high) right above the target, lying in a 50 cm deep pit hole. For the simulation of human victims, we used three water bags, each filled with 10 litres of tap water. Considering the

fact that a human body consists of more than 60% of water (Sheng, 2000) and additionally the dielectric permittivity of water ($\varepsilon_w = 81$) being comparable to muscle tissue ($\varepsilon_{mt} = 50$) (Gabriel et al., 1996; Jaedicke, 2003; Daniels, 2004) the used water bags should be a good surrogate for the simulation of human victims.

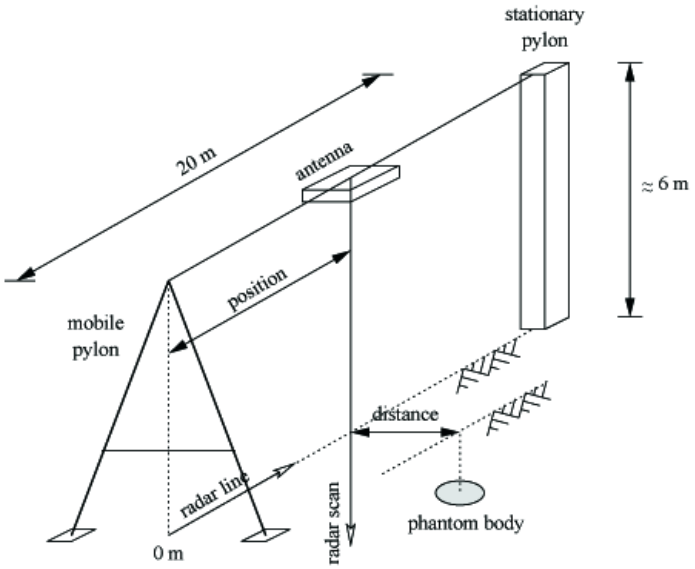

Figure 2.1.: Sketch of the aerial railway system

During winter 2006, from March until May, seven measurement series were performed and analyzed. For the first four field days, the radar surveys were conducted with both antennas, afterwards only the 400 MHz antennas were used.

2.2.2. Radar processing

The gathered radar data can be displayed in a radargram. A radargram (Fig. 2.5) consists of several single scans plotted together to form a coherent radar profile. Every single scan (radar trace) is divided, according to the chosen resolution, in n^2 samples, whereas every sample value is assigned a specific gray value. The resulting raw radar profiles were processed with the REFLEXW-Software (K.J. Sandmeier Scientific Software, Karlsruhe, Germany). This software enables the application of different filters and gain functions to visualize the resulting reflection values. We used a 1D filter (dewowing) to eliminate a possible low frequency part. Noise that occurs because of the geometry of the system, clutter, artifacts and static reflections were reduced with a background removal. The background filter subtracts reflections, which are constant over the whole radargram. Afterwards, we applied a linear gain for a clear display of the recorded radar profile. For the analysis of the resulting reflection energy, we used the envelope application.

The envelope or instantaneous amplitude is a measure for the reflectivity strength, which is proportional to the square root of the complete energy of the signal at an instant of time. The envelope on the one hand gives an overview of the energy distribution of the traces and on the other hand, it can facilitate the determination of signal first arrivals (Sandmeier, 1998), which was used for the manual snowpack extraction in section 2.3.2.

2.2.3. Snow properties

Radar reflectivity is caused by discontinuities in permittivity and/or electrical conductivity of the penetrated medium (Daniels, 2004). A change of these parameters in snow is mostly dependent on changes in snow density and snow wetness (Gubler and Hiller, 1984; Marshall et al., 2004; Yamamoto et al., 2004). Therefore, we focused mainly on these parameters and measured applying the highest possible spatial resolution. First, the radar signature of the snow was measured below the cable. Second, high-resolution penetration recordings with the SnowMicroPen (SMP) (Schneebeli et al., 1999) were performed to get spatially highly resolved information of the dielectric permittivity by empirical relations. The spacing between the SMP measurements along the radar line was constant (1 – 2 m) for each field day. The measuring depth was set to 1.5 m but could not always be achieved because of some impenetrable layers that stopped the measurement. At the end of the experiments, a conventional snow profile (e.g. Colbeck et al., 1990) was dug in the middle of the analyzed radar line. We acquired various snow parameters in this profile such as stratification, grain size, grain form, density and hand hardness. With the Dielectric Moisture Meter (DMM), we measured a relative value of the dielectric number in snow U compared to the number in air U_{ref}. The permittivity of snow ε_S was calculated relative to the value in air based on an empirical formula (Denoth, 1994):

$$\varepsilon_S = 1 + k \log_{10}(\frac{U}{U_{ref}}) \tag{2.1}$$

with the empirical constant $k = 7.41$.

2.2.4. Footprint analysis

The footprint or detectable range of an antenna is a key parameter. It influences the capability of a GPR-system as a tool for a professional search and rescue operation. We analyzed the footprint of the 400 MHz antenna at a height of 6 m above the snow surface by digging the phantom body in several distances to the aerial railway system (Fig. 2.2). The depths of the phantom body in the snow were approximately the same in all footprint experiments (around 0.5 m) and the radar line was always measured with the same antenna settings.

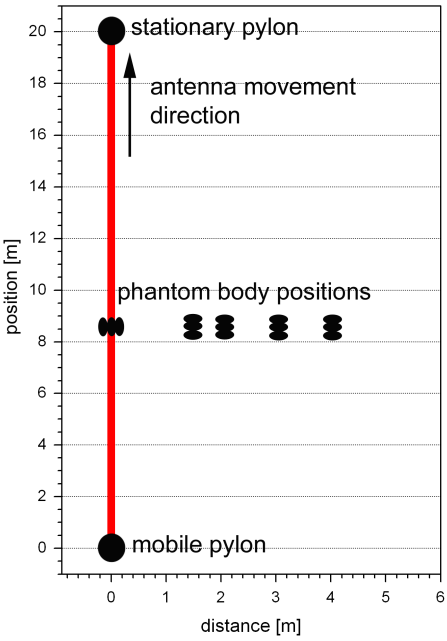

Figure 2.2.: Test arrangement for the footprint analysis. The black dots visualize the phantom body positions orthogonal and parallel to the radar line.

2.2.5. Wet snow analysis

Wet snow is known to be almost impenetrable by FMCW radar (Gubler and Hiller, 1984) and by radar using gigahertz frequencies (e.g. Gubler and Weilenmann, 1986). To our knowledge penetration depth at lower frequencies has not been studied in wet snow systematically.

Field tests

We tested this important case in a snowpack with a melting surface. The measurements during May 2006 had the same test arrangement as described before. Again, we simulated an avalanche deposit directly above the victim with a snow grooming machine. Furthermore, we dug a cave and recorded radar lines, while a life human was lying in the snow cave.

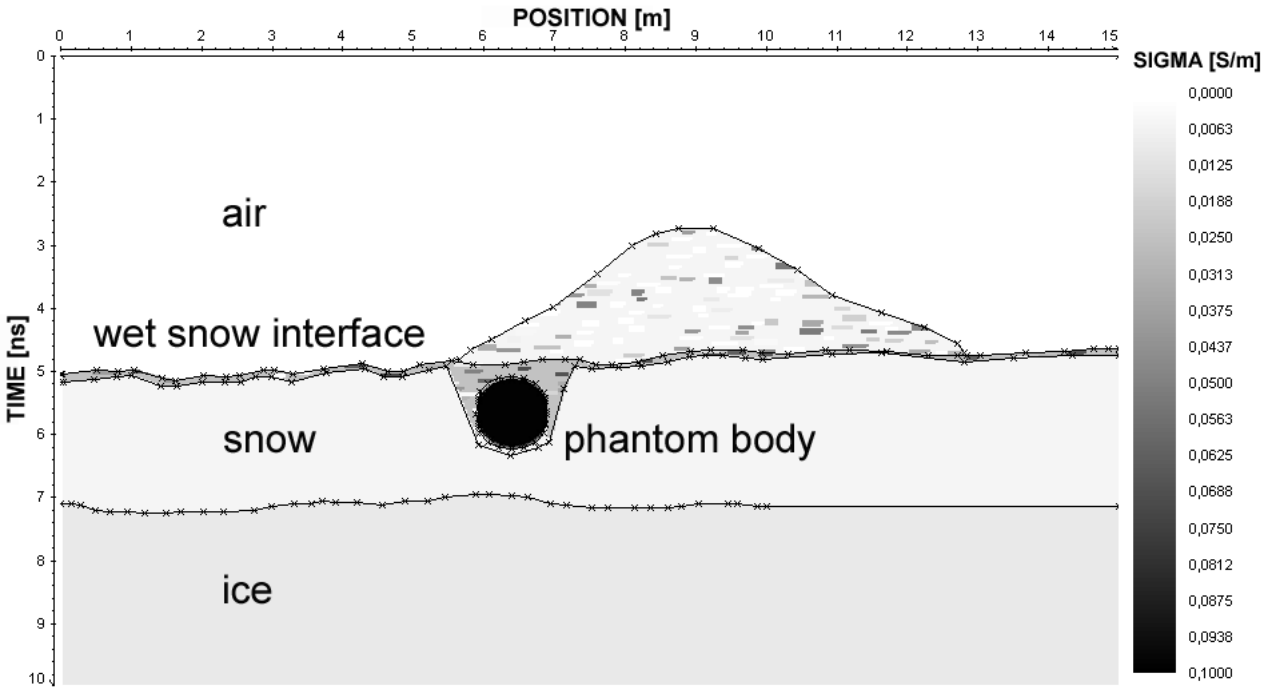

Figure 2.3.: Geometry and electrical conductivity for the numerical simulation of a radar response for wet-snow conditions. A thin surface layer of wet snow with higher conductivity than in the deeper dry snow is modelled. A randomly distributed scatter of the conductivity in the deposit due to the mixture of dry and wet snow is assumed.

Numerical simulation

We simulated the wet snow conditions by modelling the radargram with the REFLEXW software. In moist snow, not only the dielectric permittivity increases distinctly in comparison to dry snow, but also the electrical conductivity contributes to influence the signal propagation. The permittivity of moist snow is remarkably larger than that of dry conditions, as moist snow consists additionally of a water volume fraction. Three media, with various volume fractions contribute to the resulting dielectric permittivity, air ($\varepsilon_a = 1$), ice ($\varepsilon_I = 3.2$) and water ($\varepsilon_w = 81$). The electrical conductivity of dry snow is set by the mixture between ice and air, which conductivities are approximately $\sigma_I \approx 10^{-8}$ S/m (Hobbs, 1974) and $\sigma_a = 2.5 \cdot 10^{-13}$ S/m (Lide, 1996), respectively. The conductivity of liquid water is at least two orders of magnitude higher, namely $\sigma_1 = 4 \cdot 10^{-6}$ S/m for pure water and $\sigma_2 = 3 \cdot 10^{-5}$ S/m for distilled water (Czichos, 1996). With a small amount of impurities in water this value is far higher, e.g. the accepted limit value for tap water is usually $\sigma = 0.05$ S/m. A typical value for the glacier water of a catchment at Stubai glacier is $\sigma = 0.01$ S/m. Therefore, the expected vertical differences of conductivity for wet snow-avalanche conditions are assumed to be higher than the measured differences in

permittivity (Tab. 2.1). We performed two different simulations. One was performed with permittivity values according to the measurements with the Denoth Meter in the profile and constant conductivity. In a second simulation, we overlaid assumed conductivity values in the range mentioned above (Fig. 2.3). Here we modelled a wet snow interface, due to the warm day, and dry snow below, as it was observed in situ. The snow mound was physically created by scraping up the upper layers of the surrounding snowpack with a snow-grooming machine. Thus, the deposit was a mixture of wet and dry snow, as well as air filled holes. Therefore, we assume some randomly distributed scatter of the conductivity in the snow accumulation.

2.3. Calculations

2.3.1. Permittivity estimation with SnowMicroPen signals

The SnowMicroPen records the penetration force every 4 µm. Pielmeier (2003) found an empirical approach to convert the penetration force into density:

$$f = 0.0033 \cdot exp(0.018\rho_s) \tag{2.2}$$

with the force signal f in (N) and the snow density ρ_S in (kg/m^3). Thus, vertically highly resolved density profiles can be calculated using eq. (2.2). These density values can be converted into dielectric constant or permittivity values including the assumption that in dry snow the permittivity is solely a function of density, eq. (2.3) (Kovacs et al., 1995; Mätzler, 1996)

$$\varepsilon_s^b = (1 - v)\varepsilon_h^b + \varepsilon_{so}^b \tag{2.3}$$

with the empirical fitting parameters of $b = \frac{1}{3}$, the permittivity of the host medium (air) $\varepsilon_h = 0.9974$ as well as the permittivity of the solid material (ice) $\varepsilon_{so} = 3.215$; v is the ice volume fraction with:

$$v = \rho_s/\rho_I \tag{2.4}$$

where ρ_I is the density of solid ice. Mätzler (1996) and Kovacs et al. (1995) used different functions. However, the difference between the equations is below 1%. Other models like the one of Schneebeli et al. (1998), who developed a calibration function specifically for time-domain reflectometry (TDR), which has in this case a systematic error, were not applied in the present study. The average dielectric permittivity for each penetration measurement was calculated and the variation characterized using eq. (2.3).

2.3.2. Post processing of radar data

After processing the raw radar data with the methods of section 2.2.2, we extracted the snowpack manually and analyzed the reflection energy curves within these trimmed radar scans. 100 consecutive scans of a radargram, which correspond to 1 m horizontal distance, were picked out systematically around a point of interest (e.g. an apex of a hyperbola) and visualized as reflection energy curves.

Snow pack extraction

It is important for any fast automatic detection algorithm to remove the zone of air and underground in the radargram to perform the location algorithm solely in the snowpack. In this work, we conducted this manually for each scan, by using the reflection energy curves, which show distinct peaks at the two interfaces air-snow and snow-ice. However, automatic snowpack extraction was part of the ongoing research and is presented in Frühauf et al. (2009) – Paper 2.

Reflected energy analysis

The resulting trimmed reflection energy curve of each scan was analyzed statistically. We calculated the coefficient of variation for these scans but the maximum values of the reflected energy were too isolated for creating a significant pattern. Based on this experience, we calculated the quotients of the maximum over mean, maximum over median and the average of the five highest values of the respective trimmed scan (h5) over mean and median. The same analysis were likewise performed for positions in the radar line, where the influence of the reflections of the phantom body or the two railway pylons in the radargram was minimal. All the resulting quotients were averaged over the respective 100 consecutive scans and visualized in bar plots (Fig. 2.5, 2.8 and 2.9).

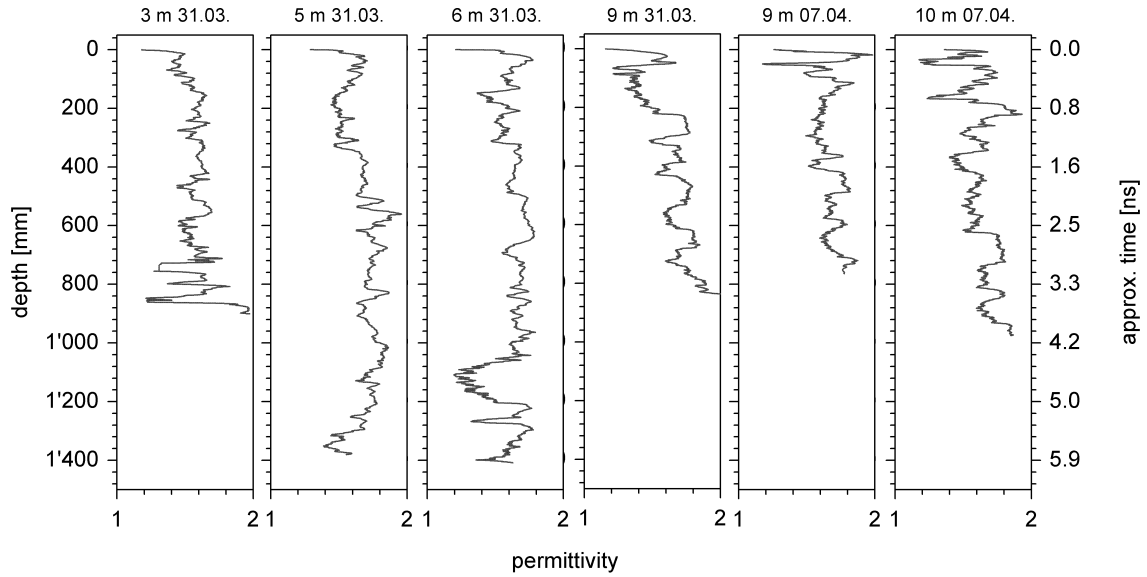

Figure 2.4.: The calculated permittivity curves from selected SMP measurements in dry snow. The positions in the mentioned radargrams are marked.

2.4. Results

The field days of winter 2006 were dedicated to various specific topics. Firstly, the effect of snow layers of different density on the recognizability of the phantom body was investigated. Secondly, the size of the radar footprint and the effect of phantom orientation were measured. Thirdly, the effect of wet snow on the perceptibility of targets was determined.

2.4.1. Permittivity of snow

SMP measurements

Around 40 SMP measurements showed a strong variation in the penetration resistance from almost 0 N up to 50 N or more. Direct density measurements in the snow pit in the undisturbed snowpack revealed values up to 400 kg/m^3 with steps of more than 100 kg/m^3 between different layers. This corresponds well with the measured hand hardness, which was measured between stage 1 (fist) and stage 4 (pencil). However, the permittivity calculated according to section 2.3.1 lies mainly between $\varepsilon = 1$ and $\varepsilon = 2$, with only very few values above $\varepsilon = 2$ (Fig. 2.4). The interquartile range (IQR) (Wilks, 1995) of the profiles decreases according to the calculations in section 2.3.1 by a factor of 10 from penetration resistance to permittivity. Compared with the permittivity of the phantom body ($\varepsilon_w = 81$) errors and uncertainties in this empirical estimation of the snow permittivity are negligible.

Dielectric Moisture Meter

The measurements of the permittivity with the Denoth Meter are summarized in Table 2.1. The overall mean value for dry snow is $\varepsilon_s = 1.5$. The mean value of the estimated permittivity from SMP tests is slightly higher, but in a reasonable agreement with this mean value. The permittivity variations predicted by the SMP tests are therefore assumed to be realistic. In the following we will use $\varepsilon = 1.5$ as mean permittivity for dry snow.

Table 2.1.: Calculated permittivity values of the dielectric numbers recorded with the Dielectric Moisture Meter (DMM) compared to the range of the several calculated SMP-permittivity values.

Date	Mean	SD	Min	Max	Mean_SMP	Max_SMP
21.03.06	1.42	0.21	1.17	1.74		
31.03.06	1.57	0.23	1.17	1.83	1.63	1.95
04.04.06	1.49	0.23	1.08	1.69		
07.04.06	1.54	0.18	1.28	1.74	1.70	1.97
28.04.06	1.65	0.34	1.24	2.35		
04.05.06	1.98	0.29	1.68	2.69		
11.05.06	1.99	0.30	1.66	2.89		

2.4.2. Effect of snow layers

The effect of snow layers of rapidly changing density was tested in several measurement series. The test arrangement of March 31, 06 is used in the following to illustrate the coherences. To simulate an avalanche deposit, a snow mound was created above the phantom body, which was located at the position of 5.4 m in the radargram. We measured the line twice with both antennas, the 400 MHz and the 600 MHz antennas. In Figure 2.5 the radargram and in Figure 2.6 the reflection energy of selected scans is displayed, measured with the 400 MHz antennas.

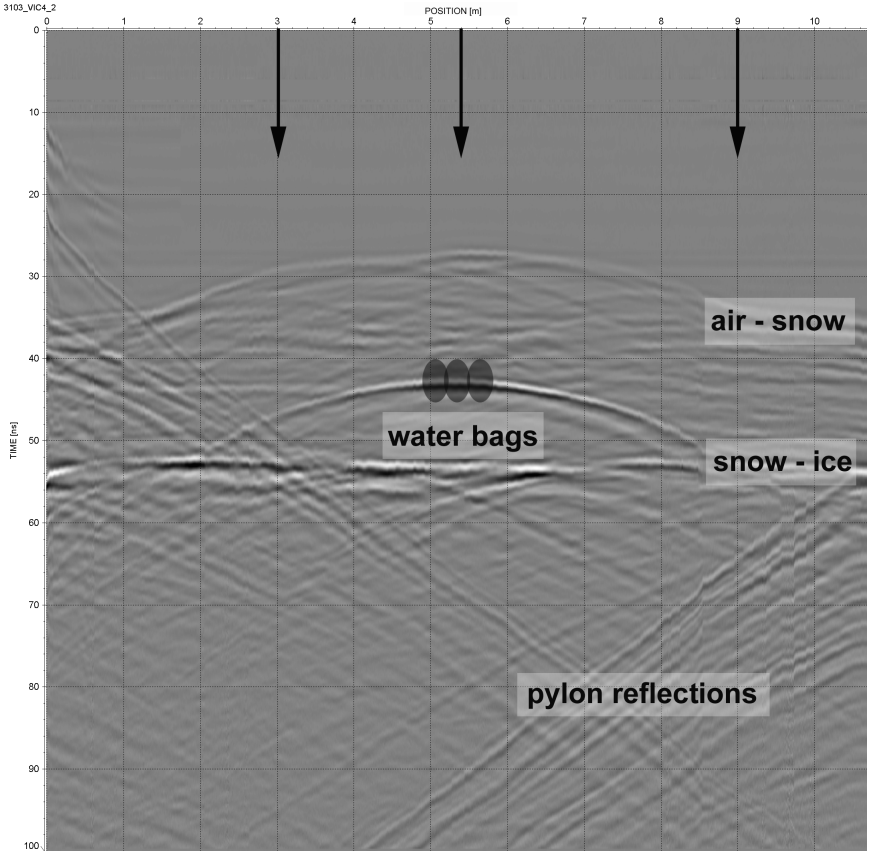

Figure 2.5.: Radargram of the measurement in dry snow (31.03.06). In horizontal direction the position and in vertical direction the two-way travel time of the signal is plotted. The air-snow transition and the snow-ice transition as well as the position and the dimension of the phantom body (dark gray dots) are marked. The arrows indicate the positions of the reflection energy profiles. The diagonal linear reflections in the radargram are artifacts caused by the two pylons.

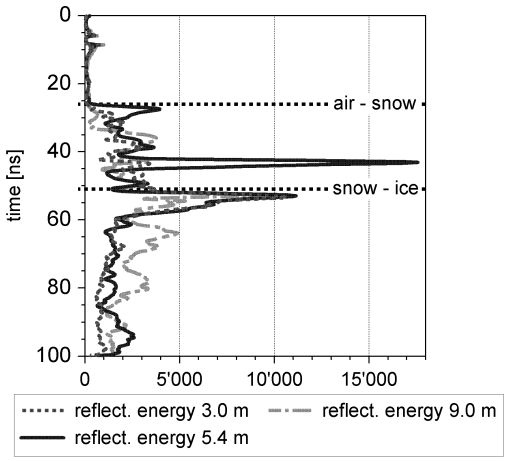

Figure 2.6.: Diagram of the relative reflection energy of selected scans of the 31.03.06 measurement.

In the radargram in Figure 2.5, the reflection above the water bags can easily be identified as hyperbola. The formation of a hyperbola as a reflection image of a point source can be explained by the velocity of propagation of the transmitted waves of a moved transmitter and the beam width of the antenna (section 1.2.3; Daniels, 2004, p.24). The apex of the hyperbola (second arrow, Fig. 2.5) is situated at a position of 5.4 m with a two-way travel time of 40–45 ns (∼15 ns in snow). With the above estimated permittivity of $\varepsilon_s = 1.5$, the velocity of propagation of electromagnetic waves in snow is calculated as $v = 0.24$ m/ns, subsequently resulting in the depth of the apex of 1.83 m in snow. The probed depth in the field was about 2 m. The reflection energy curves (Fig. 2.6) taken at 3.0 m, 5.4 m and 9.0 m show characteristic differences between features of the phantom body and the surrounding snow. It can be stated that the signal at 5.4 m shows the reflection signal of the phantom body very clearly. The first peak at a two-way travel time of 40–45 ns is the phantom body; the second is the transition snow – ice (50–55 ns). The reflection energy of the surrounding snow in Figure 2.6 is about five times smaller than the energy peak above the phantom body, consisting of three water bags. By dividing the maximum reflected energy by the statistical mean or median of the energy in the snowpack, large disparities between phantom-body scans (2. and 4. bar, Fig. 2.7) and pure-snow scans are obvious. These resulting energy quotients differ by a factor of approximately 2. For a better visualization a line is drawn in the bar diagrams at a threshold of 4 units.

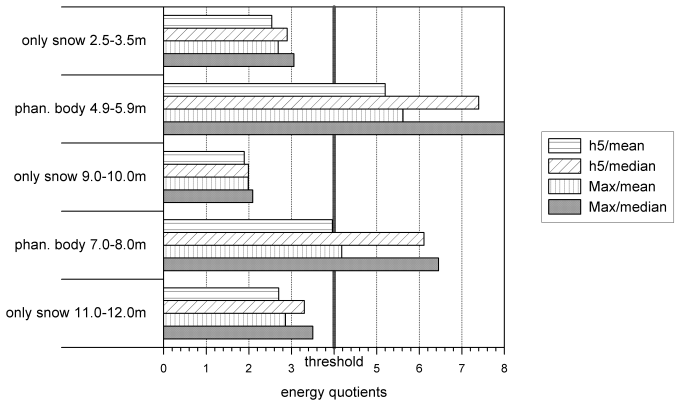

Figure 2.7.: Phantom body detection with reflection energy values for specific horizontal ranges of scans. Each of the 100 scans in the intervals are averaged over the horizontal distance, which is given in the labels. Shown is the statistical evaluation of the vertical variation of the reflected energy: the quotients of the 5 highest values (h5) and the maximum value (Max) over the mean and median value.

2.4.3. Radar footprint and effect of phantom orientation

An important feature of any radar system is the footprint or detectable range of the antennas. The interest is, up to what horizontal distance to the radar line a phantom body clearly is

detectable as hyperbola. This was analyzed by offsetting the phantom from the cable system (Fig. 2.1). Furthermore, some trials were made testing if recognizable differences exist in the radargram, whether the phantom body is overflown across or along.

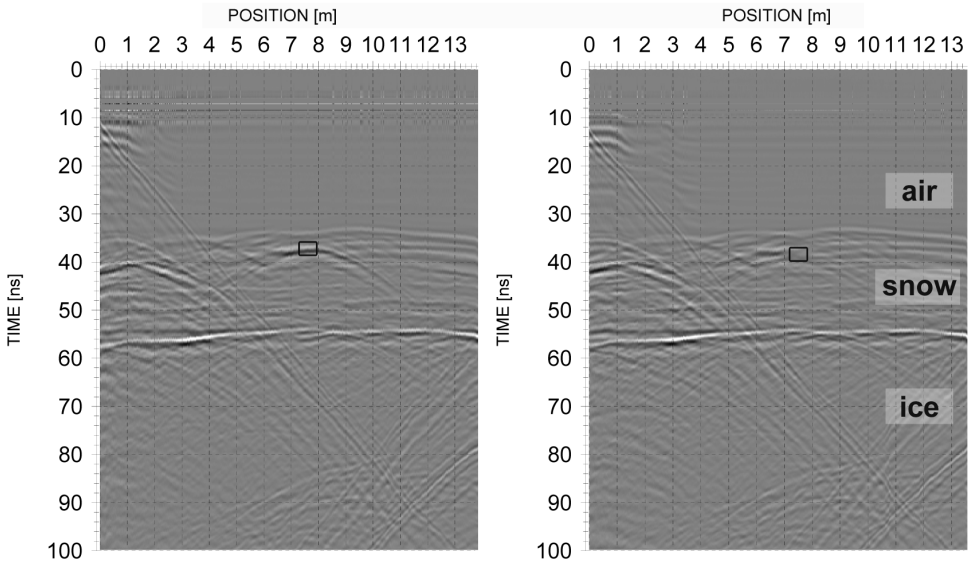

Figure 2.8.: Radargrams of two measurements with special regard to the footprint of the antenna. Left shows a radar image with a phantom body (black rectangle) in a horizontal distance of 1.5 m from the railway cable. Right displays a radargram for the phantom body in approximately 2 m distance from the railway cable. The hyperbolas with apex at 1 m are caused by the operator and the control equipment.

Both radargrams in Figure 2.8 were processed as described in section 2.3.2. In each case consecutive scans around the apex of the hyperbola and scans, where the influence of the phantom body and the disturbances of the pylons were minimal, were chosen for extraction. Figure 2.8 as well as Figure 2.9 show very distinct differences between the two radar measurements. In the left radargram in Figure 2.8 the hyperbola, particularly the apex of the hyperbola, is clearly visible. While the phantom body is situated in a distance of 2 m or more (Fig. 2.8, right radargram) no clear hyperbola is determinable. This is also seen in terms of reflective energy quotients (Fig. 2.9), whereas the energy quotients for a phantom body in 2 m distance do not differ from measurements in pure snow.

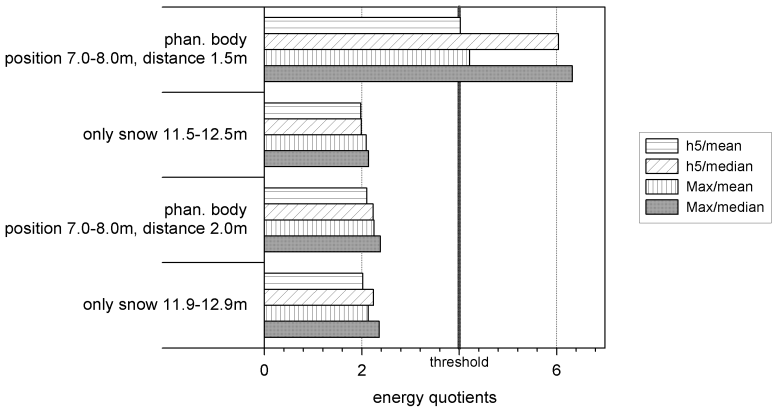

Figure 2.9.: Size of detectable range shown by reflection energy values of specific horizontal ranges of scans. Each of the 100 scans in the intervals are averaged over the horizontal distance, which is given in the labels. Shown is the statistical evaluation of the vertical variation of the reflected energy: the quotients of the 5 highest values (h5) and the maximum value (Max) over the mean and median value.

The orientation of the phantom body, parallel or across to the radar line (Fig. 2.2), influences the reflected energy as well. The mean reflection energy for the orthogonal position of the phantom body is $\sim$ 70% of the mean reflection energy for the parallel position (Fig. 2.10). The term "parallel to the radar line" corresponds to a 90° angle to the polarization of the radar antennas, but in the following we use the terms parallel and across referring to the radar line.

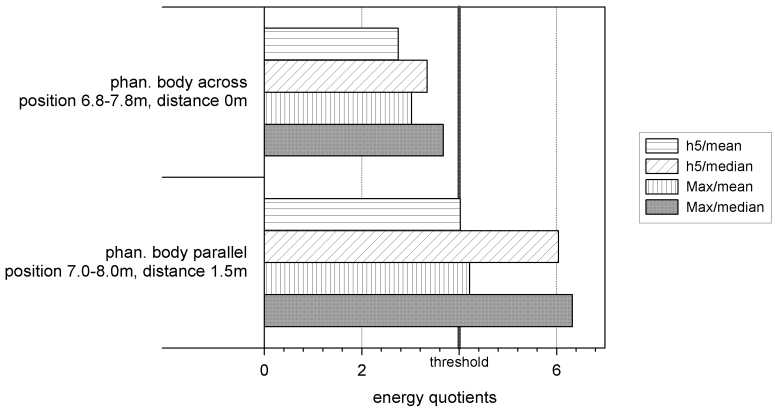

Figure 2.10.: Reflection energy of specific horizontal ranges of scans with the phantom body parallel and across to the radar line. Each of the 100 scans in the intervals are averaged over the horizontal distance, which is given in the labels. Shown is the statistical evaluation of the vertical variation of the reflected energy: the quotients of the 5 highest values (h5) and the maximum value (Max) over the mean and median value.

2.4.4. Effect of wet snow

Field tests

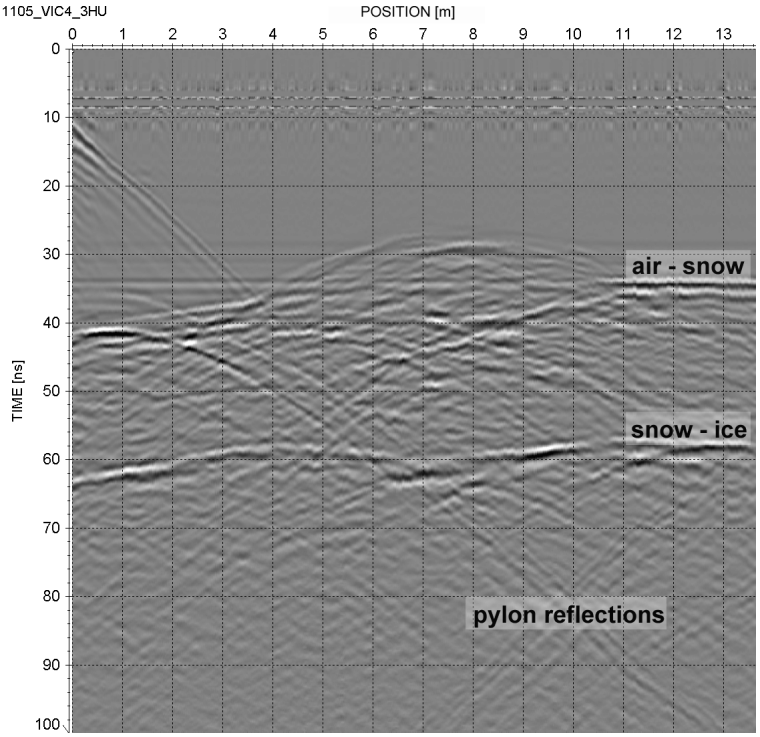

Figure 2.11.: Radargram of the measurement of the 11.05.06 in wet snow with the phantom body and a human victim lying in the snowpack. In horizontal direction the distance is plotted in meter and in vertical direction the two-way travel time of the signal in ns. The air-snow transition and the snow-ice transition are marked, the artifacts caused by the pylons are visible.

In all analyzed cases using 400 MHz antennas, neither the water bags nor a human body were identifiable as a hyperbola in the radargram (Fig. 2.11). Therefore, no reflection could be related to the targets in the snow accumulation. We did no statistical or reflection energy analysis because of the complexity of the radar picture.

Numerical simulation

With the measured permittivity values in the wet snowpack (Tab. 2.1), which are slightly higher than for dry snow, the numerical simulation showed an obvious phantom body reflection (Fig. 2.12B). Adding a randomly distributed scatter of the electrical conductivity, as mentioned in section 2.2.5, resulted in a simulated radargram as in Figure 2.12C. The clarity of the phantom-body

hyperbola decreases rapidly even - as conducted here - if only few disturbances are supplemented.

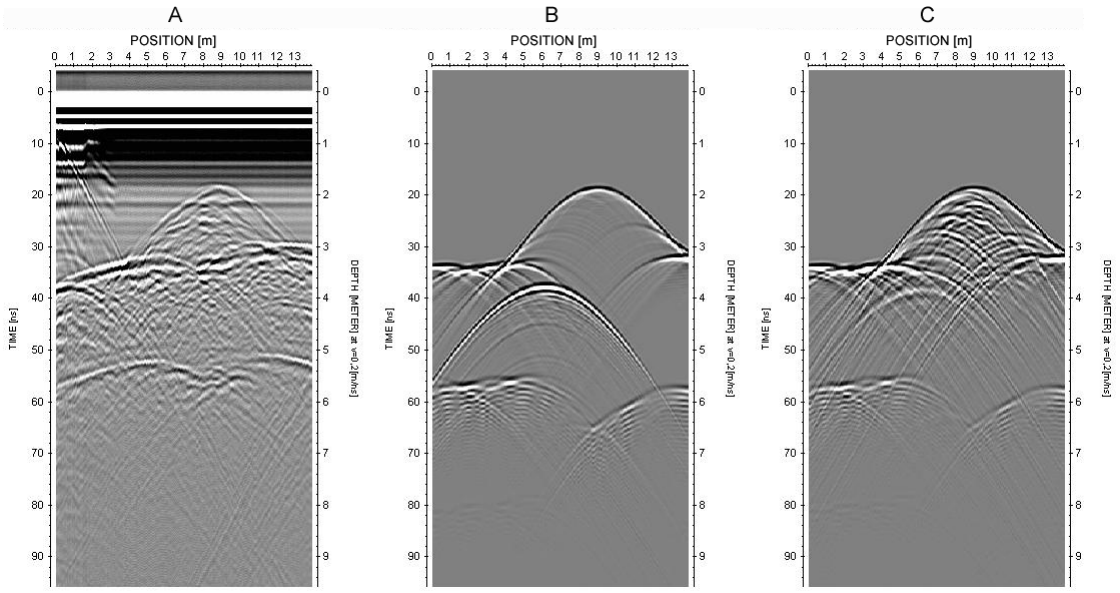

Figure 2.12.: Result of the numerical modelling. Left, the measured radargram is visualized, middle shows a simulated radargram with the measured permittivity values of the snow profile and constant electrical conductivity. Right displays a modelled radargram where randomly supplemented disturbances in electrical conductivity in the snow mound are added.

2.5. Discussion

Using the aerial railway system together with a GPR, we were able to simulate airborne detection of avalanche victims. The 6 m high railway was probably still too low for the simulation of helicopter flights, but it offers a possibility to measure the effect on radar at a distinct distance to the snow surface. Avalanche deposits were simulated by scraping up a snow mound with a snow-grooming machine. Several SnowMicroPen measurements and density analysis were conducted in two dry snow avalanches, triggered by snow recreationalists, to analyze the spatial variability of snow parameters in avalanche debris. These data correspond very well to the SMP values gathered of the artificial deposits in our experiments. A future task will be to analyze the statistical significance of the similarity between avalanche and artificial deposits. The mean value and the variation of the permittivity of dry snow turned out to be much lower than the permittivity of water or a human body. This guarantees a strong reflection of radar waves by a victim, which was clearly observed in our field tests. Therefore, this victim should be detectable in dry snow, even if the stratigraphy shows a large variability. On the other hand,

our experiments with moisture in the snowpack confirmed earlier conclusions that the detection of bodies within a wet snow avalanche is probably very difficult or impossible with radar. The numerical model showed that this could be due to the mixture of dry and wet snow and some air filled voids in the accumulation. This mixture causes a strong variability in electrical conductivity. Thus, the radar reflection is scattered too much by the deposit, with the consequence that the remaining phantom body reflections in or below a deposit are too attenuated for being recognizable clearly as hyperbola. In our experiments, with the antennas at a height of 6 m, the reflection energy decreases rapidly for objects that are situated in a lateral distance of more than 1.5 m from the radar line. This result would lead to a search strip of only 3 m, which is obviously extremely narrow for a helicopter flight. Measurements in winter 2007 with a chair lift in 12 m height, what is a feasible height for helicopter applications, showed that the footprint size only slightly increases. In addition, using two antennas mounted in various distances to each other orthogonally to the radar line showed that the overall detectable range can be further increased. The orientation of the phantom body with respect to the radar line influenced the reflected energy. Less energy was reflected by objects oriented perpendicular to the radar line, which means for the used GPR-system, parallel to the polarization of the antenna. This resulted in a further reduction of the footprint for cross-orientation. Therefore, the flight pattern for a helicopter should be a grid of orthogonal lines to minimize the influence of the orientation. One of the ultimate goals of this research project is to develop an automatic detection software (see Frühauf et al., 2009 – Paper 2). The idea is that an algorithm informs an operator in the helicopter by a signal when a suspicious object is situated in the snowpack. The four analyzed test series showed that simple thresholding may be sufficient for the algorithm. A thorough statistical analysis is not yet possible because of the limited number of tests. Further steps towards the aimed fool-proof detection system will require helicopter flights and the development of an online snowpack extraction and hyperbola location software. An important task will be georeferencing the position of the hyperbola apex. In summary, the utilized GPR-system is not yet capable for rescue operations based on helicopters. For an adequate operation, a footprint created by at least two antenna devices in an array should be used, mounted parallel to each other on a beam. Multiple antennas can be controlled using multi-channel control units. The distance between the antennas may not exceed the width of the footprint of one antenna. The flight pattern should be an orthogonal grid with the maximum mesh width not larger than the created footprint. A differential GPS could be a promising possibility to follow this grid accurately and to georeference the gathered data.

2.6. Conclusion

We conclude that even strong changes in stratigraphy in dry snow have a small effect on the perceptibility of phantom bodies with dielectric properties similar to humans using a 400 MHz GPR system. In contrast, wet snow with a similar stratigraphy as in an avalanche deposit makes a phantom body impossible to detect. Although the height of 6 m is too low for a helicopter flight, we could show that a flight operated system can be feasible. The automatic detection algorithm works well for the four analyzed datasets but is entirely dependent on a proper snowpack extraction, which in an automated form is still a challenge. Our measurements covered a realistic range in snow avalanche conditions but it is still necessary to validate the algorithm with a higher number of samples.

Acknowledgement

Financial support for this research was provided by the Centre of Natural Hazard Management (alpS) and Wintertechnik Engineering GmbH. IDS Ingegneria dei Sistemi kindly supported us with the radar system. For assistance in the field we thank E. Bollmann, L. Furtenbach, M. Huttenlau, P. Mair, H.-M. Schuler and M. Thöni. We would also like to thank K.J. Sandmeier for performing the modelling and K.J. Sandmeier and J. Schweizer for discussions that helped to improve the present study. Furthermore, we thank the anonymous referees for valuable suggestions to improve the paper.

Bibliography

Arcone, S., Delaney, A., 2000. GPR images of hidden crevasses in Antarctica. In: Proceedings of the Eighth International Conference on Ground Penetrating Radar. Gold Coast, Australia, pp. 760–765.

Colbeck, S., Akitaya, E., Armstrong, R., Gubler, H., Lafeuille, J., Lied, K., McClung, D., Morris, E., 1990. The international classification for seasonal snow on the ground. Tech. rep., International Commission of Snow and Ice of International Association of Scientific Hydrology / prep. by Working group on Snow Classification.

Coumes, A., 1983. Systems radioélectriques passifs pour la detection les victims d' avalanches. In: Tagung Elektronik und Lawinen '79. Graz, Austria, pp. 158–168.

Czichos, H. E., 1996. Hütte- die Grundlagen der Ingenieurwissenschaften, 30th Edition. Springer-Verlag, Berlin, Germany.

Daniels, D., 2004. Ground Penetrating Radar, 2nd Edition. The Institution of Electrical Engineers, London, UK.

Denoth, A., 1994. An electronic device for long-term snow wetness recording. Annals of Glaciology (Proceedings of the Symposium on Applied Ice and Snow Research 1993) 19, 104–106.

Frühauf, F., Heilig, A., Schneebeli, M., Fellin, W., Scherzer, O., 2009. Experiments and algorithms to detect snow avalanche victims using airborne ground-penetrating radar. IEEE Transactions on Geoscience and Remote Sensing 47 (7), 2240–2251.

Fuks, P., 1983. Multifrequency radar for detection of avalanche victims. In: Tagung Elektronik und Lawinen ´79. Graz, Austria, pp. 169–176.

Gabriel, S., Lau, R., Gabriel, C., 1996. The dielectric properties of biological tissue: III. parametric models for the dielectric spectrum of tissues. Physics in Medicine & Biology 41, 2271–2293.

Gubler, H., Hiller, M., 1984. The use of microwave FMCW radar in snow and avalanche research. Cold Regions Science and Technology 9, 109–119.

Gubler, H., Weilenmann, P., 1986. Seasonal snow cover monitoring using FMCW radar. In: ISSW International Snow Science Workshop 1986. pp. 87–97.

Hobbs, P., 1974. Ice Physics. Oxford University Press, Oxford, UK.

Instanes, A., Lonne, I., Sandaker, K., 2004. Location of avalanche victims with ground-penetrating radar. Cold Regions Science and Technology 38, 55–61.

Jaedicke, C., 2003. Snow mass quantification and avalanche victim search by ground penetrating radar. Surveys in Geophysics 24, 431–445.

Kovacs, A., Gow, A., Morey, R., 1995. The in-situ dielectric constant of polar firn revisited. Cold Regions Science and Technology 23, 245–256.

Lide, D., 1996. Handbook of Chemistry and Physics, 76th Edition. CRC Press, USA.

Machguth, H., Eisen, O., Paul, F., Hoelzle, M., 2006. Strong spatial variability of snow accumulation observed with helicopter-borne GPR on two adjacent Alpine glaciers. Geophysical Research Letters 33 (13).

Mair, R., 2006. Lawinenunfälle in Österreich im Winter 2005/06. Sicherheit im Bergland, pp. 218–239.

Marshall, H., Koh, G., Forster, R., 2004. Ground-based frequency-modulated continuous wave radar measurements in wet and dry snowpacks, Colorado, USA: an analysis and summary of the 2002/03 NASA CLPX data. Hydrological Processes 18, 3609–3622.

Modroo, J., Olhoeft, G., 2004. Avalanche rescue using ground penetrating radar. 10 th International Conference on Ground Penetrating Radar, Delft, Netherlands, 785–789.

Mätzler, C., 1996. Microwave permittivity of dry snow. IEEE Transactions on Geoscience and Remote Sensing 34 (2), 573–581.

Niessen, J., Kliem, E., Poehlking, E., Nick, K., 1994. The use of ground penetrating radar to search for persons buried by avalanches. 5 th International Conference on Ground Penetrating Radar, Kitchener, Canada, 507–517.

Osterer, F., 1983. Radar zur Suche Lawinenverschütteter. In: Tagung Elektronik und Lawinen '79,. Graz, Austria, pp. 139–147.

Paul, W., 1983. Ortung von Lawinenverschütteten durch Reflexionsmessungen. In: Tagung Elektronik und Lawinen ´79. Graz, Austria, pp. 148–157.

Pielmeier, C., 2003. Textural and mechanical variability of mountain snowpacks. Ph.d. thesis, University of Berne, Berne, Switzerland.

Sandmeier, K., 1998. Reflexw version 4.1 manual.
URL `http://www.sandmeier-geo.de/Download/reflexwmanual.pdf`

Schneebeli, M., Coléou, C., Touvier, F., Lesaffre, B., 1998. Measurement of density and wetness in snow using time-domain reflectometry. Annals of Glaciology 26, 69–72.

Schneebeli, M., Pielmeier, C., Johnson, J., 1999. Measuring snow microstructure and hardness using a high resolution penetrometer. Cold Regions Science and Technology 26, 101–114.

Sheng, H., 2000. Body fluids and water balance. In: Stipanuk, M. (Ed.), Biochemical and physiological aspects of human nutrition. Saunders, Philadelphia, USA, pp. 843–865.

SLF, 2007. Lawinenunfälle. [access date 19.04.2007].
URL `http://www.slf.ch/avalanche/avalanche--de.html`

Tschirky, F., Brabec, B., Kern, M., 2000. Lawinenunfälle in den Schweizer Alpen – Eine statistische Zusammenstellung mit den Schwerpunkten Verschüttung, Rettungsmethoden und Rettungsgeräte. Ammann, W.J., Davos, Switzerland, Ch. Durch Lawinen verursachte Unfälle im Gebiet der Schweizer Alpen, pp. 125–136.

Wilks, D., 1995. Statistical methods in atmospheric sciences. San Diego, USA.

Würtl, W., 2003. Lawinenereignisse in Österrreich - Winter 2002/03. Sicherheit im Bergland, Innsbruck, Austria, pp. 49–82.

Würtl, W., 2004. Lawinenereignisse in Österrreich im Winter 2003/04. Sicherheit im Bergland, Innsbruck, Austria, pp. 170–190.

Würtl, W., 2005. Lawinenunfälle in Österrreich im Winter 2004/05. Sicherheit im Bergland, Innsbruck, Austria, pp. 206–222.

Yamamoto, T., Matsuoka, K., Naruse, R., 2004. Observation of internal structures of snow covers with a ground–penetrating radar. Annals of Glaciology 38, 21–24.

Zweifel, B., 2004. Lawinenunfälle in den Schweizer Alpen. Winter 2002/03. Personen- und Sachschäden. Davos, Switzerland.

Zweifel, B., 2005. Lawinenunfälle in den Schweizer Alpen. Winter 2003/04. Personen- und Sachschäden. Davos, Switzerland.

3. Experiments and Algorithms to Detect Snow Avalanche Victims Using Airborne Ground-Penetrating Radar [1]

Florian Frühauf, Achim Heilig, Martin Schneebeli, Wolfgang Fellin and Otmar Scherzer

[1] published in similar form as: Frühauf, F., Heilig, A., Schneebeli, M., Fellin, W., Scherzer, O., 2009. Experiments and algorithms to detect snow avalanche victims using airborne ground-penetrating radar. IEEE Transactions on Geoscience and Remote Sensing 47 (7), 2240–2251.

Abstract

Snow avalanche victims have only a good chance to survive when they are located within short time. This requires that they wear an active beacon or very rapid deployment of a search-and-rescue team with dogs. Customary ground-penetrating radar (GPR) instruments used on the snow surface are not able to reduce fatality numbers, because they are slow to search a field. A potential alternative could be an airborne search using radar. An airborne radar search is technologically challenging, because a very large data-stream has to be processed and visualized in real time, and the interaction of the electromagnetic waves with snow, subsurface and objects must be understood. Experiments and simulations showed that body-equivalent objects in the snowpack reflect radar waves and appear as diffraction hyperbolas in the recorded radar data. Here, we studied a two-step algorithm to locate such hyperbolas. In the first step, a fast active contour method is used to segment the snowpack, in the second step, a matched filter locates the diffraction hyperbolas. This algorithm detects body-like objects in real-time. The algorithm was validated using realistic test arrangements and conditions using an aerial tramway. The distance dependence of the reflection energy with increased flight heights, the coherence between the use of more antennas and the detectable range and the reflection images of different avalanche victims were measured. The algorithm detected the object hyperbola for each investigated case where the reflection energy of the scans was higher than for scans of pure snow. Two antennas in monostatic arrangement almost doubled the detectable range, which would decrease the length of the flightline. Airborne GPR has a large potential to become a rapid search method in dry snow avalanches. However, a fully operational version still requires substantial improvements in hard- and software.

3.1. Introduction

The detection of snow avalanche victims, which are not equipped with a localization device is a demanding problem for rescue operations. The development of alternatives to traditional search methods like dogs or snow probing teams is a challenge, which is urgently at issue. There have been several research groups working on the possibilities of ground penetrating radar (GPR) for the detection of avalanche victims (Niessen et al., 1994; Jaedicke, 2003; Instanes et al., 2004; Modroo, 2004; Olhoeft and Modroo, 2006). These studies have in common that the radar system is used directly upon the snow surface. The snow surface of an avalanche is usually blocky and difficult to walk. An airborne radar system would be attractive, because this seems to be the only way to decrease the search time to improve survival probability according to Brugger et al. (2001). Olhoeft and Modroo (2006) systematically measured the signature of different objects buried in a snowpack. They show that a human body mass equivalent has a distinct radar signature.

Heilig et al. (2008) investigated fundamental questions relevant to an airborne application of GPR-systems: (i) the influence of the snow properties on the radar signal, (ii) the maximum horizontal distance of a victim from the flight direction and (iii) the influence of the orientation of the victim with respect to the flight direction. Additionally, it is essential for a fast and successful airborne search operation with GPR that the objects in the snowpack are located automatically by a software algorithm. A manual real-time detection on a computer screen is impossible because of difficult light conditions and various forms of appearances of the hyperbolas caused by different radar antenna orientation. Due to these facts, further development towards a feasible automatic avalanche victim localization system and algorithm were undertaken.

Airborne radar data recording consists of at least three materials: air, snow and underlying layer, either soil, bedrock, talus or ice. The boundaries of the materials appear as nearly straight lines in the radargram, caused by the high reflection due to changes in permittivity and/or electrical conductivity. A buried point-like object reflecting the electromagnetic radiation, manifests itself as a diffraction hyperbola (Daniels, 2004). Thus the goal of the detection algorithm is to find these hyperbolas in the snowpack in real-time.

A two-step approach was chosen. First a parametric active contour method (Kass et al., 1987; Blake and Isard, 1998) for automatic extraction of the snowpack is applied. Such an active contour approach is currently not used for the processing of GPR data. Next a matched filter algorithm was applied to enhance the diffraction hyperbolas in the radargrams. The optimal choice of a template diffraction hyperbola, similar to the gathered radar data, turned out to be crucial.

Building on the work of Heilig et al. (2008), we measured at a more realistic height of 12 m above the snow surface. Measurements and the subsequent processing indicate that an airborne search is feasible in real scenarios.

3.2. Methods

First we introduce the localization algorithm, then the experimental setup and finally a statistical method to evaluate radar reflectivity and signal quality.

3.2.1. Location algorithm

A human victim or a body mass equivalent manifests itself as a diffraction hyperbola in the radargram. However, radargrams from a snowpack and the underlying ground often contains additional hyperbolas, caused by boulders in the subsurface of the snowpack. Therefore, in a first step the snowpack must be extracted, and then the hyperbolas in the snowpack must be

localized.

The extraction and de-noising of the snowpack is performed in three steps. First, the radargram is pre-processed. Second, the snowpack is segmented using an active contour algorithm, and finally the extracted snowpack is post-processed to improve the signal to noise ratio of the hyperbola. The localization step is conducted by searching for hyperbolas in the snowpack by a matched filter.

In the following, we describe the snowpack extraction step of the algorithm for the first n_x scans. The dynamic implementation of these steps is gained by adding a new incoming scan to the radar data and discard the oldest. The result of the snowpack extraction steps is stored. Then we create a template of a hyperbola to match it with the stored result of the first three steps. This fourth step of the algorithm uses the last scans in such as that the size of the generated template fits.

We assume that the antenna moves across a straight line with a constant velocity v. We use the following notations: Let ξ be the position of the antenna, Ξ be the position after n_x scans, θ be the time and Θ be the range (the receiving time for each scan). Then we consider a radargram as a mapping

$$u_0 : \begin{cases} [0,1] \times [0,1] & \to & \mathbb{R} \\ (x,t) & \mapsto & u_0(x,t) \end{cases}$$

where $x = \frac{\xi}{\Xi}$ and $t = \frac{\theta}{\Theta}$. The digitalized radargram is composed of the samples of u_0 at $x_i := (i-1)/(n_x-1)$ and $t_j := (j-1)/(n_t-1)$, with $i = 1\ldots, n_x$ and $j = 1, \ldots, n_t$. We describe the methods in a continuous setting and discretise it for the implementation.

Preprocessing

We follow the preprocessing steps proposed in Daniels (2004). First we reduced the clutter from the raw data u_0 as in Haltmeier et al. (2005). Moreover, we included a linear gain function and after that we applied a median filter and denote the result by u_1. In Figure 3.1 we see the raw data u_0 and in Figure 3.2 the result u_1 after the mentioned preprocessing steps were applied.

This data derived from measurements on a glacier, where the antenna was mounted on a chairlift. The air-snow ($\theta \approx 68$ ns), the snow-ice boundary ($\theta \approx 80$ ns) and the position of the apex of a hyperbola (15.75 m, 70.5 ns) are observable.

Extraction of the snowpack

We describe an active contour model to automatically detect the boundaries of the snowpack. Parametric active contour models are extensively used to locate object boundaries in images

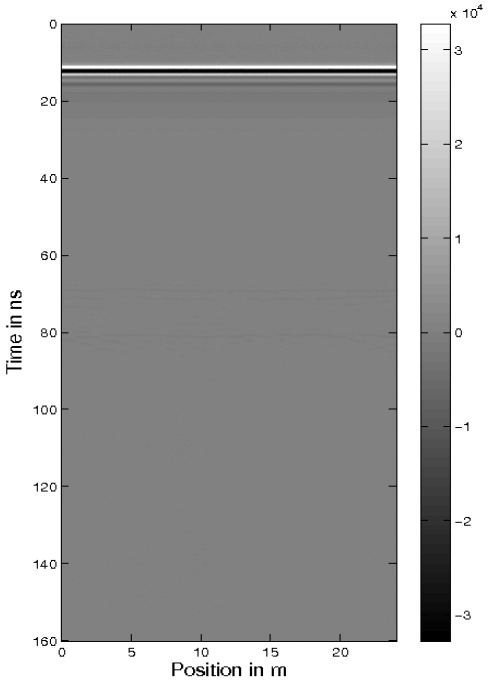

Figure 3.1.: The raw radar data u_0. The spatially constant high signals in the upper area are derived from reflections of the aperture.

(Kass et al. (1987); Blake and Isard (1998)). Many real life application of computer vision including segmentation (Aubert et al., 2003), motion tracking (Leymarie and Levine, 1993) and shape modeling (Terzopoulos and Fleischer, 1988) are based on active contour models.

To apply an active contour method on our data we use an *average amplitude* Φ_λ, which depends on a scaling parameter λ. Therefore we introduce the function

$$\psi_{ab} : \begin{cases} [a,b] & \to & [0,1] \\ \tau & \mapsto & \frac{\ln(\tau)-\ln(a)}{\ln(b)-\ln(a)} \end{cases},$$

$0 < a < b$. In the following we denote by $\psi(|u_1(x,t)|)$ the function $\psi_{ab}(|u_1(x,t)|)$, where $a = \min\{|u_1(x,t)| : 0 \le t \le 1\}$ and $b = \max\{|u_1(x,t)| : 0 \le t \le 1\}$.

We search for a function f, which minimizes the one dimensional Bounded Variation (BV) functional

$$\int_0^1 \left(f(t) - \psi(|u_1(x,t)|)\right)^2 dt + \lambda \int_0^1 \left|f'(t)\right| dt\,, \tag{3.1}$$

where the prime $'$ denotes the derivative with respect to t. A minimizer f_λ of (3.1) has values in $[0,1]$ due to the normalization of ψ. To sharpen the air-snow boundary we introduce a threshold

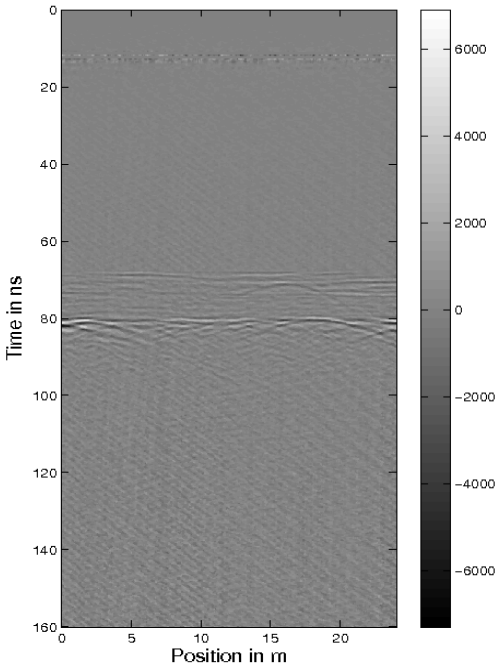

Figure 3.2.: The data u_1 after the preprocessing steps.

c_1 and define the average amplitude

$$\Phi_\lambda(x,t) := \begin{cases} f_\lambda(t) & \text{if } f_\lambda(t) \geq c_1 \\ 0 & \text{otherwise}\,. \end{cases}$$

On the left hand side in Figure 3.3 we can see Φ_λ with $\lambda = 0.75$ and $c_1 = 0.4$ and on the right hand side a plot of $\Phi_\lambda(x,\cdot)$.

There are two reasons why we use here a one dimensional BV functional to create the average amplitude:

1. A minimizer of (3.1) can be calculated by using the fast Tautstring algorithm in the one dimensional case (see Grasmair, 2007 for the equivalence and Davies and Kovac, 2001 for the implementation).
2. The total variation of a function f, i.e., the second term in (3.1) is small, if f consists of intervals with the same function value. Hence, for a sufficient large λ a minimizer of (3.1) is a piecewise constant function. Here, we expect large values of the function at the area of the air-snow and the snow-subsurface boundary, while the other parts should have small function values.

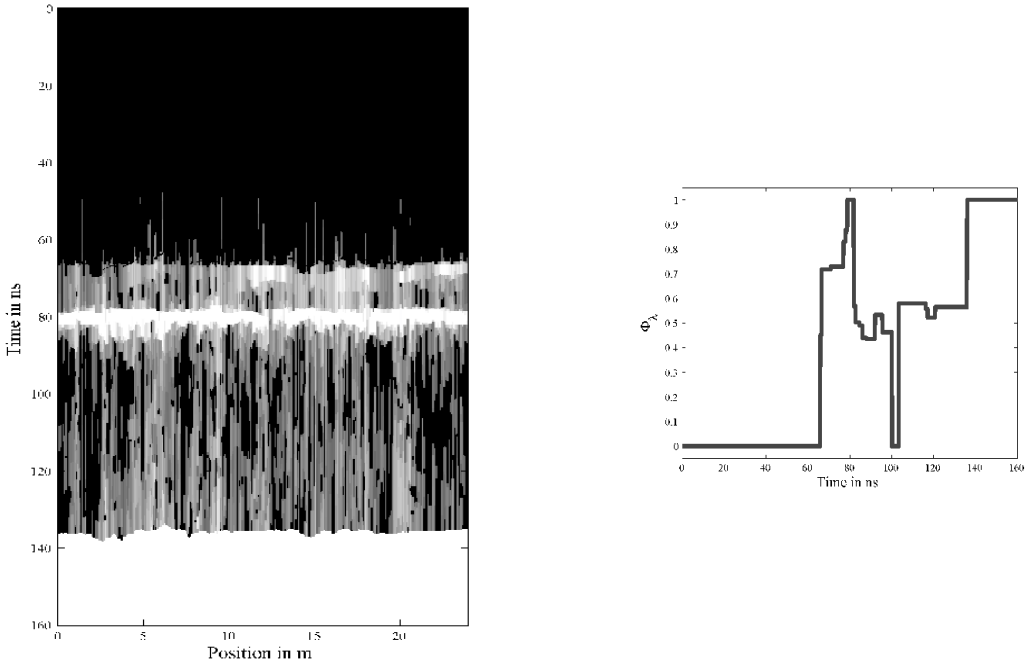

Figure 3.3.: Left: The average amplitude Φ_λ. Right: A plot of $\Phi_\lambda(x, \cdot)$. The air-snow boundary is characterized by the first jump of $\Phi_\lambda(x, \cdot)$.

The air-snow boundary corresponds to the first edge within the image Φ_λ to which we apply the parametric active contour as in Haltmeier et al. (2005). We define the potential

$$p_x : \tau \mapsto -\gamma\tau + \Phi_\lambda(x, \tau) \tag{3.2}$$

for a fixed x and $\gamma > 0$. In Figure 3.4 we see a schematic plot of p_x. The idea of the active contour method is to find the first local minimum of p_x. This is indicated in the picture by the rolling ball.

Since the boundary can be represented as a function $h(x)$, we consider the energy functional

$$\int_0^1 p_x(h(x))dx + \frac{\alpha}{2}\int_0^1 h'(x)^2 dx\,. \tag{3.3}$$

We choose the air-snow boundary as a local minimizer h_1 of (3.3). We calculate h_1 numerically by a steepest descent method. The first term in (3.3) forces $h_1(x)$ to be in the first local minimum, while the second term makes h_1 smooth. The parameter α controls the influence of the two terms. Here we use the squared norm of the derivative of h instead of the total variation, since we want to find a smooth envelope of the snow, i.e. a smooth function without jumps. Note that

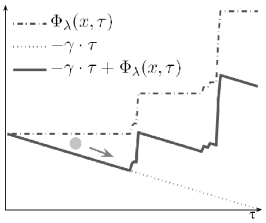

Figure 3.4.: The potential p_x is illustrated. The air-snow boundary corresponds to the first edge of $\Phi_\lambda(x,\cdot)$ or the first local minimum of p_x. The procedure of the active contour is pictured by the ball, which rolls down and stops rolling at a minimum.

$h_1(x) \in (0,1)$ for $x \in (0,1)$, since we assume the snow boundary to be inside the radargram. Then the minimizer h_1 is obviously element of $W_2^1((0,1))$, the Sobolev space of squared integrable functions with a squared integrable weak derivative, and hence continuous and almost everywhere differentiable, (Wlodka, 1982).

To determine the snow-subsurface boundary h_2, we use the knowledge of h_1. We set

$$u_i(x,t) := \begin{cases} \int_{h_1(x)}^{t} |u_1(x,\tau)|d\tau & \text{if } t > h_1(x) \\ 0 & \text{otherwise}\,. \end{cases}$$

Then the function

$$\overline{u}(x,t) := \min\left\{1, \kappa\cdot\frac{u_i(x,t)}{\max(u_i(x,\cdot))}\right\},$$

has an edge at the snow-subsurface boundary, since this boundary is observable by a high reflection in the radargram. In the left picture of Figure 3.5, we see $\overline{u}$ with $\kappa = 1.8$, where at $t \approx 80$ ns the edge is visible. We define

$$\Psi(x,t) := \begin{cases} \overline{u}(x,t) & \text{if } \overline{u}(x,t) \geq c_2 \\ 0 & \text{otherwise} \end{cases}$$

with a second threshold c_2. In the right picture of Figure 3.5 we see a plot of one scan of Ψ (fat line) with $c_2 = 0.35$ and of $\overline{u}$ (thin line). Note, that the parameter $\kappa > 0$ affects the location of h_2, since an edge occurs earlier if κ is greater.

Then we apply the active contour method described above where we substitute Φ_λ by Ψ, i.e., we search for a local minimizer h_2 of

$$\int_0^1 \left(-\gamma h(x) + \Psi(x,h(x)) + \frac{\alpha}{2}h'(x)^2\right)dx$$

to get the snow-subsurface boundary. The snow boundaries h_1 and h_2 are shown in the radargram

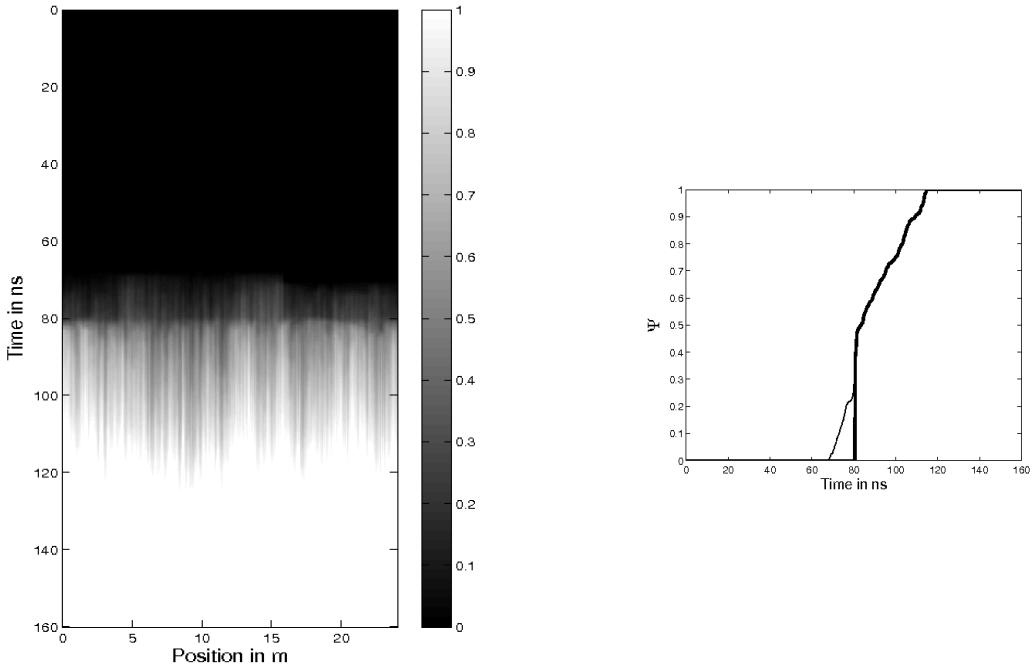

Figure 3.5.: Left: The function $\overline{u}$. At $t \approx 80$ ns an edge is visible. Right: One plot of $\Psi(x, \cdot)$. The edge at $t \approx 80$ ns corresponds to the snow-subsurface boundary. The thin line between 65 and 81 ns shows $\overline{u}(x, \cdot)$.

in Figure 3.6 and the extracted snowpack $u_S = u_1 \cdot \chi_S$ is displayed in the left picture of Figure 3.7, where

$$\chi_S(x) := \begin{cases} 1 & \text{if } x \in S \\ 0 & \text{otherwise} \end{cases}$$

is the characteristic function of

$$S := \{(x, t) : h_1(x) \leq t \leq h_2(x)\} .$$

We used $\alpha = 0.3$ and $\gamma = 0.6$ in the active contour method for both boundaries.

Preparation of the snowpack

By applying the matched filter to amplify the intensity of the hyperbola to u_S, perturbations occur at the boundaries of the snowpack such as that the detection of the hyperbola will get difficult (right picture in Fig. 3.7).

To prevent these perturbations, we introduced a postprocessing step after extraction of the raw

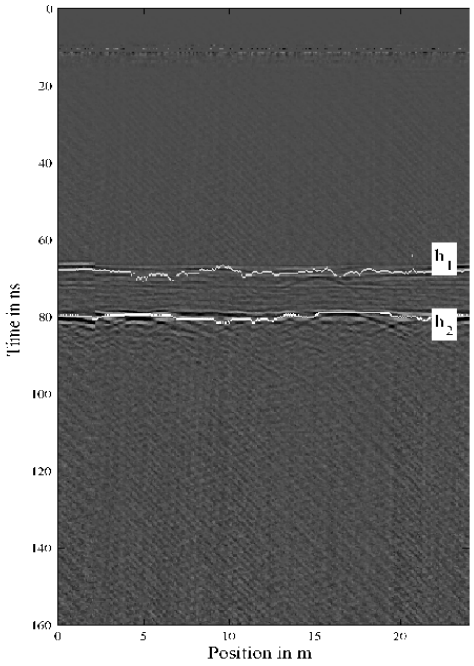

Figure 3.6.: In the radargram we displayed the boundaries h_1 and h_2. Note that the colors of the radargram are changed to make the boundaries more clearly visible.

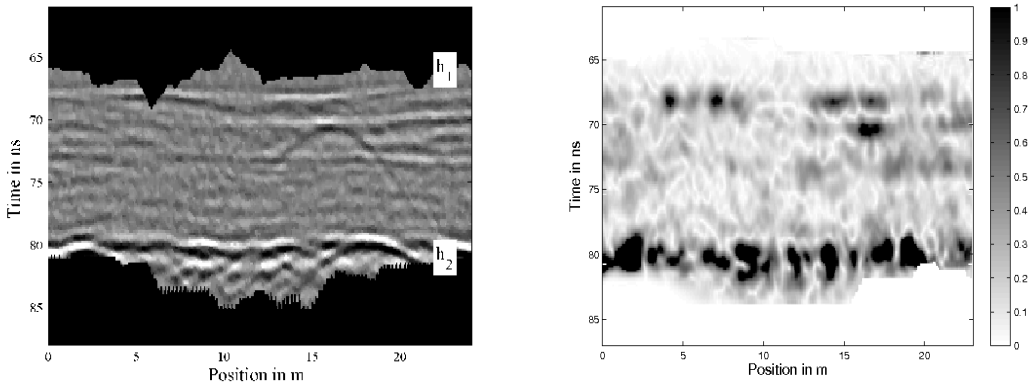

Figure 3.7.: Left: The extracted snowpack is shown. Here the displayed range is between -1000 and 1000 to point out the higher values at the boundaries of the snowpack. Right: The result of the matched filter to u_S without preparation of the snowpack. Perturbations at the boundaries appear.

snowpack. High amplitudes of the signal, which occurred only near the boundaries caused the perturbations. Thus, we absorbed the high amplitudes by a scaling function, see Figure 3.8. The

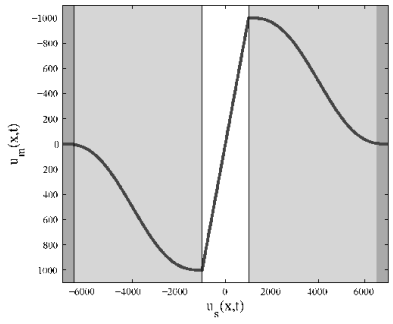

Figure 3.8.: A scaling function for u_S. High amplitudes get low values while low amplitudes keep their values.

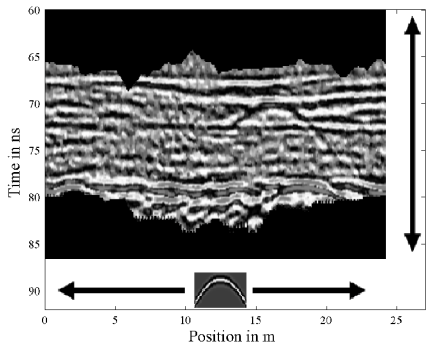

Figure 3.9.: The prepared snowpack can be seen. The diffraction hyperbola is emerged. The method of the matched filter algorithm is indicated by the synthetic hyperbola. We match the snowpack with such a hyperbola-mask.

scaling function is divided in three regions. The first region contains the small values of $|u_S|$, i.e. the white area in Figure 3.8 is given by $|u_S| \leq \eta\,(= 1000)$ where the values of u_S were kept. The second region is marked by the dark gray area in Figure 3.8 ($|u_S| \geq 6500$), where the values of u_S were set to zero. The third region is determined by the remaining values and marked by the light gray area in the figure. The values of u_S were damped in this region by the two polynomials of degree 5, which interpolate $(-6500, 0), (-\eta, -\eta)$ and $(\eta, \eta), (6500, 0)$, respectively. Moreover, the first and the second derivative of these polynomials have the value 0 at the interpolating points. With it, the polynomials are uniquely determined.

We denote the scaled snowpack by u_M (Fig. 3.9). The high values at the boundaries disappeared and the diffraction hyperbola is clearly emerged.

Matched filter enhancing the diffraction hyperbolas

There are a couple of methods to enhance the diffraction hyperbolas and thus to locate the position of a possible avalanche victim (Daniels, 2004; Osumi and Ueno, 1984). Here we use a matched filter algorithm presented in Haltmeier et al. (2005). We compared the snowpack u_M with a template m of a diffraction hyperbola. The principle of the matched filter is shown in Figure 3.9. For the sake of completeness, we briefly repeat the approach.

For a better understanding, we explain how diffraction hyperbolas occur. Assume that the positions of the antenna and a victim are in a plane. Then we can choose a coordinate system such as that the positions of the antenna are given by $(\xi, 0)$ and the victim lies at (ξ_o, h_o). We disregard the refraction of the signal at the air-snow boundary and we assume that the propagation speed v_r of the radar signal is constant with the same value in air and in snow. The runtime of the radar signal from the antenna to the victim and back is given by

$$\theta(\xi) = 2\frac{\sqrt{(\xi - \xi_o)^2 + h_o^2}}{v_r}\,.$$

A hyperbola is obtained by varying ξ with maximum $(\xi_o, 2h_o/v_r)$. We use this formula to construct the template m by convolutions with a Ricker Wavelet (Frühauf, 2007). Note that the template m depends on the settings of the radar equipment, the flight altitude and the velocity of the helicopter.

The definition of the measure of similarity of two images is most important for any concrete implementation of a matched algorithm. Here we used the squared Euclidian distance

$$\int_0^1 \int_0^1 \left(u_M(x,t) - m(x - x_0, t - t_0)\right)^2 dxdt \tag{3.4}$$

between u_M and the template m at position (x_0, t_0). Under certain assumptions the magnitude of the distance measure (3.4) is determined by a convolution term (Lewis, 1995; Haltmeier et al., 2005)

$$(u_M * m)(x_0, t_0) := \int_0^1 \int_0^1 u_M(x,t) m(x - x_0, t - t_0) dxdt\,.$$

Expressing the similarity as a convolution allows a fast calculation with the Fast-Fourier-Transformation (FFT) algorithm.

As last step we took the Hilbert envelope (Michaelis et al., 1997) of the result of the convolution, denote it by u_r and introduce a threshold parameter L. Then we display

$$u_o(x,t) = \begin{cases} \frac{u_r}{L} & \text{if } u_r \le L \\ 0 & \text{otherwise.} \end{cases}$$

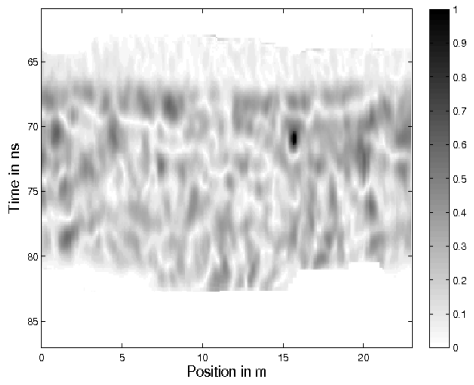

Figure 3.10.: The result of our data processing algorithm. The position of the diffraction hyperbola is marked by the dark area around (15.75 m, 70.5 ns).

In Figure 3.10 we show the result of the location algorithm with $L = 10^5$.

The snowpack is displayed by light gray values, while one dark area is visible at the position of the diffraction hyperbola $(\xi, \theta) \approx (15.75 \text{ m}, 70.5 \text{ ns})$.

3.2.2. Instrumentations for the data acquisition

Radar measurements were performed to validate the algorithm and to determine the effects of environmental parameters and radar settings on the data. A RIS One GPR instrument (IDS Ingegneria dei Sistemi, Pisa, Italy) was assembled for the fieldwork. Measurements were conducted with 400 MHz antennas. We conducted tests with an aerial tramway system (Heilig et al., 2008) 6 m above the snow surface and with a chairlift about 12 m above the snow surface. The radar scans were triggered by an odometer wheel with the resolution of one vertical scan per horizontal centimeter on tests on the tramway, where the radar antenna was moved along a steel cable in one direction. The scans of the chair lift had to be triggered by constant time intervals. The sampling rate was set to at least 512 samples per scan.

Avalanche debris was simulated by scraping up a snow accumulation with one push forward of a snow-grooming machine (4 m wide, around 2 m high) right above the target lying in an about 0.5 m deep pit hole (Fig. 3.11). We operated with volunteers and with phantom bodies consisting of three 10 l bags filled with tap water to simulate human victims. The dimension of the three bags placed in a row, were about 1.0 m in length, 0.4 m in width and 0.1 m in height. Heilig et al. (2008) assumed that the phantom body is comparable to a real human.

Furthermore, we performed additional tests with two antennas on the aerial tramway system. The antennas were mounted parallel to each other on a cross beam with a spacing up to 1.5 m. The orientation of the antennas was orthogonal to the radar line. It is possible to arrange the

Figure 3.11.: The creation of the artificial avalanche mound above the phantom body.

transmitting and receiving antennas in two different ways by using a multichannel control unit:

- monostatic antenna mode: both antennas transmit and receive radar signals separately in consecutive time intervals
- bistatic antenna mode: one antenna transmits, the other receives the radar signal in a distinct time interval. In the following interval the role of the antennas is switched.

A more realistic comparison to a helicopter flown radar is a flight on a chairlift at about 12 m above the snow surface. The antennas were mounted on the footpeg under the chair lift. We performed radar scans with different scan rates per second while the lift speed was constant at about $v_{cl} = 4.2$ m/s. The horizontal resolution in scans per second depends on the used radar equipment. The resolution of the IDS-system is limited by the number of samples and the applied stacking rate.

3.2.3. Processing of the radargrams

For evaluating the described localization algorithm, we developed a method to quantify the clearness of the hyperbola reflections in comparison to the surrounding snowpack. The raw radar profiles were processed with the REFLEXW-Software (K.J. Sandmeier Scientific Software, Karlsruhe, Germany). The processed radargrams were quantified similar to the techniques described in Heilig et al. (2008). We calculated the absolute values of the received radar signals for each sample of each single scan in the radargrams. After that we extracted consecutive scans (between 55 and 100) upon an area of interest (apex of a hyperbola) and performed manually a removal of the scan ranges in air and ice. For the resulting scans of the snowpack, we calculated a relative reflection energy quotient. In detail, we calculated the quotients of the 5 highest sample-values

(h5) over the median of the scan range of the snowpack for each single scan. The mean of these reflection energy quotients of the extracted consecutive scans as well as the values of the relative reflection difference between objects in the snow and pure snow are shown in Table 3.1 and 3.3. The reflection energy quotients calculated by the absolute values are around a factor of 1.5 higher than calculated with the envelope application (Heilig et al., 2008). The algorithm quantifies the reflection magnitude of the object hyperbolas in relation to the surrounding snow and offers the possibility to verify the results of the introduced localization algorithm independently.

3.3. Results

Field tests were performed on the selfmade aerial tramway system 6 m above ground and with the help of a chair lift in a skiing area 12 m above the snow surface. These test arrangements seem to be sufficiently realistic to be compared to real helicopter flights.

3.3.1. Aerial tramway data

The results obtained with the aerial tramway system are described in the following subsections.

Two antenna tests

We measured with two IDS 400 MHz GPR antennas. However, due to the reason that GPR-antennas are usually single-unit productions, sometimes with different electronic devices, the electromagnetic specifications of the antennas were different. Therefore, the gathered raw reflection energies of these antennas were different and not comparable. Measurements of the same snowpack at nearly the same time interval resulted in mean reflection energy differences of more than a factor of 1.5 between the two antennas. The results of the detectable range of both antennas in monostatic mode confirmed the measurements of Heilig et al. (2008) of an object perceptibility of 1.5 m horizontal distance to both sides of the antennas. Consequently, if we use two antennas mounted on a cross beam spaced by 3 m, the search strip can be doubled to a width of 6 m. Using the bistatic mode did not enlarge the detectable range. The resolution of the radargram deteriorated compared to the monostatic mode.

Phantom body variations

We varied the phantom body and the snow-avalanche parameter on a test series in March 2007 using the aerial tramway system in a height of 6 m above the snow surface.

First, we measured the radar line with the water bags without an avalanche mound above (A),

second we created an avalanche mound with a snow-grooming machine above the water bags (B) (Fig. 3.11). Next we dug a hole in the snow mound and placed a person lying perpendicular to the radar line in the snow cave (C). After these test arrangements, water bags were put at the former location of the person, but now with an air gap of approximately 30 cm above the phantom body (E). Finally we measured the radar line with an air hole of 100 cm width, 75 cm length and 45 cm height in radar movement direction (F). The calculated relative reflection energy quotients of these series are displayed in Table 3.1 and the results of the detection algorithm are presented in Figure 3.12.

Table 3.1.: Reflection energy quotients of various GPR-signals with different phantom bodies and pure snow values with (aval) or without (no aval) an avalanche mound above the victim. A: phantom body 4.6-5.6 m no aval; B: phantom body 4.7-5.7 m aval; C: human body 4.9-5.9 m aval; D: only snow 9.0-10.0 m; E: phantom body + air 4.9-5.9 m aval; F: air hole 4.6-5.6 m aval

	A	B	C	D	E	F
median refl. energy quot.	4.914	5.006	5.888	3.649	5.605	3.914
factor times pure snow	1.347	1.372	1.614	1	1.536	1.073

The reflection energy quotients in Table 3.1 show the effect of the hyperbola on the reflection coefficient. The measurements with and without an artificial avalanche mound (Tab. 3.1 A and B) above the phantom body confirm the results of Heilig et al. (2008) that the snow properties are almost negligible compared to the reflection values of water bags. The third column (Tab. 3.1 C) describes the reflection energy amplification of a human body in a snow cave. This quotient is remarkably higher than for water bags (factor 1.17), which is contrary to the expectation that the permittivity of water is assumed to be much higher (factor 1.6) than that of human bodies. However, the volume of the human body is much larger compared to the phantom body ($V_{human} = 0.34$ m^3, $V_{waterbags} = 0.02$ m^3). The person wore common skiing or snowboarding clothes without any additional sports equipment (skis, snowboard, helmet etc).

While an air gap is added to the phantom body (Tab. 3.1 E), we gathered reflection magnitudes comparable to the human body. Analyzing the air cave only resulted in reflection energy values corresponding to that of pure snow, although a permittivity contrast between air and snow exists. However, this contrast is very small in relation to the contrast to water or humans: ($\varepsilon_{air} = 1$, $\varepsilon_{snow} = 1.6$, $\varepsilon_{water} = 81$, $\varepsilon_{human} \approx 50$; (Jaedicke, 2003; Daniels, 2004; Heilig et al., 2008).

The result of the localization algorithm (Fig. 3.12) showed dark areas at positions, where a diffraction hyperbola is detected. The snowpack is displayed by light gray areas. The reflection energy quotient and the contrast of the hyperbola are correlated. Moreover, we apply a global threshold $c_{\text{thresh}} = 0.9$ on the results shown in Figure 3.12. Then we detect the phantom body and the human body in all test cases (A, B, C and E), while for D and F nothing is detected.

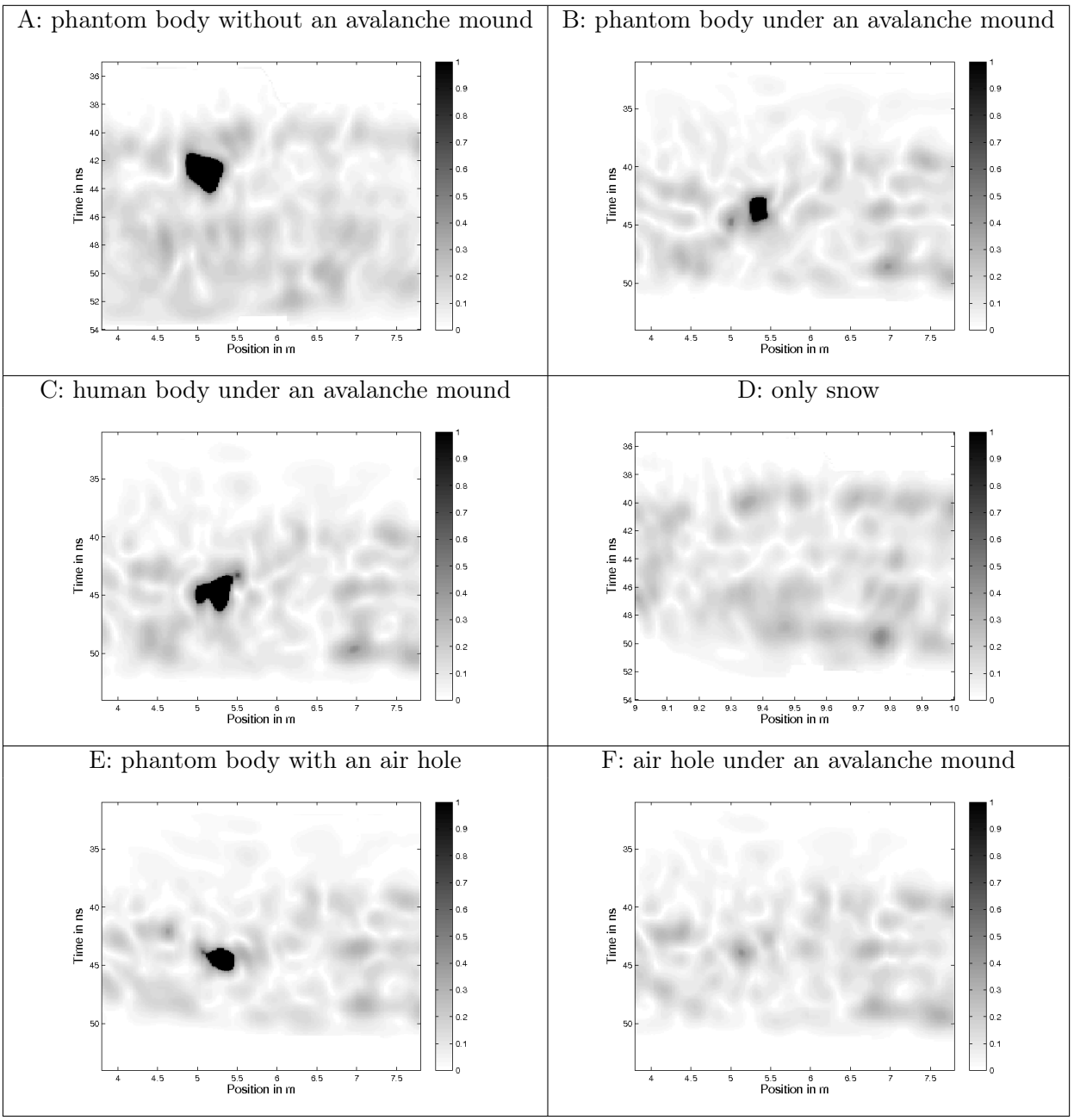

Figure 3.12.: Results of the detection algorithm with different phantom bodies and pure snow values, with or without an avalanche mound above the victim. Detected victims are marked by dark areas and the position of the hyperbolas are defined by the x-axis. The adjustment of the pictures corresponds to Table 3.1 (from left to right).

This yields a hit rate of the localization algorithm of 100% for the railway data without false detections.

3.3.2. Chairlift data

The reflection energy decreases with increasing distance of the radar source to the target (Yamamoto et al., 2004). The empirically defined equation for distances from 0.8 m to 5 m of Yamamoto et al. (2004) is: $A = 1.11/10^4 \cdot d^{-0.97}$, with A as the GPR reflection amplitude and d the distance in meter. We compared this empirically defined equation to the data from 6 and 12 m height above ground. We analyzed the mean raw reflection amplitude snow-only areas for 100 consecutive scans. The snow properties were very similar in the chairlift and aerial tramway test arrangements (Table 3.2).

Table 3.2.: Results of the comparison of the distance dependence of radar reflection amplitudes

Date	Snow surface distance	Sample #	Scan #	Mean	Median
09.02.07	12 m	64	100	73.36	67.00
30.03.07	6 m	62	100	153.79	150.00

The mean of the raw (unprocessed) reflection magnitude of snow in a vertical distance of 6 m to the radar source is 2.08 times higher than the snow-reflection values in a distance of 12 m. The empirical equation (Yamamoto et al., 2004) predicts a factor of 1.96, which is in a good agreement with our value. The decay of the reflection magnitude influences all processed values, like the reflection energy quotients and the brightness of the detected spots. However, the relationship is nonlinear due to the processing procedure.

Furthermore, the relative reflection energy quotients of an arrangement, where the phantom body is situated at a horizontal distance of 3 m correspond to snow-only energy quotients (Tab. 3.3). The detectability borders increases from 1.5 m at 6 m height to approximately 2.5 m at 12 m height. These results are confirmed by the automatic localization algorithm. In Figure 3.13, we see results of the algorithm described in Section 3.2.1 where the phantom body is buried in varying horizontal distances to the chairlift. We apply a threshold $c_{\text{thresh}} = 0.9$ on these images to identify a detected hyperbola. For the up to 2 m horizontal distance, the algorithm detects a hyperbola (dark areas in the images). The 3 m horizontal distance was analyzed by two measurements. The first measurement was performed by an uphill-fly by with the chairlift and the second with a downhill-fly by. In this case, the phantom body was only detected, while flying uphill with reflection energy quotients very close to that of pure snow. Again the localization algorithm yields a hit rate of 100% without false detections on these extracted data. A general detection and error statistic of the algorithm for the chairlift data is difficult because of perturbation caused for instance by the chairlift column. This statistic is an essential task in future work in particular for data taken from helicopter flights.

Table 3.3.: Reflection energy quotients of GPR signals measured from the chair lift. G: phantom body - 75 scans - 12 m vertical distance H: only snow - 75 scans - 12 m vertical distance; I: phantom body - 70 scans - 12 m vertical and 1 m horizontal distance; K: phantom body - 70 scans - 12 m vertical and 2 m horizontal distance; L: phantom body - 55 scans - 12 m vertical 3 m horizontal distance.

	G	H	I	K	L
median refl. energy quot.	4.467	2.963	3.223	3.098	2.928
factor times pure snow	1.508	1	1.088	1.046	0.988

We conclude that the usable detectable range is between 2 and 3 meter for a radar altitude 12 m above ground.

3.4. Discussion

3.4.1. Field data

We used GPR from a chair lift in a distance to the snow surface corresponding to a realistic flight height for a helicopter. Reflection energy decreased about linearly with height. More focused antennas could be an advantage for higher altitudes of flight (Marshall and Koh, 2008). Our tests from the chairlift were conducted at relatively benign conditions: low wind, constant speed, and almost constant distance between ground and antenna. A helicopter-borne system will have to deal with these complications, which make the evaluation of the data more challenging. Using more focused antennas will lead to the application of an array of equal antennas because the detectable range is inversely related to the focus of the antenna. We analyzed a system with two antennas on a cross beam. This configuration increased the detectability borders, when we use both antennas as individual transmitters and receivers. Additonal antennas could be used, but at the expense of increased costs.

The field data confirmed the results of the preliminary work of Heilig et al. (2008). The reflection energy quotients were not affected by snow properties in dry snow. Also, an air gap above the body was not disturbing the avalanche victim detection.

The reflection energy quotients above a relative big air cave in a snow mound are similar to that of pure snow measurements. This can be explained by the very small difference between the permittivity of snow and air. Consequently, the generated reflection will be rather small as confirmed here. Air gaps in avalanche debris and above an avalanche victim created only negligible reflections. A small air gap above the phantom body did not reduce the relative reflection energy quotient of the buried object. A phase shift as described in Modroo (2004), as a result of the double permittivity change, could not be observed. In contrast to Modroo

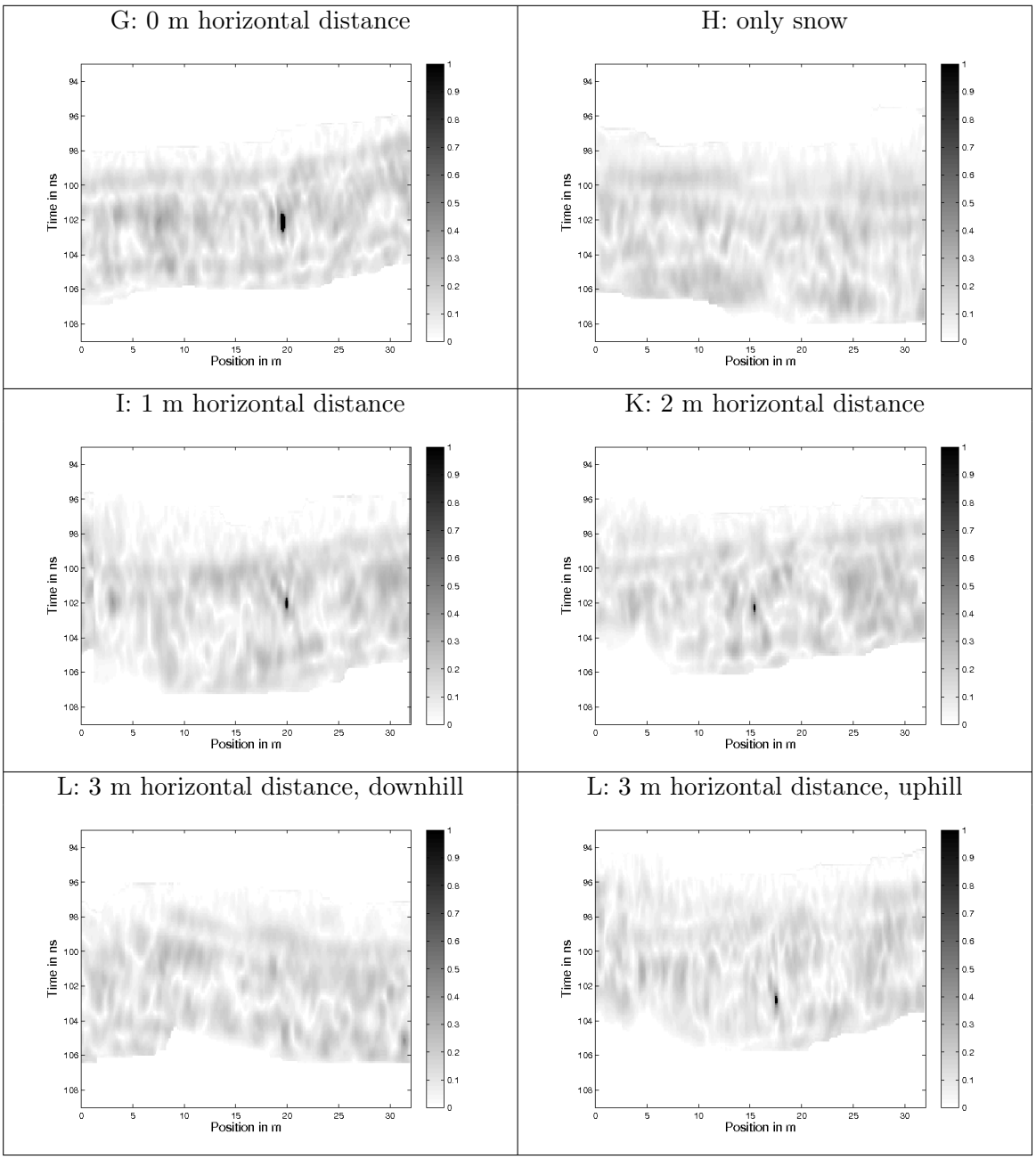

Figure 3.13.: Results of the detection algorithm with increasing horizontal distances of the phantom body and pure snow values. Detected victims are marked by dark areas. The arrangement of the pictures corresponds to Table 3.3 including the display for the downhill fly-by.

(2004) the persons that were employed in our test arrangement with a temperature of 37° C had an insulating layer around and were buried out after a few minutes. No ice layer was formed in the hole which would amplify the permittivity differences. Additionally Table 3.1 proves the

Table 3.4.: Required processing times of the used procedures.

Function	BV-Min.	Preproc.	Migr.	AC
aver. calc. time in ms	0.11	0.15	1.77	0.04

assumption of Heilig et al. (2008) that the water bags are a good surrogate for human bodies in avalanche debris. The resulting reflectivity values of the three bags are in a good agreement with the buried person.

3.4.2. Feasibility of the automatic processing algorithm

We developed an algorithm, which automatically detects hyperbolas in radargrams. In a first step the snowpack is extracted and processed. The extraction of the snowpack has two advantages: (i) perturbing reflections in the subsurface do not affect the match filter and (ii) the computing time is minimized by reducing the area of interest for the match filter. Runtime tests of the algorithm are shown in Table 3.4.

The preprocessing steps are not complex operations and therefore not time consuming. To minimize the BV functional, we can use the Tautstring algorithm and the active contour method is applied just to $n_x = 4$ successive scans and hence both methods can be calculated fast. All other calculation steps can be disregarded with respect to the calculation time, except for the matched filter. In our examples the matched filter is done by a two dimensional convolution, where the size of m is greater than (40×80) and the size of the snowpack is more than 100 pixel.

The percentage of the snowpack in the radargram and the size of the template m affected the real-time calculation. For typical settings of $n_t = 1024$, a range $\Theta = 1.6 \cdot 10^{-7}$ seconds and a stack of 3, a real time processing for a flight velocity of $v = 5$ m/s was possible for a snowpack with a depth thinner than 3 meters.

We interfaced the radar equipment over a 100 Mb Ethernet with a notebook [2], and used our software to analyze the data simultaneously. We tested this configuration on the Hintertux Glacier and in Obergurgl, Austria in a chairlift. The feasibility of the real time processing with direct data transfer was confirmed by both tests, when we chose the settings discussed here. Nevertheless, there are possibilities to improve the efficiency of the algorithm.

The choice of the parameters of the algorithm depended on the height and the velocity of the flight and on the percentage of the snowpack. In particular the extraction of the snowpack required different parameters for the chairlift and the aerial tramway data. In section 3.2.1 we state a choice of the parameters, which are used for the analysis of the chairlift data ($\lambda = 0.75$, $c_1 = 0.4$, $\kappa = 1.8$, $c_2 = 0.35$, $\alpha = 0.3$, $\gamma = 0.6$, $\eta = 1000$ and $L = 10^5$). All tested chairlift data

[2] DELL Latitude D820 with a Intel Centrino Duo, 1.66 GHz, 1 GB RAM. FSB 664 MHz, L2 cache 2

sets were analyzed with the same setting and the results were quite good. For the interpretation of the aerial tramway data the parameters had to be changed, but a fixed setting ($\lambda = 1$, $c_1 = 0.5$, $\kappa = 1.4$, $c_2 = 0.7$, $\eta = 1500$ and $L = 5 \cdot 10^7$, the other parameters were kept) was used for all these data sets and yielded good results. Based on these results, the processing of radar data flown in a helicopter should be possible after adjusting the parameter setting. The sensitivity of the parameters was not large, i.e., a variation of 10% of one parameter did not change the result significantly. A future goal will be to reduce the number of parameters further.

Our experiments showed that the underground material (ice, rock, talus) did not affect the processing steps for the extraction of the snowpack. The detectability of avalanche victims in a snowpack seems to be independent of the underground. The decisive condition for the detection of the victims is the change in electromagnetic material properties between the snow and the target.

As mentioned in Section 3.3 a general study of the quality of the algorithm with c_{thresh} has still to be performed. In particular this statistic is essential for data taken from a helicopter flight over a real avalanche. In the test cases of this paper, we yield a tip rate of 100% without false detections.

3.5. Conclusion

An automated real-time detection of avalanche victims without transceiver or responder devices is feasible by the described hard- and software system. We confirmed the empirical results of Yamamoto et al. (2004) of the decrease of reflection magnitude for larger distance between antennas and target. This will restrict the distance between snow surface and the GPR on the helicopter for rescue operations. The use of two antennas, mounted on a cross beam in twice the distance of the detectability range approximately doubles the space of the flight lines but requires well balanced antennas. Air holes in the snowpack are not detectable. In addition a small air gap above an object does not degrade the detectability of hyperbolas by attenuating the reflection energy values.

Acknowledgement

For assistance in the field we thank S. Link, S. Unterader, M. Huttenlau and P. Koessler. We would also like to thank D. Bardenz, K.J. Sandmeier and H.-M. Schuler for discussions that helped to improve the paper. Furthermore, we thank the anonymous referees for valuable suggestions to improve the paper.

Author contributions

F. Fruehauf and A. Heilig contributed equally to the work.

Bibliography

Aubert, G., Barlaud, M., Faugeras, O., Jehan-Besson, S., 2003. Image segmentation using active contours: Calculus of variations or shape gradients? SIAM J. Appl. Math. 63 (6), 2128–2154.

Blake, A., Isard, M., 1998. Active Contours: The Application of Techniques from Graphics, Vision, Control, Theory and Statistics to Visual Tracking of Shapes in Motion. Springer-Verlag, Secaucus, USA.

Brugger, H., Durrer, B., Adler-Kastner, L., Falk, M., Tschirky, F., 2001. Field management of avalanche victims. Resuscitation 51, 7–15.

Daniels, D., 2004. Ground Penetrating Radar, 2nd Edition. The Institution of Electrical Engineers, London, UK.

Davies, P. L., Kovac, A., 2001. Local extremes, runs, strings and multiresolution. Ann. Statist. 29 (1), 1–65.

Frühauf, F., 2007. Erstellung einer Software zur Auswertung von Radardaten für die automatisierte Ortung von Lawinenverschuetteten. Endbericht des alpS Projektes B 2.6, AlpS, Centre of Natural Hazard Management.

Grasmair, M., 2007. The equivalence of the taut string algorithm and BV-regularization. J. Math. Imaging Vision 27 (1), 59–66.

Haltmeier, M., Kowar, R., Scherzer, O., 2005. Computer aided location of avalanche victims with ground penetrating radar mounted on a helicopter. Digital Imaging and Pattern Recognition, 30th. Workshop of the Austrian Association for Pattern Recognition, OAGM/AAPR, Obergurgl, 19–28.

Heilig, A., Schneebeli, M., Fellin, W., 2008. Feasibility study of a system for airborne detection of avalanche victims with ground penetrating radar and a possible automatic location algorithm. Cold Regions Science and Technology 51 (2-3), 178–190.

Instanes, A., Lonne, I., Sandaker, K., 2004. Location of avalanche victims with ground-penetrating radar. Cold Regions Science and Technology 38, 55–61.

Jaedicke, C., 2003. Snow mass quantification and avalanche victim search by ground penetrating radar. Surveys in Geophysics 24, 431–445.

Kass, M., Witkin, A., Terzopoulos, D., 1987. Snakes: Active contour models. Int. J. of Computer Vision 1 (4), 321–331.

Lewis, J., 1995. Fast template matching. In Vision interface, 120–123.

Leymarie, F., Levine, M., 1993. Tracking deformable objects in the plane using an active contour model. IEEE Trans. Pattern Anal. Mach. Intell. 15 (6), 617–634.

Marshall, H., Koh, G., 2008. FMCW radars for snow research. Cold Regions Science and Technology 52, 118–131.

Michaelis, D., Gramss, T., Strube, H., 1997. Glottal-to-noise excitation ratio - a new measure for describing pathological voices. ACUSTICA acta acustica 83, 700–706.

Modroo, J. J., 2004. Ground penetrating radar location of buried avalanche victims. Master's thesis, Colorado School of Mines, [Online]. Available: http://www.modroo.com/files/JjM2004MSc.PDF.
URL `[Online].Available:http://www.modroo.com/files/JjM2004MSc.PDF`

Niessen, J., Kliem, E., Poehlking, E., Nick, K., 1994. The use of ground penetrating radar to search for persons buried by avalanches. 5 th International Conference on Ground Penetrating Radar, Kitchener, Canada, 507–517.

Olhoeft, G., Modroo, J., 2006. Locating and identifying avalanche victims with GPR. The Leading Edge 25 (3), 306–308.

Osumi, N., Ueno, K., 1984. Microwave holographic imaging method with improved resolution. IEEE Transaction on Antennas and Propagation 32 (10), 1018–1026.

Terzopoulos, D., Fleischer, K., 1988. Deformable models. The visual Computer 4, 306–331.

Wlodka, J., 1982. Partielle Differenzialgleichungen. Teubner, Stuttgart.

Yamamoto, T., Matsuoka, K., Naruse, R., 2004. Observation of internal structures of snow covers with a ground–penetrating radar. Annals of Glaciology 38, 21–24.

4. Upward-looking Ground-Penetrating Radar for Monitoring Snowpack Stratigraphy [1]

Achim Heilig, Martin Schneebeli, Olaf Eisen

[1] accepted as: Heilig, A., Schneebeli, M., Eisen, O., in press. Upward-looking ground-penetrating radar for monitoring snowpack stratigraphy. Cold Regions Science and Technology.doi:10.1016/j.coldregions.2009.07.008

Abstract

Operational remote monitoring of snowpack stratigraphy, melt water intrusions and their evolution with time for forecasting snowpack stability is not possible to date. Determination of the spatial variability of snowpack conditions on various scales requires a number of point measurements with various methods. These methods are either destructive or do not provide information about the internal structure of the snowpack. The application of a remotely controlled non-destructive sensor system would help to gain a higher spatio-temporal resolution about information of the snowpack. In this study we present results from upward-looking ground-penetrating radar (GPR) surveys from horizontal caves dug in the front wall of snow pits at the bottom of the snowpack. GPR data are compared with vertical profiles of snow hardness and density, obtained in the snow pit. Data were acquired in different areas with varying snow conditions with various GPR systems, frequencies and polarizations. Radar experiments with high frequencies (> 1 GHz) detect internal layers in the snowpack in dry snow, but fail to provide clear reflections at the upper snow-air transition because of attenuation. In wet snow, the radar signals < 1 GHz are capable to penetrate a meter-thick snowpack and detect the snow surface, although the signal is strongly attenuated. Analysis of reflection phases and magnitudes allows interpretation of their physical origin in terms of changes in dielectric permittivity. Varying antenna polarization causes a strongly different signal response, likely induced by the snow-pit wall present in our set-up. Forward calculation of density-based reflection coefficients between neighboring layers of varying hardness, yields ambiguous results in terms of correspondence with observed radar reflections apart except for interferences of neighboring reflections. Moreover, we identify several pitfalls for future applications. The system set-up used here represents a basis for further developments towards a system, which is capable of improving information on the spatial and temporal snowpack characteristics.

4.1. Introduction

Avalanche warning centers forecast the snowpack stability and monitor the current snow distribution and precipitation amounts for areas that range from mountain regions to provinces and to entire countries in Alpine mountains. The spatial and temporal variability of seasonal snowpacks is large, even when focusing on homogeneous slopes (Schweizer et al., 2008). Regarding a whole mountain region, a few observations are definitely insufficient to determine the spatial and temporal variability of e.g. internal weak layers or snow drift accumulations at ridges and in avalanche paths. Evaluation of snow height, snow distribution and observations of the temporal evolution of the snowpack are some of the major tasks facing avalanche forecasting. Temporal snowpack monitoring of the same bulk of snow is impossible, if the method is destructive (e.g. conventional

snow profiles). Ultrasonic snow-height sensors should be used only in flat areas (Gubler, 1981). No reliable results can be gathered in snow-deposition areas along ridges or in avalanche paths, where snow displacements are large and inhomogeneous and dangerous to observe on-site. The use of explosives for determining and reducing the current avalanche danger in such areas is an insufficient trial and error method. For the validation and improvement of snowpack simulation models, it is of high importance to measure snowpack conditions with a high spatial resolution in real-time on various scales (Lehning and Fierz, 2008). Additionally, ground-truth measurements for evaluation of remote satellite-based snow monitoring is a task, which will be in high demand in the future (Wingham et al., 2005). Snowpack monitoring on steep slopes, avalanche paths or along ridges requires a system working regardless of the current avalanche danger. Furthermore, it must not be destroyable by avalanches and should provide data in all weather conditions. A feasible solution would be a system monitoring the snowpack from below. Upward-looking GPR is a suitable method to fulfill these requirements. Data gathered with this GPR application, i.e. snow height, specific layer features and their locations (including wet layers), their evolution with time and changes in density in the snowpack above the GPR, provide a supplemental data set of standard observations, which can support avalanche warning centers in decision making.

The non-destructive recording of snowpack properties has been of major interest to snow scientists for more than 30 years. The use of impulse radars with high frequencies (2–7 GHz) to measure snow stratigraphy in an mountain snowpack was firstly described by Vickers and Rose (1973). Ellerbruch et al. (1977) and Boyne and Ellerbruch (1979) measured snow properties with a frequency modulated continuous wave (FMCW) radar. Gubler and Hiller (1984) conducted similar measurements with a FMCW system from above and beneath the snowpack. Marshall and Koh (2008) review the research done on the use of FMCW for snow analysis. Continuous wave radar systems provided convincing results for measuring the snow stratigraphy from above the surface. On the other hand, the used FMCW at X- and Ku-band frequencies failed to penetrate a moist snowpack (e.g. Gubler and Hiller, 1984; Gubler and Weilenmann, 1986). This was only possible with C-band frequencies (Marshall et al., 2004). A few FMCW-radar systems are used for near-continuous observations of avalanche flow dynamics and avalanche entrainment measurements (e.g. Sovilla and Bartelt, 2002). Moreover, there is no commercial manufacturer of FMCW-systems in the frequency range suitable for applications from beneath the snowpack. Previous studies used custom-made single units, which makes it very difficult to establish the method as a standard monitoring tool. Single units differ usually in various system parameters, as no standard manufacturing norm exists. This fact complicates the development of normalized processing steps to reduce clutter and noise. Furthermore, the price and the feasibility of reproduction in higher unit numbers favors the concentration on pulsed radar systems. Other methods, such as time domain reflectrometry (TDR), turned out to be not suitable for an application in slope areas (Schneebeli et al., 1998; Waldner et al., 2001). The installation of TDR

requires poles reaching the transition from snow to air above the surface, which makes the system prone to avalanche destruction.

Recently, various research has been conducted on the use of impulse radar for estimating snowpack properties. These radar systems are commercially available and already have a wide field of applications. In Scandinavia and in alpine regions, impulse radar systems such as ground-penetrating radar are used to measure snow-water equivalent (SWE) (Lundberg et al., 1999; Lundberg and Thunehed, 2000; Marchand et al., 2001), snow depth and snow accumulation variability (Harper and Bradford, 2003; Machguth et al., 2006) as well as to detect avalanche victims (Modroo, 2004; Heilig et al., 2008). In Arctic and Antarctic regions, GPR was successfully applied in snow and glacier studies, e.g. for determining internal layering in the firn column for accumulation studies (e.g. Richardson et al., 1997; Eisen et al., 2008).

For the development of an automatic snowpack monitoring system focusing on snow height and internal layering based on GPR technology, it is essential to evaluate various system components to investigate their capabilities and pitfalls. This study analyzes the potential of GPR in snow stratigraphy mapping for both dry and wet snow conditions. Our approach considers three main objectives: (i) find a measurement arrangement for impulse radar antennas from beneath the snowpack, which is able to provide reliable measurements of the snowpack for short-time data requests several times a day; (ii) analyze the reflection response of different snow stratigraphic boundaries and the penetration depth for various snow conditions; (iii) compare various antennas, set-ups and GPR systems in terms of their reliability as an automated snowpack monitoring system. We first describe the utilized systems and the theoretical background, measurement set-ups and studies conducted. Subsequently, the measurements are analyzed separately for dry and wet snow conditions, polarization and frequency dependencies. The results suggest that further research on this topic is necessary and the improvement of hardware components for a remote controlled operation is desirable.

4.2. Methods

4.2.1. Data acquisition

GPR-system

We used a RIS One GPR instrument (IDS, Pisa, Italy) with shielded 900 MHz and 2 GHz bipolar antennas and a RAMAC system (MALA Geoscience, Malå, Sweden) with shielded 800 MHz antennas. In all measurements the signals were time-triggered. For further processing and interpretation steps, it is important to distinguish between snow stratigraphic reflections and noise or internal antenna signals caused by the antenna design or other external influences. The

antenna noise in pulsed radar systems from beneath the snowpack partly masks the reflections caused by the snow stratigraphy, which makes it difficult to detect the snow signals. In order to remove this effect, we generated an alternation of the response signal for different recordings (i.e. for the duration of the whole acquisition consisting of several tens of traces, which is not identical to the recording time of an individual trace). We moved the antenna vertically for the alternation of the signal. For this feasibility study, the option to operate the radar at various locations with different antenna systems argued against a long-time installation of the system.

Additionally, we used a bipolar antenna concept (No. 4, Tab. 4.1) operating at 2 GHz. The bipolar antennas measured one pulse after another with each antenna measured separately. Thus, with one test arrangement, we created two different measurements almost simultaneously, while each antenna operated individually. The antennas were orientated orthogonal to each other. To investigate polarization effects with the conventional 900 MHz and 800 MHz antennas in a similar manner as for the bipolar antennas, we also rotated each shielded transmitter/receiver pair horizontally by 90°.

Snow-data

A conventional snow profile (e.g. Colbeck et al., 1990) with high resolution density measurements was made to interpret the radar measurements and to compare the resulting reflections with snowpack properties. We took at least two snow samples with a 100 cm^3 density shovel of each recognized layer to determine the average layer density. The hand-hardness values were determined according to the guidelines of Colbeck et al. (1990), where different objects are gently pushed into the snow with a penetration force of about 50 N. The different objects are the fist (F), describing the loosest part of the snowpack, followed by four fingers (4Fi), one finger (1Fi), pencil (P) and finally a knife blade (K) to penetrate the hardest layers. The determination of the liquid water content in our study is qualitative, since we were not able to use instruments for moisture measurements. We used the approximation by Colbeck et al. (1990), who defined four terms of liquid water content in the snowpack and distinguished between the classes by an approximate range of water volume fraction. Dry snow is defined to zero liquid water in the snowpack, wetness class I corresponds to moist conditions, where the liquid water is not yet visible at 10 times magnification (approximate range of liquid water content in the snowpack $\nu_w < 3\%$). Class II - wet - and III - very wet - contain visible liquid water and are distinguished by the possibility to press out water by moderately squeezing the snow in the hands (class II: $3 < \nu_w < 8\%$; class III: $8 < \nu_w < 15\%$). Class III contains an appreciable amount of air between the pores in contrary to the next higher class IV, which is defined as "slush" ($\nu_w > 15\%$). We determined the liquid water content of the whole snowpack using the collected wetness classes of the field data and applying the upper and lower borders from Colbeck et al. (1990).

Data-processing

The raw data sets were all processed in a similar way. We applied a dewow filter of 5 ns length to calculate a running mean value, which is subtracted from the central point for each trace independently. This removes the low frequency components from the traces. A linear gain increasing with travel time helped to enhance upper parts of the radargram (i.e. snow surface) and a bandpass-butterworth filter was employed to reduce clutter and noise with the cut-offs set at about ±50% of the nominal frequency. A background removal was only applied if remarkable improvement of the visibility of non horizontal reflections was achieved. Subsequently, a static correction was used to change the height-frame of reference from the antennas direct wave to the snow surface reflection. From this it followed that all reflections parallel to the snow surface were horizontally planar after the correction, whereas the direct wave and other instrumentally caused signals appear in an inverse (triangular) oscillation to the vertical movement (Fig. 4.6). The resulting radargram was stacked over a fraction of all scans (about a tenth or a third of the whole data set). Next, the resulting scans (typically 10 or 3) were averaged over the number of samples of one reflection half cycle. With this processing, reflections not parallel to the surface were remarkably attenuated and the parallel reflections not significantly influenced. A spiking deconvolution function (Sandmeier, 1998) was utilized to improve the visibility of the existing reflections, if the record parameters were not optimally set. With this processing, we were able to isolate recognizable snow reflections, which were generated by stratigraphy, and to remove multiple reflections and antenna ringing caused by the set-up and antenna design. To be consistent in all radargrams, we define the signal's first arrival as the start of the first half cycle of a reflection.

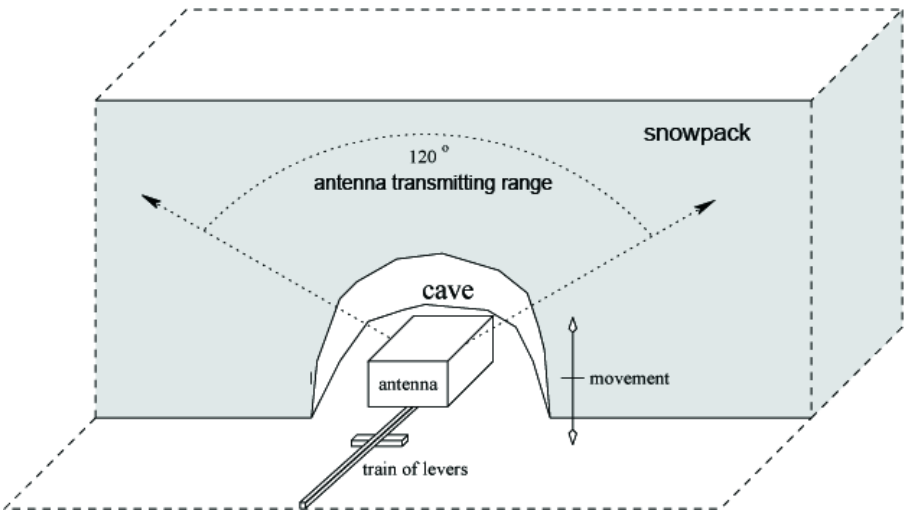

Figure 4.1.: Sketch of the test arrangement for measurements with vertically moved antennas with the use of a lever. The antennas and the lever are operated from a snow pit.

4.2.2. Test arrangement

As the transmitted wave of impulse radar systems is not modulated, snow stratigraphy reflections are displayed horizontally planar in the radargram, as are the direct wave and other instrumentally caused signals. Therefore, measuring with such systems from below the snowpack requires either horizontal or vertical movement of the antennas to apply the mentioned data processing to separate stratigraphy-caused reflections. Otherwise the impulse radar must be operated over a time period with considerable modifications of the observed snowpack. A realizable effort in the test arrangement with a horizontal movement from beneath the snowpack (maximal 0.5 m - 1.0 m horizontal movement) did not produce data, which could be evaluated sufficiently. Therefore, we arranged an experimental set-up with vertically moved antennas (Fig. 4.1). We tried different test arrangements and varied the distance of movement as well as the speed and manner. The variation of the distance of the vertical movement ranged between 0.1 m and 0.3 m and the speed ranged from less than five seconds (lever system) to more than 30 seconds for one 30 cm uplift, using a pneumatic system.

After recording the conventional snow profile, the GPR antennas were buried in an excavated cave at the bottom of the snowpack, in which they were moved by a lever system (Fig. 4.1). The cave was about 60 cm wide and 60 cm long. The distance of the antennas to the profile wall was usually about 10 to 20 cm. We measured the snowpack conditions with two different antenna arrangements, with the polarization of the antennas parallel ($\parallel$-polar) or orthogonal ($\top$-polar) to the profile wall. After the antennas were installed beneath the snowpack, the duration of each measurement was only about 1 to 2 minutes.

4.2.3. Field data

Measurements were conducted in two regions of the Austrian Alps, the Stubai Valley and the Oetz Valley, Tyrol as well as on the Colle Gnifetti, Monte Rosa, Valais, Switzerland. At all sites we measured far above the treeline, at an elevation of about 2700 m a.s.l in Austria and above 4400 m a.s.l. in Switzerland. One data set was created in mid-winter conditions in January with temperatures below the melting point (No.1, Tab. 4.1), another one in spring conditions (end of April) at a mean day-time temperature significantly above the melting point (+ 7°C) (No.2, Tab. 4.1). The same snowpack was investigated the next morning again after a cold night with a temperature minimum of -7°C (No. 3, 4). The wet snowpack from the day before was refrozen after the night. The third test was conducted in August, at almost mid-winter conditions above 4400 m (No.5). The given vertical resolution is only a theoretical value. The exact limit of detectability of horizontal layers depends on the contrasts in dielectric permittivity between adjacent layers as well as on the length of the wavelength in the medium. For thin layers, scattering at layer or object boundaries begins to be noticeable at about 1/10 of the wavelength

in the material (Olhoeft, 1998).

Table 4.1.: Date, time, location, altitude, used antennas, snow conditions and resulting theoretical vertical resolution limits according to Daniels (2004) for the different radar surveys.

No.	date time	location	altitude [m a.s.l.]	antennas [MHz]	vertical resolution with $\delta z_{min} = \frac{v}{2f}$ [m]	snow conditions
1	21.01.08 10:00	Stubai Glacier Austria	2840	900	0.132	dry
2	29.04.08 17:30	Vernagtferner Austria	2740	900	0.108 - 0.116	wet
3	30.04.08 7:30	Vernagtferner Austria	2740	900	< 0.132	refrozen
4	30.04.08 7:30	Vernagtferner Austria	2740	2000 bipolar	< 0.059	refrozen
5	28.08.08 11:00	Colle Gnifetti Switzerland	4450	800 both polarizations	0.14	dense dry

4.2.4. Theory

Dry snow conditions

Kovacs et al. (1995)and Mätzler (1996) state that in dry snow the ordinary relative dielectric permittivity ε_r is solely a function of density. Kovacs slightly improved the fit of the equation by Robin et al. (1969) to

$$\varepsilon_r = (1 + 0.845\rho)^2 \tag{4.1}$$

with ρ the density of snow or ice (in g/cm^3). Mätzler (1996), however, applied several mixing formulas on known ice-volume fractions in various snowpacks and compared the results to the effective medium formula of Polder and van Santen (1946). He concluded that the influence of a liquid layer is not detectable in dry snow conditions. In his results the Looyenga formula

(Looyenga, 1965, eq. 4.2)

$$\varepsilon^b = (1-\nu)\cdot\varepsilon_a^b + \nu\cdot\varepsilon_I^b, \tag{4.2}$$

where ν describes the ice volume fraction, the quotient of snow density over ice density, with the empirical fitting parameters for air (a) and ice (I) $\varepsilon_a = 0.9974$ and $\varepsilon_I = 3.215$ respectively and b $= \frac{1}{3}$ provided good results and the parameter are in between 1.1 % compared to the given values (e.g. Daniels, 2004). Both equations (4.1) and (4.2) differ less than 2 % in the resulting dielectric permittivity when applying density records measured at the test sites in the Austrian Alps of the last three winters (Tab. 4.2).

Table 4.2.: Comparison of the two different dielectric permittivity determinations of density based on eq. (4.1) and eq. (4.2). The ratio of the equations and the sample size N of the respective data sets are displayed.

year	N	mean $\varepsilon_{Kov}/\varepsilon_{Maet}$ [%]
06	50	1.8
07	57	1.9
08	14	1.9

As the wave speed of radar in snow and therefore the stratigraphic relation of the radargram depends on the relative dielectric permittivity ε_r, we analyzed various data sets for changes in the calculated dielectric permittivity. These values were derived from manual density measurements. To calculate the electromagnetic wave speed in snow, we use the approximation for low-loss media (Daniels, 2004)

$$\upsilon = \frac{c}{\sqrt{\varepsilon_r}} \tag{4.3}$$

where υ is the velocity in snow and c the speed of light in vacuum.

The determined mean wave speed in dry snow is displayed in Table 4.3. The average value of the velocity is $\bar{\upsilon} = 0.237$ m/ns, the standard deviation of these 121 measurements is $\sigma_\upsilon = 0.015$ and the resulting coefficient of variation (defined as $CV = \frac{\sigma}{\bar{\upsilon}}$) amounts to $CV = 6\%$.

Reflection coefficient

The magnitude of a reflection depends on the permittivity change. If in dry snow the density is the sole parameter influencing the permittivity (see Kovacs et al., 1995; Mätzler, 1996), we can use the magnitude to estimate the dielectric permittivity values at a two-media transition. The reflection coefficient r_i for a single interface between two semi-infinite half spaces is determined by

Table 4.3.: Converted annual mean dielectric permittivity values ($\bar{\varepsilon}$) for density measurements conducted between 2006 and 2008 for dry snow conditions. The permittivity has been calculated with eq. (4.1) and the mean velocity of propagation values ($\bar{v}$) were calculated with eq. (4.3). N is the sample size and σ is the standard deviation of the respective data set.

year	$\bar{\varepsilon}$	σ_ε	CV	$\bar{v}$ [m/ns]	σ_v[m/ns]	CV	N
06	1.6552	0.2298	14 %	0.235	0.017	7 %	50
07	1.5889	0.1674	10.5 %	0.239	0.013	5.5 %	57
08	1.5839	0.5839	8.5 %	0.239	0.011	5 %	14
mean	1.6162	0.1946	12 %	0.237	0.015	6 %	121

$$r_i = \frac{\sqrt{\varepsilon_i} - \sqrt{\varepsilon_{i+1}}}{\sqrt{\varepsilon_i} + \sqrt{\varepsilon_{i+1}}} \tag{4.4}$$

with i counting the layers vertically upward in our case. To cover more realistic scenarios in a natural snowpack, Marshall et al. (2007) applied an iterative equation, which takes the layer thickness and the used frequency at each layer transition into account to determine the effective reflectivity R_i.

$$R_i = |\Gamma_i|^2 \tag{4.5}$$

where Γ_i is the reflection response of the i-th snow layer in the direction of wave propagation (from the ground upwards in our application),

$$\Gamma_i = \frac{r_i + \Gamma_{i+1} e^{-2jk_i\Delta z_i}}{1 + r_i\Gamma_{i+1} e^{-2jk_i\Delta z_i}} \tag{4.6}$$

with k_i the wave number, Δz_i the layer thickness and $\Gamma_{i=1}$ the reflection response of the lowest boundary, in our case the transition from air to snow in the cave. Contrary to Marshall et al. (2007), who measured from above the snow surface, $\Gamma_{i=m}$ is the uppermost transition at the snow surface as we measured from beneath the snowpack. The iteration is initialized at the snow surface, with $\Gamma_m = r_m$. The layer thickness Δz_i was determined from the snow profile.

Wet snow conditions

In wet snow conditions the equations for relating density to permittivity as in dry snow are no longer applicable (e.g. Lundberg and Thunehed, 2000). Dielectric permittivity and electrical conductivity are influenced by the moisture content in the snowpack. Thus, the moisture fraction has to be taken into account, leading to more complicated mixing formulas. Empirical relationships between the effective permittivity of wet snow ε_{eff} and the water-volume fraction ν_w were performed by various research groups (e.g. Sihvola and Tiuri, 1986; Roth et al., 1990; Denoth,

1989, 1994). Based on these previous studies, Lundberg and Thunehed (2000) determined a parameter for the calculation of an average permittivity and thus the SWE in wet snow. They used the empirical relation

$$\varepsilon_{eff} = 1 + c_3\rho_s + c_4\rho_s^2 + c_5\nu_w + c_6\nu_w^2 \tag{4.7}$$

for the wet-snow permittivity based on the snow density and the volume fraction of water, previously defined by Sihvola and Tiuri (1986), Sihvola and Kong (1988) and Denoth (1989, 1994). This equation was derived from the theoretical three phase mixing model of the co-existing media - ice, air and water,

$$\varepsilon_{eff}^{\frac{1}{3}} = \nu_I\varepsilon_I^{\frac{1}{3}} + \nu_a\varepsilon_a^{\frac{1}{3}} + \nu_w\varepsilon_w^{\frac{1}{3}}, \tag{4.8}$$

applied to the model of Looyenga (1965) and discussed in detail by Wilhelms (2005) for firn with two media. The indices refer to ice (I), air (a) and water (w).

The variables c_j in (4.7) are constants derived by Roth et al. (1990), where $\nu_w + \nu_s + \nu_a = 1$ and $\rho_s = \nu_w\rho_w + \nu_a\rho_a + \nu_I\rho_I$ is the measured density of snow. Roth et al. (1990) found a good agreement between calculated and measured ε using the phase mixing model with the derived constants of $c_3 = 1.7 \cdot 10^{-3}$, $c_4 = 7.244 \cdot 10^{-7}$, $c_5 = 15.06$, $c_6 = 56.7$, the permittivity of water $\varepsilon_w = 88$ and the permittivity of ice $\varepsilon_I = 3.18$ (Daniels, 2004) (note that e.g. Roth et al., 1990 state that ε_w is temperature and frequency dependent and therefore different to the known $\varepsilon_w = 81$ for 20°C e.g. Daniels, 2004). Sihvola and Kong (1988) developed an empirical model to compare measured data with theoretically calculated relative dielectric permittivity values for wet snow,

$$\varepsilon_{eff} = 1 + 1.7\rho_d + 0.7\rho_d^2 + (0.1\nu_w\rho_w + 0.8(\nu_w\rho_w)^2)\varepsilon_w \tag{4.9}$$

with the density of dry snow $\rho_d = \rho_s - \nu_w\rho_w$. In addition to the application of these mixing formulas, we applied equation (4.3) for a further determination of ε_{eff} by utilizing the probed snow height above the antennas for the conversion of the two-way travel time in the radargram to wave speed.

In these approaches different forms for the water inclusions (spherical, ellipsoidal, etc.) are not considered. This seems not to be important in snow, because the shape of water inclusions is always similar unless heavy melting takes place and drainage pathways might develop. This influence is, however, beyond the scope of this paper.

4.3. Results

4.3.1. Dry snow conditions

Utilizing a lever system, the height of the uplift of the antennas has an influence on the radargram. The antennas describe a circular movement on the lever (Fig. 4.1). The longer the uplift the more of a circular movement is described by the antennas. We applied various movement heights with the lever system. The divergence angle between the vertical of the profile and the antenna direction increases the longer the uplift. With an uplift of $d_1 = 0.1$ m the antenna will be turned away from the vertical by $\alpha_1 = 5.7°$, with an uplift of $d_2 = 0.3$ m, α will increase to $\alpha_2 = 17.5°$. A 5° turn of the antenna is negligible in our opinion. To keep the results reliable, we only considered data sets with a maximum uplift of about 0.1 m. An error occurs by the conversion of two-way travel time values to depth values. We used the calculated mean wave speed in dry snow (Tab. 4.3), but measured the two-way travel time (TWT) across two media, air and snow. As the air layer above the antennas was removed in the radargrams (Fig. 4.2 – 4.6), this error has no influence on the data. Nevertheless, estimating layer positions with the determined mean average wave speed in snow results in a slight impreciseness in the displayed snow-height and layer-position accuracy converting TWT to height values (Tab. 4.3). We compared the calculated wave speed of each layer of the two referred measurements using equation (4.1) to the mean average velocity of propagation in dry snow of Table 4.3. The mean values were calculated according to the respective layer thickness, neglecting the snow layers where the snow cave was excavated. Even the radar measurements in August 2008 on a high alpine site are within the variation range of the determined average wave speed for dry snow conditions (Tab. 4.3).

Table 4.4.: Calculated mean values of the density determinations of the referred measurements No.1 and No.5 (Tab. 4.1) in comparison to the mean wave speed of Table 4.3.

Date	21.01.08	28.08.08
$\bar{\rho}$ [kg/m^3]	291.63	396.08
$\bar{\varepsilon}$	1.554	1.781
CV ε	0.08	0.14
$\bar{v}_s$	0.241	0.225
CV v_s	0.04	0.06
$\Delta\bar{v}$ [%]	1.7	5.3

The radargrams, obtained from the operation of different systems from beneath the snowpack in dry snow conditions, are compared with the hand hardness and density profile. Figure 4.2 shows a radar record with the IDS system (No.1, Tab. 4.1) and Figure 4.3, a record with the RAMAC system (No.5, Tab. 4.1). Both radargrams are turned upside down to have the snow surface at the top of the figure to investigate the relation between prominent internal layers, visible in the

radargram, with the transitions in the physical properties data set as determined from the snow profiles. The effective reflectivity values of $R_i \gtrsim -70$ dB of snow-pit density records calculated from eq. (4.5) as well as the corresponding layer thicknesses and density differences are listed in Tables 4.5 and 4.6.

In both figures the reflections related to the transitions from air to snow at the cave ceiling and from snow to air at the snow surface are distinctly developed (Fig. 4.2, 4.3; horizontal lines). The direct wave and the reflection caused by the transition air-snow beneath the snowpack overlap. Therefore, the phase sequence cannot be clearly related. However, various internal reflections can be related to the recorded snow parameters. The measured dominant change in density of $+80$ kg/m^3 in radar wave propagation direction (Tab. 4.5) at 107 cm snow height in the Stubai data set result in a remarkable reflection in the radargram (referred to as ref#2, Fig. 4.2). Furthermore, the strong density decrease above 133 cm can be related to the respective reflection (ref#1). Other density steps resulting in lower reflectivity values (Tab. 4.5) are not distinguishable in the radargram. Likely, because of the location adjacent to the dominating media transitions, constructive interference at 146 cm and destructive interference at 62 cm prevented the evolution of these reflections in the radargram. Additionally, both layers recorded as reflections (ref#1, ref#2) are thicker or equal to the theoretical layer resolution in snow (Tab. 4.5), (Daniels, 2004). The utilized processing standard for these data enabled a visualization without artifacts via the static correction and the stack of the scans.

The measurements conducted on the Colle Gnifetti (No.5, Tab. 4.1) indicates that the snowpack stratigraphy causes various reflections. With the applied static correction at the snow surface, we were able to attenuate multiple reflections and antenna noise but could not completely remove them. The range in the radargram (Fig. 4.6) between 132 cm snow height and the surface is dominated by multiple reflections, as analyzed by comparison of different polarization measurements further discussed below in section 4.3.3. The radar records of this high alpine site (Fig. 4.3) are more influenced by artifacts caused by the system design (several half cycles of the direct wave, test arrangement, etc.) than the records performed in January 2008 (Fig. 4.2) on the Stubai glacier. Several strong changes in density and hand hardness are observeable at 132 cm (ref#1), below 118 cm (ref#2, only hardness), below 80 cm and between 48–62 cm (ref#3) snow height (Fig. 4.3). These snow stratigraphy changes correspond to reflections in the processed radargram (displayed in grayscale) as well as in the averaged wiggles. The ice layer at a depth of 132 cm in the snow profile is difficult to assign to ref#1 in the radargram. It is likely that the ice layer corresponds to this remarkable reflection as the transition from snow to ice cause a reflection although the layer thickness is too thin for the vertical resolution of the radar (Olhoeft, 1998; Marshall et al., 2007). The next remarkable internal reflection (ref#2), at first sight, has only a corresponding snowpack structure in the hand hardness to explain the reflection occurrence. The analyzed snowpack was influenced by several melting periods resulting in various

ice lenses, which were more or less horizontally consistant. Reflection ref#3 can be related to the density step of $\Delta\rho \simeq +50$ kg/m^3 at 50–62 cm snow height, also recorded as a remarkable hardness increase in the profile. The calculated effective reflectivity (eq. 4.6) is about -70 dB (Tab. 4.6). The density and hardness rise from 70–80 cm has a slight equivalence in reflection response. The effective reflectivity hardly differs from that of at 50 cm snow height (Tab. 4.6). The radar responses situated below 30 cm snow height are characterized by the dominant overlap of the direct wave. Similar to the measurement No.1 (Tab. 4.1), the dominant reflections at the transitions from air to snow and snow to air are interfering with the reflections likely caused by the near-surface and the near-cave ceiling layers.

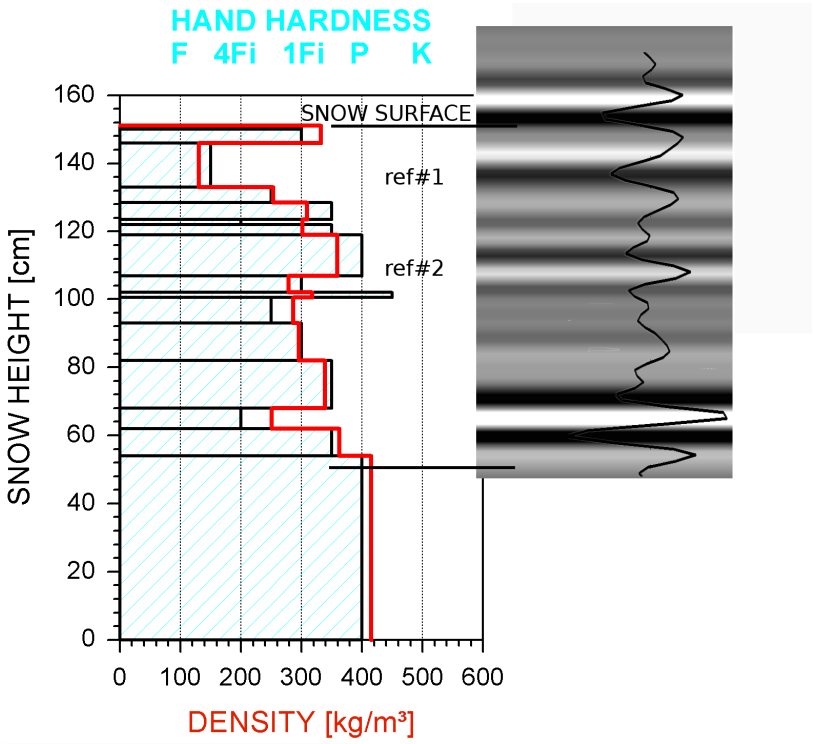

Figure 4.2.: Data set No. 1 measured on the Stubai glacier, Austria (Tab. 4.1). Comparison of radar records obtained with the 900 MHz system in dry snow conditions to snow hardness (blue) and density (red line). The horizontal lines relate the snow surface and the cave ceiling to the corresponding reflections. The statically corrected and stacked radargram and an averaged wiggle view over 30 traces of the presented range are shown.

Table 4.5.: Location of the respective density gradient in radar direction, reflectivity from eq. (4.5) and layer thickness of specific snow layers with a reflectivity larger than -70 dB of the analyzed measurement No.1 from the Stubai Glacier, Austria.

height	$\Delta\rho$[kg/m³]	R_i[dB]	layer thickness [cm]
150	-332.34	-18.5	
146	201.69	-51.2	4
133	-123.20	-54.4	13
128.5	-55.64	-68.7	5
119	-58.12	-68.5	3
107	80.48	-62.8	12
68	57.61	-68.5	14
62	-81.47	-62.6	6
55	362.64	-33.6	7

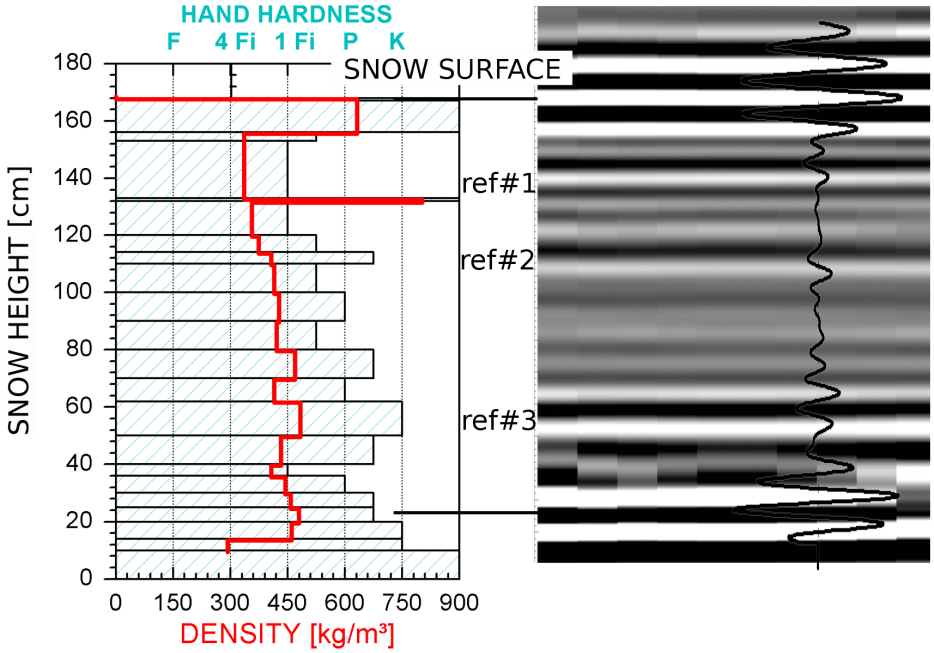

Figure 4.3.: Data set No. 5 ⊤-polar measured on the Colle Gnifetti, Switzerland (Tab.4.1). Comparison of radar records obtained with the 800 MHz system in dry snow conditions to snow hardness (blue) and density (red line). The horizontal lines relate the snow surface and the cave ceiling to the corresponding reflections. The statically corrected and stacked radargram with an averaged wiggle view over 30 traces of the presented range are shown.

Table 4.6.: Location, density gradient in radar direction, reflectivity (eq. 4.5) and layer thickness of specific snow layers with a reflectivity larger than -70 dB of the analyzed measurement No.5 from the Colle Gnifetti, Switzerland.

height	$\Delta\rho$[kg/m^3]	R_i[dB]	layer thickness [cm]
167	-631.31	-13.6	
156	295.25	-41.6	7
133	-465.22	-34.2	20
132	445.16	-36.6	1
70	55.24	-70.3	10
62	-69.55	-66.3	8
50	51.79	-71.5	12
24	457.73	-34.8	6

4.3.2. Wet snow conditions

In a moist snowpack the previously applied conversions of travel time to depth or density to dielectric permittivity values are no longer applicable. The roughly determined average volume fraction of water for the entire analyzed snowpack (Fig. 4.4) was about $\nu_w = 4.2\%$ utilizing the upper boundaries of the ranges defined by Colbeck et al. (1990) and $\nu_w = 2.9\%$ if the lower boundaries are utilized. This results in an uncertainty of about 30% for the average water volume fraction. Calculating the effective permittivity of the snow results in different values for all equations introduced above (eq. 4.3, 4.7, 4.9). The effective permittivity calculated from the measured TWT in the analyzed wet snowpack using eq. (4.3) results in $\varepsilon_{eff4.3} = 2.76$ (the subscript indicates the respective equation). The empirical approach by Lundberg and Thunehed (2000) result in $\overline{\varepsilon}_{eff4.7} = 2.36\pm0.12$ ($\pm5\%$) for the given wetness range and the equation by Sihvola and Kong (1988) result in $\overline{\varepsilon}_{eff4.9} = 2.08\pm0.08$ ($\pm4\%$). The differences for these assumed values is 14% between the empirical approaches and almost 30% between eq. (4.3) and eq. (4.9). Taking the wettest layer in the profile and adopting the upper range given by Colbeck et al. (1990) the difference between the two empirical equations increases to 17%. The values determined with eq. (4.9) correspond adequately within the three-phase mixing model eq. (4.8) $\overline{\varepsilon}_{eff4.8} = 2.18 \pm 0.08$ ($\pm3.5\%$). Independent of the equation used, the average effective permittivity of the whole snowpack and the permittivity of certain wet layers differ by more than a factor of 2 at most. This variation is higher than the dielectric permittivity variation of dry snow (e.g. Heilig et al., 2008). Additionally, this variation has no linear gradient with depth, but can be present from one layer to the next. In Figure 4.4 the wetness variations are displayed in addition to hardness and density. The occurrence of different wetness classes one after another in the snowpack in Figure 4.4 results in travel-time conversion to depth with respect of each layer separately, contrary to dry snow conditions, where permittivity differences among snow layers

can be neglected for the wave speed determination.

In the completely isothermal snowpack (temperature constant at 0° C) in Figure 4.4, the snow surface reflection is strongly attenuated. The emitted 900 MHz signal is still able to penetrate the snowpack as proven by targets (Aluminum shovel put onto the snow surface for a short time, see reflection hyperbola in Fig. 4.4) in the radargram, but the detection of the surface reflection is hardly possible without such target reflections (Fig. 4.4). However, it is clearly visible that in addition to density steps, wetness differences cause reflections in this radargram and actually seem to be the major cause. The two remarkable internal reflections seem to correspond to the strong increases in wetness at about 110 cm and 150 cm height of the snow profile (Fig. 4.4).

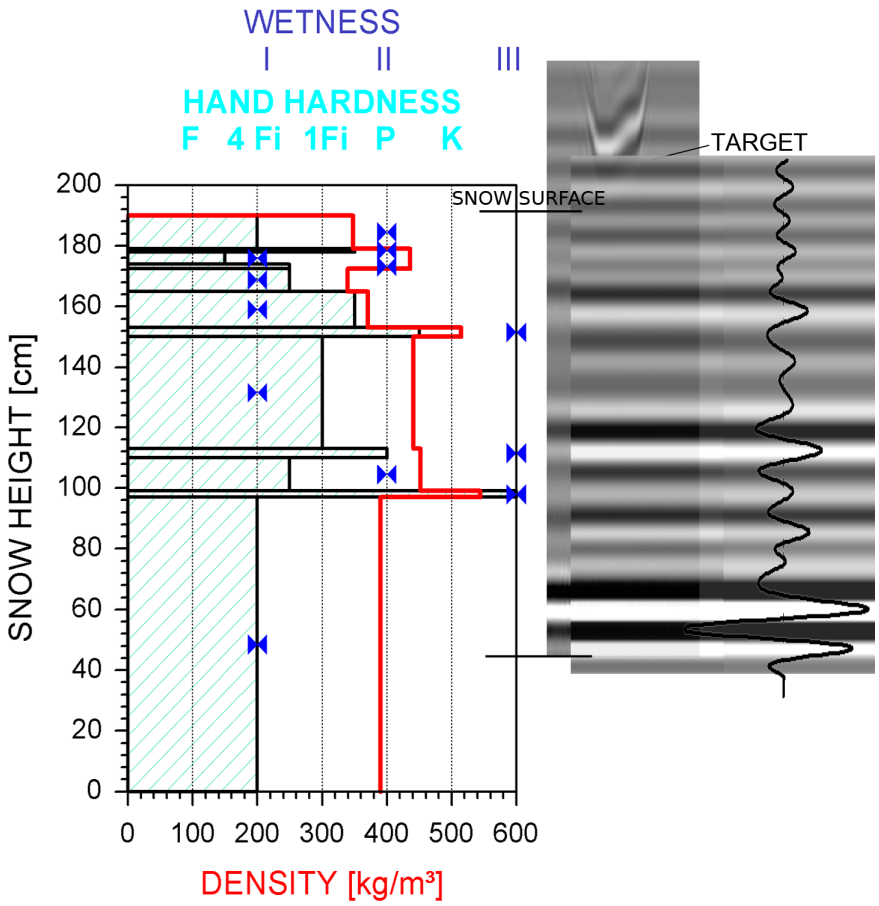

Figure 4.4.: Data set No. 2 measured on the Vernagtferner, Austria (Tab. 4.1). Comparison of radar records obtained with the 900 MHz system in wet snow to snow hardness (light blue), density (red line) and wetness (blue stars). The horizontal lines relate the snow surface and the cave ceiling to the corresponding reflections. Visualized is the statically corrected and stacked radargram with an averaged wiggle view over 30 traces of the presented range. Furthermore the reflection from the snow surface-target (Aluminum shovel) is displayed in the background.

4.3.3. Polarization and frequency dependence

The application of pulsed radar systems, where the bandwidth is predetermined according to the antennas used, allows two possibilities of variation, which influence the radar record. Firstly, it is possible to vary the frequency and, secondly, one can vary the polarization of the antennas. The frequency determines the penetration depth and the bandwidth the vertical resolution (Marshall et al., 2007). A lower frequency enables a deeper penetration into the medium and a higher frequency has higher sensitivity to layer transitions. A larger bandwidth or frequency range results in improved vertical resolution. Figure 4.5 illustrates these relations by the use of two different antenna systems for analyzing the same snowpack on Vernagtferner (Tab. 4.1, No. 3 and 4). The previously mentioned 900 MHz antenna (Fig. 4.5 A) is compared with a 2 GHz bipolar antenna (Fig. 4.5 B and C). The measurements were conducted before the daily warming occurred.

The three radargrams of the same snowpack are plotted together in Figure 4.5 to compare corresponding reflections. The most obvious differences occur at the snow surface. While for the 900 MHz antennas the transition from snow to air at the snow surface is distinctly visible (Fig. 4.5 A, at about 15 ns), the appearance of this transition for the 2 GHz antennas is very much attenuated and hardly recognizable (Fig. 4.5 B, C). Reflections from the surface target in the 2 GHz antennas are only visible by applying an extra gain at the snow surface range. Below the surface transitions, the next horizontal persistent reflections, which occur in all three radar records are located at about 12–13 ns. The 900 MHz antenna shows a strong reflection structure, while in both 2-GHz records the signal is strongly attenuated. Further persistent reflections consistently occurring in all three radargrams are situated at about 10 ns and the reflection from the cave ceiling. However, radargram B and C, recorded with two different polarizations, are not identical. Differences occur in reflection strength of the signal and the location of the reflection with height. Both records were processed in the same way. Horizontally persistent reflections, which are observable in both radargrams are at 12 ns, at about 10 ns and above 8 ns. The occurrence of other reflections do not correspond to each other. This is, for instance, the case between 13–14 ns and below 6 ns. This indicates that these signals depend on the polarization of the antenna and should rather be considered some kind of geometry-related noise, which is not a proxy for the snowpack stratigraphy.

Furthermore, especially for the parallel-polarized arrangement, various artifacts are observable throughout the profile (Fig. 4.5C). We also observed these occurrences of artifacts in the data set No.5 conducted with 800 MHz antennas (Fig. 4.6). The strong symmetrical phase and amplitude structures in the wiggle view and the radargrams indicate that these reflections are very likely multiples or ringing. Interestingly, these artifacts occur mainly in the areas before and after the uplift with air between the antennas and the cave ceiling. In contrast, regarding

the orthogonal-polarized arrangement (Fig. 4.6), these artifacts are concentrated on the range of the antennas' uplift and thus deleted or strongly attenuated by the applied processing procedure.

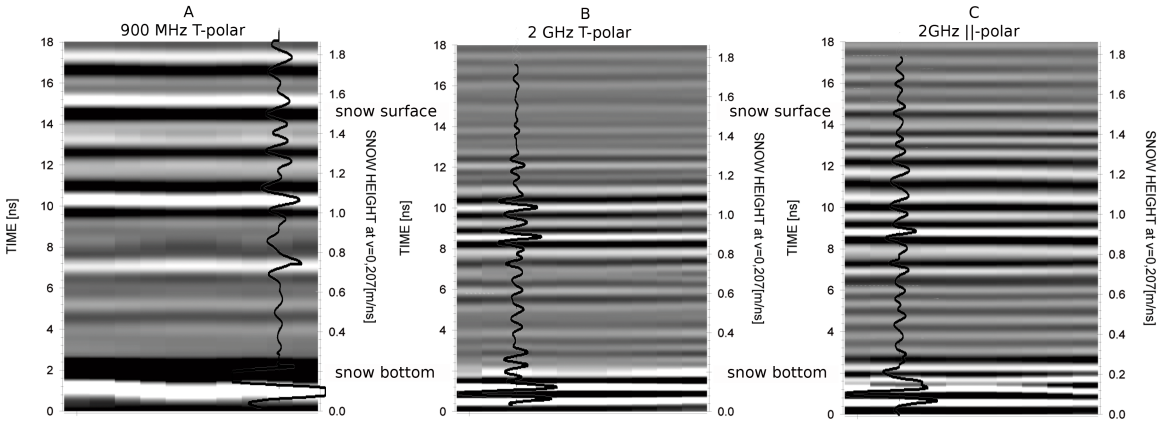

Figure 4.5.: Data sets No. 3 and No. 4 measured on the Vernagtferner, Austria (Tab. 4.1). Comparison of radar records of the same refrozen snowpack obtained with 900 MHz (A) and 2 GHz (B,C) bipolar antennas. The two-way travel time (left y-axis) is related to depth values (right y-axis). Visualized are the statically corrected and stacked radargrams with an averaged wiggle view over 30 traces of the presented range.

4.3.4. Physical origin of reflections

Studies of GPR in Antarctic regions (Arcone et al., 2004, 2005) showed that the radar phase structure enables interpretation of the stratigraphic characteristics in dry snow. Arcone et al. (2005) and Hubbard and Glasser (2005) describe the relation between permittivity and phase polarity sequences. We analyzed the phase structure of two data sets in dry snow conditions (No. 1, Stubai Glacier, Austria; No.5, Colle Gnifetti, Switzerland, Tab. 4.1) and one data set obtained in wet snow conditions (No. 3, Vernagtferner, Austria, Tab. 4.1) with respect to the above mentioned results. The observed source wavelet's phase structure for the IDS antennas is a sequence of 3 half cycles with a negative – positive – negative amplitude sequence (- + -) while the used RAMAC antennas have at least 4 half cycles also starting with a negative half cycle (- + - +) as source wavelet. We display the radar data such that a positive half cycle corresponds to a white colored amplitude and a negative half cycle to a black colored amplitude in the grayscale plot (Fig. 4.2; 4.3, wiggle). From the physical principles laid out in section 4.2.4 (eq. 4.4), we would therefore expect that a change from low to high permittivity (air-snow interface at the cave ceiling) causes a phase reversal ($r < 0$), whereas a change from high to low permittivity (snow-air interface at the snow surface) causes a reflection without a phase reversal ($r > 0$) . As mentioned above, in dry snow conditions, density is the sole parameter (Kovacs et al., 1995;

Mätzler, 1996) influencing the permittivity. Therefore, phase polarity changes can be related to the sign of a density change (Arcone et al., 2004, 2005). The phase structure of the reflection from the cave ceiling in Figure 4.2 consists of 4 half cycles starting with a positive amplitude (+ - + -) and at the snow surface of 2 1/2 half cycles (- + (-)) without phase reversal. The phase sequences of these two reflections are consistent with the underlying changes in permittivity. In Figure 4.2, the first positive oscillation at the cave ceiling is interfering with the direct wave and therefore slightly attenuated, but visible in the wiggle display. The internal reflection at 107 cm height (ref#2) in this figure has a reversed phase characteristic (+ - +) and the reflection at 133 cm (ref#1) has no reversal of 2 half cycles starting with a negative amplitude. Both reflections correspond to the determined density gradient, which is positive (resulting in a phase reversal) at 107 cm and negative (np phase reversal) at 133 cm. The reflectivity values of these two changes in density of Table 4.5 are both above $R = -70$ dB. For the data set no. 5 (Fig. 4.3) obtained on Colle Gnifetti, Switzerland, the cave ceiling is difficult to define due to interferences and overlapping of the direct air and ground wave, therefore no phase analysis is reliable. At the snow surface the reflection starts with a strong positive half cycle due to the strong density change to the uppermost layer ($R = -41.5$ dB, Tab. 4.6). It is not possible to distinguish the transition from snow to air from the snow surface to this layer reflection because of the length of the wavelet, which is at least 3 half cycles long. The three previously discussed internal reflections (Fig. 4.3, ref#1 – ref#3) have a similar phase sequence starting with a positive amplitude (+ -). Comparing to the measured densities for ref#1 and ref#3 these phase reversals are reproduced in the corresponding density increase (Fig. 4.3). As the density increase related to ref#2 is missing in the snow pit data (Fig. 4.3), we assume that a thin layer with a strong increase in density existed but has not been measured. An increase in hand hardness at this depth was observed at 110 cm height (Fig. 4.3). The phase sequence is in accordance with the previously mentioned theoretical principles as well. The reflectivity values (Tab. 4.6; Fig. 4.6) are at about $R_i \simeq -70$ dB and above. The density step at 70 cm height can be related to a just recognizable reflection in the radargram (Fig. 4.3, wiggle view). The calculated reflectivity is $R = -70.3$ dB.

Also for the reflections in wet snow conditions, the observed phase structure corresponds to permittivity changes. In this case, the dielectric permittivity depends in addition to the density on moisture content. The internal layers with a higher moisture content at 110 cm and 155 cm in Figure 4.4 are represented by a + - phase structure, indicating an increase in dielectric permittivity. The snow-surface transition displays the opposite structure (- +), although it is hardly recognizable.

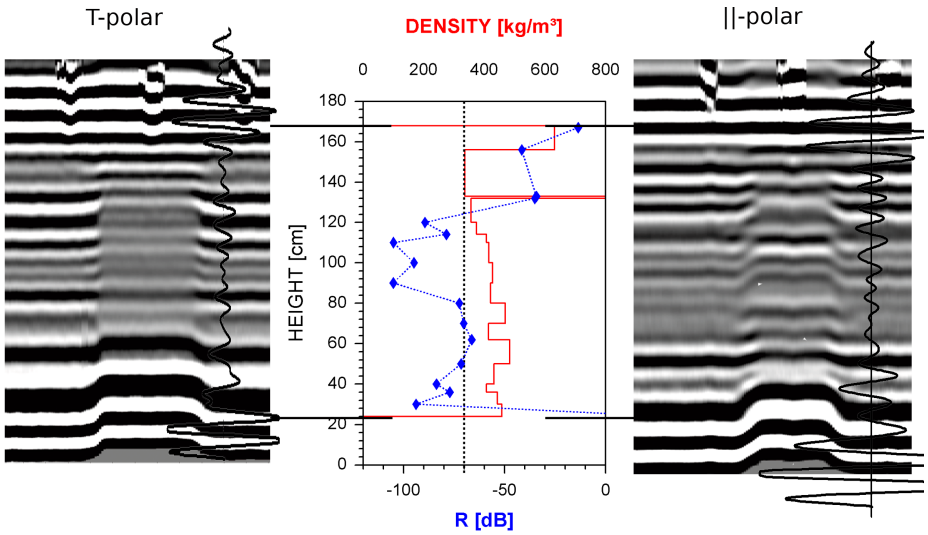

Figure 4.6.: Data set No. 5 measured on the Colle Gnifetti, Switzerland (Tab. 4.1). Effective reflectivity (blue diamonds) determined with eq. (4.5) and density (red line) compared to recorded radargrams. Visualized are a ⊤- and a ||- polarization in respect to the profile wall recorded with 800 MHz antennas. The diamonds display the effective reflectivity where the density changes from one layer to another. The radar records are additionally processed with a static correction but not stacked for a better visualization of the multiple reflections.

4.4. Discussion

In the following we address the three objectives: (i) find a measurement arrangement for the application of radar beneath the snowpack, which is able to provide reliable results for short-time data requests at specific times during a day; (ii) analyze the reflection response of different snow stratigraphies and the penetration depth for various snow conditions; (iii) compare various antenna and GPR systems in terms of their reliability as an automated snowpack monitoring system.

For a short-term data request, it is essential that one is able to distinguish between antenna effects and snow stratigraphy causing reflections. As the snowpack is usually not changing while a measurement is conducted and the frequency structure of the source signal is constant for impulse systems, moved antennas will improve the interpretability and the reliability of the received data. A horizontal movement requires an effort for the design of the test arrangement, which is not applicable beneath the snowpack. Therefore, the vertical uplift is the most effective solution. Reflections caused by the snow stratigraphy or by media transitions will be reproduced in the radar record with a significant movement structure. This structure is the basis for further processing steps. We were able to identify artifacts and multiples (Fig. 4.2–4.6) by our processing

procedure. The applied static correction allowed us to separate reflections non-parallel to the snow surface, the stacking over selected scan ranges helped to identify artifacts and the horizontal average attenuates the non-horizontally planar reflections. Reflections caused by the stratigraphy in the snowpack can be separated from other reflection sources with the applied test arrangement and processing. The presented movement technique via a lever system is naturally not applicable for an installation of the system on the top ground surface. A remote controlled lifting platform is essential for a long-term installation. Nevertheless, for this feasibility study the lever system worked well and provided reliable results with an uplift of about 0.1 m.

Dry snow

The results of the field measurements in dry snow conditions are very encouraging. Strong density changes with an adequate layer thickness produce distinct reflections. In high winter conditions without a melt period affecting the snowpack, which means that no ice lenses are in the snow cover, the reflections were caused by density changes with a layer thickness larger than the resolution limit of the applied antennas (Daniels, 2004; Marshall et al., 2007). Whether thinner layers could possibly be detected cannot be answered with these data sets. Observed thin layers with a distinct density step and therefore a calculated reflectivity $R_i > -70$ dB were situated too close to the snow-air media transitions in the radargram. The transition from air to snow and snow to air caused constructive and destructive interferences, which prevented identification of possible layer reflections of these thin layers (Tab. 4.5; Fig. 4.2). While melt processes have affected the snowpack, resulting thin ice layers were detectable because of the strong density transitions and the resulting strong increase in dielectric permittivity (Fig. 4.3, ref#1). Occasionally, their vertical location in the snow pit does not exactly correspond to the location of the reflection. This could happen if the snowpack was not undisturbed and the recorded layer in the profile not perfectly parallel to the snow surface. In addition, application of an average wave speed also slightly influences the traveltime-depth conversion and contributes to small depth differences. In the profile in Figure 4.3 more than one ice lens was observed. However, horizontally non-persistent ice layers were not recorded in the observed profile. It is very likely that the reflection ref#2 was caused by other ice intrusions, whose density was not recorded because of their lateral discontinuity. Nevertheless, a corresponding strong increase in hand hardness could be recorded in the profile. The location of internal layers and the determined snow height, calculated with an average wave speed, is within the variation range of 6% (Tab. 4.3; 4.4), even for the measurements in August on a high alpine site. Considering a snow height with a two-way travel time of 20 ns, a variation range of 6 % to the mean average wave speed will result in 2.31 m snow height with an uncertainty of ± 0.15 m. This is an adequate accuracy regarding the spatial variability of probed snow heights (Föhn, 1989).

Wet snow

Due to the lack of an adequate instrument for measuring the liquid water volume fraction in snow, the presented results cannot be taken as a fully quantitative analysis of the influence of specific amounts of liquid water on radar reflections. The uncertainty in the determination of the water volume fraction of the whole snowpack is about 30%. By regarding the calculated permittivity values, this uncertainty decreases to about ±5%. Two different empirical approaches for the calculation of the effective permittivity were used. The values of the approach by Lundberg and Thunehed (2000) differ by more than 15% from the results by Sihvola and Kong (1988). This is why permittivity values were not converted to reflectivity. Lundberg and Thunehed used the measured density of wet snow and Sihvola and Kong developed an empirical relation for the density of dry snow. Which empirical conversion of water volume fraction to effective permittivity fits best, has to be analyzed in a future dedicated measurement series with objective determinations of the moisture fraction in the snowpack. However, various qualitative relations can be derived from this data set. The signal of the utilized GPR 900 MHz antennas was strongly attenuated by the moisture in the snowpack, but it was still able to penetrate the snow all the way to the surface and back. The assumed average moisture values for the whole snowpack were probably at the lower end of the actual values, especially for the upper parts of the profile. However, distinct layers reached water contents up to 12% and more, which is very wet (Colbeck et al., 1990). We conclude that the analyzed snow conditions defined the upper-end member of possible moisture contents, where the application of impulse radar systems with higher frequencies seems still be possible and reliable. Two internal layers were recorded with radar, which corresponded to layers of high moisture content. A temporal observation of wet layers in snowpacks is a strong argument for the intended sensor system and can be a decisive application possibility for the prediction of wet slab avalanches. However, more field work is required for the application in wet snow conditions, e.g. to determine an average wave speed value for the snow height estimation or an algorithm for the identification of the snow surface.

Comparison of density-base reflectivity distribution with observed reflections

The introduction of the phase structure and the reflection coefficient or effective reflectivity relates specific reflections in dry snow to specific snow parameters. The analyzed phase structures for dry and wet snow conditions correlated well with the observed density or calculated dielectric permittivity changes. This result helps to identify and follow specific snow layers with time. The results of the calculated reflectivity showed that potentially a reflection is caused by an effective reflectivity threshold larger than $R = -70$ dB. It is not yet possible to quantitatively analyze reflections. In the current study a quantitative analysis is hampered by the fact that we utilized two different radar systems and that for this scope our sample size is too small. However, further

development and application of the radar equation seems possible. Note that in a homogeneous medium (without ice layers) the detectable thickness of snow layers is inversely proportional to the used frequency range or bandwidth. For a reliable conclusion about the reflectivity more field data are needed to relate thresholds to snowpack parameters.

Comparison of different antenna and GPR system

In this feasibility study we employed different radar systems and various antennas. The aim of this variation was to identify the best radar set-up for future long-term field measurements and to define the possible problems in snowpack monitoring by GPR. The most obvious problems occurred with the application of the 2 GHz antennas. Even a dry snowpack with a high average density caused so much attenuation that the snow surface reflection and targets at the snow surface were hardly detectable. In addition, the penetration length was only about 1.4 m. On the contrary, the 900 MHz antennas provided distinct surface reflections and were able to detect the targets even in a wet snowpack. This lets us conclude that the 2 GHz impulse radar is not feasible for a whole season application, especially if water infiltrates the snowpack. Additionally, the two different polarizations with 2 GHz created reflections, which could not be assigned to snowpack features and therefore are likely noise or multiples. Especially in the upper parts of the snowpack, reflections caused by the stratigraphy were hardly detectable in the radargrams and a different reflectivity between both polarizations was apparent. Supplemental radar records for the two analyzed different polarizations were measured with the 800 MHz antennas as well. The 800 MHz antennas confirm the polarization results observed with the 2 GHz antennas. Antennas polarized parallel to the snow-pit wall produce remarkably more signals in the radargram than orthogonal polarized antennas. The generation of the multiples and side reflections is propably due to the fact that the emittance of the radar did not cover a laterally homogeneous snowpack. The discussed test arrangement obviously contributes to the problem, as one side of the snowpack was excavated and could cause reflections from the vertical wall. As the records were measured closely to the profile wall, it is very likely that the multiple reflections and artifacts are caused by radar waves traveling at the profile wall up and down and reaching media transitions at slightly different travel times than the direct waves. The antenna touched the snowpack at the cave while it was lifted up. This is probably the reason for the occurrence of these artifacts in the orthogonal-polar arrangement. A polarization parallel to the profile wall means that the main part of the emitted radar lobe is not directed to the profile wall, resulting in a large portion of the radar wave being radiated to the media transition in the bulk. While the antennas are lifted up, the range transmitted in the open space is reduced and thus fewer multiples are generated.

A future permanent installation of the system beneath a snowpack for the entire season will prevent these polarization problems. We estimate the influence of polarization relatively marginal

for our usage. It is assumed that the stratigraphy is very homogeneous and quasi-parallel for the small section the radar footprint is covering, even in steep slopes.

4.5. Conclusion

The imaging of snow stratigraphy with an upward-looking GPR system deployed beneath the snowpack is feasible. Even a wet snowpack was penetrable by the utilized radar system. The use of 800–900 MHz antennas for commercial pulsed radar systems provides the best trade-off between vertical resolution and penetration depth. 2 GHz antennas were not able to penetrate a snowpack with a higher average density. For very wet snowpacks or for larger snow heights the performance of higher frequencies than 1 GHz are insufficient. The application of theoretical and empirical relations to allocate reflections to changes in snow density and moisture content was possible, especially for the phase structure. The allocation of the reflections' magnitude provided qualitative results. If these results will be confirmed in further field works, it will be possible to follow the temporal development of the snowpack especially in snow height and specific density changes (crusts). Continuous radar profiles and some evaluation measurement in combination with weather data can provide detailed information about the further evolution of the snowpack and by this means validate snowpack models. For a reliable quantification of the reflectivity, more field data are required, especially highly resolved density records and for wet snow conditions continuous measurements of the moisture content. Application of dielectric profiling on the centimeter scale within the area of the GPR footprint could provide very detailed information about the coherences of snow density variations and permittivity, enabling a better comparison of snow-based reflection coefficients and observed GPR reflections.

Acknowledgement

This research is partly funded by grant DFG EI672/5-1 to O.Eisen, PIEPS GmbH, WSL Swiss Federal Institute for Snow and Avalanche Research and r-hm Risk and Hazardmanagement. For assistance in the field we thank the Commission of Glaciology of the Bavarian Academy of Sciences, S. Leimgruber, P. Bohleber, R. Drews, C. Hofstede, Air Zermatt for helicopter support and the CAI Capanna Margherita for accommodation. We would also like to thank H.-M. Schuler and K.J. Sandmeier for discussions that helped to improve the paper and the anonymous referees for valuable suggestions.

Bibliography

Arcone, S. A., Spikes, V. B., Hamilton, G. S., 2005. Phase structure of radar stratigraphy horizons within Antarctic firn. Annals of Glaciology 41, 10–16.

Arcone, S. A., Spikes, V. B., Hamilton, G. S., Mayewski, P., 2004. Stratigraphic continuity in 400 MHz short-pulse radar profiles of firn in West Antarctica. Annals of Glaciology 39, 195–200.

Boyne, H., Ellerbruch, D., 1979. Microwave measurements of snow stratigraphy and water equivalence. In: Proc. 47th Annual Western Snow Conference.

Colbeck, S., Akitaya, E., Armstrong, R., Gubler, H., Lafeuille, J., Lied, K., McClung, D., Morris, E., 1990. The international classification for seasonal snow on the ground. Tech. rep., International Commission of Snow and Ice of International Association of Scientific Hydrology / prep. by Working group on Snow Classification.

Daniels, D., 2004. Ground Penetrating Radar, 2nd Edition. The Institution of Electrical Engineers, London, UK.

Denoth, A., 1989. Snow dielectric measurements. Advanced Space Research 9, 233–243.

Denoth, A., 1994. An electronic device for long-term snow wetness recording. Annals of Glaciology (Proceedings of the Symposium on Applied Ice and Snow Research 1993) 19, 104–106.

Eisen, O., Frezzotti, M., Genthon, C., Isaksson, E., Magand, O., van den Broeke, M., Dixon, D., Ekaykin, A., Holmlund, P., Kameda, T., Karlöf, L., Kaspari, S., Lipenkov, V., Oerter, H., Takahashi, S., Vaughan, D., 2008. Ground-based measurements of spatial and temporal variability of snow accumulation in East Antarctica. Reviews of Geophysics 46 (RG2001).

Ellerbruch, D., Little, W., Boyne, H., Bachman, D., 1977. Microwave characteristics of snow. In: Proc. 45th Annual Western Snow Conference.

Föhn, P., 1989. Snow cover stability tests and the areal variability of snow strength. In: Proceedings ISSW International Snow Science Workshop 1988, Whistler, B.C. Canada. pp. 262–273.

Gubler, H., 1981. An inexpensive remote snow-depth gauge based on ultrasonic wave reflection from the snow surface. Journal of Glaciology 27 (95), 157–163.

Gubler, H., Hiller, M., 1984. The use of microwave FMCW radar in snow and avalanche research. Cold Regions Science and Technology 9, 109–119.

Gubler, H., Weilenmann, P., 1986. Seasonal snow cover monitoring using FMCW radar. In: ISSW International Snow Science Workshop 1986. pp. 87–97.

Harper, J., Bradford, J., 2003. Snow stratigraphy over a uniform depositional surface: spatial variability and measurement tools. Cold Regions Science and Technology 37, 289–298.

Heilig, A., Schneebeli, M., Fellin, W., 2008. Feasibility study of a system for airborne detection of avalanche victims with ground penetrating radar and a possible automatic location algorithm. Cold Regions Science and Technology 51 (2-3), 178–190.

Hubbard, B., Glasser, N., 2005. Field Techniques in Glaciology and Glacial Geomorphology. Wiley and son, Chichester. Great Britain.

Kovacs, A., Gow, A., Morey, R., 1995. The in-situ dielectric constant of polar firn revisited. Cold Regions Science and Technology 23, 245–256.

Lehning, M., Fierz, C., 2008. Assessment of snow transport in avalanche terrain. Cold Regions Science and Technology 51, 2-3 (2-3), 240–252.

Looyenga, H., 1965. Dielectric constant of heterogeneous mixtures. Physica 21, 401–406.

Lundberg, A., Thunehed, H., 2000. Snow wetness influence on impulse radar snow surveys theoretical and laboratory study. Nordic Hydrology 31 (2), 89–106.

Lundberg, A., Thunehed, H., Bergström, J., 1999. Impulse radar snow surveys - influence of snow density. Nordic Hydrology 31 (1), 1–14.

Machguth, H., Eisen, O., Paul, F., Hoelzle, M., 2006. Strong spatial variability of snow accumulation observed with helicopter-borne GPR on two adjacent Alpine glaciers. Geophysical Research Letters 33 (13).

Marchand, W.-D., Bruland, O., Killingtveit, A., 2001. Improved measurements and analysis of spatial snow cover by combining a ground based radar system with a differential global positioning system receiver. Nordic Hydrology 32 (3), 181–194.

Marshall, H., Koh, G., 2008. FMCW radars for snow research. Cold Regions Science and Technology 52, 118–131.

Marshall, H., Koh, G., Forster, R., 2004. Ground-based frequency-modulated continuous wave radar measurements in wet and dry snowpacks, Colorado, USA: an analysis and summary of the 2002/03 NASA CLPX data. Hydrological Processes 18, 3609–3622.

Marshall, H., Schneebeli, M., Koh, G., 2007. Snow stratigraphy measurements with high-frequency FMCW radar: Comparison with snow micro-penetrometer. Cold Regions Science and Technology 47 (1-2), 108–117.

Modroo, J. J., 2004. Ground penetrating radar location of buried avalanche victims. Master's thesis, Colorado School of Mines, [Online]. Available: http://www.modroo.com/files/JjM2004MSc.PDF.
URL `[Online].Available:http://www.modroo.com/files/JjM2004MSc.PDF`

Mätzler, C., 1996. Microwave permittivity of dry snow. IEEE Transactions on Geoscience and Remote Sensing 34 (2), 573–581.

Olhoeft, G., 1998. Electrical, magnetic and geometric properties that determine ground penetrating radar performance. In: Proceedings of GPR '98. 7th International Conference on Ground Penetrating Radar. pp. 177–182.

Polder, D., van Santen, J., 1946. The effective permeability of mixtures of solids. Physica 12 (5), 257–271.

Richardson, C., Aarholt, E., Hamram, S.-E., Holmlund, P., Isaksson, E., 1997. Spatial distribution of snow in western Dronning Maud Land, East Antarctica, mapped by a ground-based snow radar. Journal of Geophysical Research 102 (B9), 20, 343–353.

Robin, G. d., Evans, S., Bailey, C., 1969. Interpretation of radio echo sounding in polar ice sheets. Phil. Trans. R. Soc., Ser. A 265 (116), 437–505.

Roth, K., Schulin, R., Flüler, H., Attinger, W., 1990. Calibration of time domain reflectrometry for water content measurement using a composite dielectric approach. Water Resources Research 26, 226–273.

Sandmeier, K., 1998. Reflexw version 4.1 manual.
URL `http://www.sandmeier-geo.de/Download/reflexwmanual.pdf`

Schneebeli, M., Coléou, C., Touvier, F., Lesaffre, B., 1998. Measurement of density and wetness in snow using time-domain reflectometry. Annals of Glaciology 26, 69–72.

Schweizer, J., Kronholm, K., Jamieson, B., Birkeland, K., 2008. Review of spatial variability of snowpack properties and its importance for avalanche formation. Cold Regions Science and Technology 51 (2-3), 253–272.

Sihvola, A., Kong, J., 1988. Effective permittivity of dielectric mixtures. IEEE Transactions on Geoscience and Remote Sensing 26 (4), 420–429.

Sihvola, A., Tiuri, M., 1986. Snow fork for field determination of the density and wetness profiles of a snow pack. IEEE Transactions of Geoscience and Remote Rensing 24, 717–721.

Sovilla, B., Bartelt, P., 2002. Observations and modelling of snow avalanche entrainment. Natural Hazards and Earth System Sciences 2, 169–179.

Vickers, R., Rose, G., 1973. High resolution measurements of snowpack stratigraphy using a short pulse radar. In: Proceedings of the Eighth International Symposium on Remote Sensing of the Environment. pp. 261–277.

Waldner, P., Huebner, C., Schneebeli, M., Brandelik, A., Rau, F., 2001. Continuous measurements of liquid water contents and density in snow using tdr. In: Dowding, C. (Ed.), Proceedings 2. International Symposium and Workshop on Time Domain Reflectometry for Innovative Geotechnical Applications. pp. 446–556.

Wilhelms, F., 2005. Explaining the dielectric properties of firn as a density-and-conductivity mixed permittivity (decomp). Geophysical Research Letters 32.

Wingham, D., Francis, C., Baker, S., Bouzinac, C., Brockley, D., Cullen, R., de Chateau-Thierry, P., Laxon, S., Mallow, U., Mavrocordatos, C., Phalippou, L., Ratier, G., Rey, L., Rostan, F., Viau, P., Wallis, D., 2005. Cryosat: A mission to determine the fluctuations in earth's land and marine ice fields. Natural Hazards and Oceanographic Processes from Satellite Data 37 (4), 841–871.

5. Temporal Observations of a Seasonal Snowpack using Upward-Looking GPR [1]

Achim Heilig, Olaf Eisen, Martin Schneebeli

[1]Paper submitted to the journal *Hydrological Processes* the 23.09.09.

Abstract

An increase of the spatial and temporal resolution of snowpack measurements in Alpine or Arctic regions will improve the predictability of flood and avalanche hazards and improve the spatial validity of snowpack-simulation models. In the winter season 2009, we installed a ground-penetrating radar (GPR) system beneath the snowpack to measure snowpack conditions above the antennas. The radar observed the temporal increase and decrease of the snow height above the antennas over more than 2 1/2 months. Three persistant melt crusts, which formed at the snow surface and were buried by further new snow events, could be used as reflecting tracers to follow the snow-cover evolution. The height in two-way travel time (twt) of each layer changed over time as a cumulative effect of settlement and variation of wave speed in response to densification and liquid-water content. For a quantitative analysis accurate wave-speed measurements of each individual layer are necessary. The presented data showed, that with moved antennas it is possible to record the snow height at least with a uncertainty of less than 8% in comparison to the probed snow height. The infiltration of liquid water with depth during melt processes was clearly observed at one instance. All recorded reflections appeared in concordance with the physical principles (e.g. in phase structure) and one can assume that an effective reflectivity of $R_i \geq -70$ dB results in remarkable reflections in the radargram. The accuracy of the used impulse radar system in determining the snow water equivalent (SWE) is in good agreement to previous studies, which used continuous wave radar systems. The results of this pilot study encourage further investigations with radar measurements using the described test arrangement on a daily basis for continuous destruction-free monitoring of the snow cover.

5.1. Introduction

The determination and forecast of snowpack properties is an important feature contributing to the daily avalanche warning bulletin as well as to the prediction of hydrological hazards and run-off amounts. In hydrological forecasting the snow water equivalent (SWE) and therefore the possible melt rates for the prediction of streamflow and reservoir inflows are of high interest (Turcotte et al., 2007). In Arctic regions spring snow melt amounts up to 80% of the annual river flow (König and Sturm, 1998). In the European Alps slightly lower rates are observable. The contingent of the spring snow melt for the annual run-off in a mountainous areas in the Austrian Alps is at about 60% (Escher-Vetter et al., 2009; Comm. Glaciology, 2009). These run-off rates are concentrated on relative short time periods in spring. Therefore, it is important for the managing of hydroelectric power plants or for regional hazard authorities to determine the amounts of SWE in a catchment area as accurate as possible to enable the forecast of the run-off. For hydrological questions, weekly-based information about the snowpack is sufficient but with

interest in spatially highly resolved knowledge about the catchment area. However, for avalanche forecast information on a daily basis of changing snowpack conditions are necessary. For the data assimilation in snow cover models as e.g. ALPINE3D (Lehning et al., 2006) or SNOWPACK (Lehning et al., 1999) the accuracy and spatial resolution depends on the input data. To date, the spatial resolution of these models is dependent on the spatial distribution of automatic snow height stations (Bavay et al., 2009). As reliable automatic snow-height data with sonic sensors are usually only gained in almost flat areas (Gubler, 1981), a lack of data exists especially in slope areas. The regional representativeness of point measurements at weather stations concerning the daily amount of new snow, which is an important factor for daily avalanche hazard prediction and artificial avalanche release (McClung and Schaerer, 2006), shows an increasing uncertainty with increasing daily new snow amounts (Schneebeli and Laternser, 2004). Schneebeli and Laternser noticed, that large daily new snow events with about 50 cm accumulated snowfall and more are often unobserved by automatic snow height stations. It is recommended by Egli (2008) that the measuring site must be placed as close as possible to the critical hazard zone. Concerning the manual data acquisition, especially in slope and ridge regions the data volume of snowpack changes and internal layering is limited by accessability. Thus, for the prediction of avalanches the spatial snow distribution in combination with snowpack stability is a key parameter (McClung and Schaerer, 2006; Kronholm and Schweizer, 2003). The determination of the snowpack stability, however, relies on data on the internal layering, preferable in combination with stability tests (Schweizer and Wiesinger, 2001). Additionally, redistribution by wind is mostly neglected in snowpack simulations, which leads to uncertainties in the total amount of snow and the addition of potential slab structures over former surface features at ridges or in slopes. This information is especially important for the forecasting of self-released avalanches (Schweizer and Wiesinger, 2001). An increase in the number of automatic snow-monitoring sensors will improve the spatial resolution of snowpack models and decrease the size of the grid cells. For further developments in predicting the spatially distributed avalanche danger automatically, the lack of data representing snowpack features especially for mountainous areas is an additional weakness for approaches like nearest neighbor methods (Pozdnoukhov et al., 2008). Either in hydrological application for the prediction of melt rates or for avalanche warning services further automatic sensor systems, working on both plain and slope areas, are an important support for the regional risk and hazard management.

In regions where avalanches occur, an automatic monitoring system must be secured against destruction by avalanches. A possible snowpack-sensor system could be realized by the application of upward-looking pulsed radar systems (Heilig et al., in press). Our implemented radar system operates from beneath the snowpack measuring in an upward direction. Gubler and Hiller (1984) performed early snow-cover observations with frequency modulated continuous wave (FMCW) radars in a similar way. The previous work on the application of FMCW radar for the record

of the snow cover is summarized by Marshall and Koh (2008). In this study the feasibility of impulse radar systems to answer scientific and technical questions is analyzed. As radar systems determine the snowpack non-destructively a temporal observation of the evolution of the snow height, internal layers and settlement speed is possible. Heilig et al. (in press) described the system requirements for an all-season penetration of the snowpack with sufficient layer resolution. In accordance with the there presented results, we designed a test arrangement for the installation of an upward-looking GPR-system at a single test site.

The following pilot study presents an upward-looking impulse radar system recording snowpack properties. We will first describe the data acquisition and the test arrangement, next the data processing and visualization and conclude with the meteorological conditions for the measurement period from the beginning of February until the beginning of April. Results of snow height determinations and the record of internal layers and their changes with time are presented. Furthermore, we analyze reflections with respect to the physical properties of the snowpack.

5.2. Methodology

5.2.1. Data acquisition

To measure the temporal evolution of a snowpack throughout a winter season (Table 5.2.1), we installed fixed GPR antennas from the middle of January 2009 until the beginning of April 2009 at a test site in the Bavarian Alps on an almost flat area (5–9° slope angle).

Table 5.1.: Radar measurements in winter 2009 to record the temporal evolution of snowpack properties.

date	notation	snowpack conditions
13.02.09	a	dry
19.02.09	b	dry
20.02.09	c	dry
06.03.09	d	dry
12.03.09	e	dry
14.03.09	f	dry
18.03.09	g	dry
25.03.09	h	dry
06.04.09	i	wet

The test site is located at 1420 m a.s.l. at the lake Grünsee, near the city of Schliersee, Germany. Although the site is below treeline, it is situated in open space, but it is located nearby a narrow terrain edge. We used a RAMAC system (MALA Geoscience, Malå, Sweden) with shielded 800

MHz antennas. The antennas (transmitter and receiver) were mounted on a hydraulic hoist system, which was fixed at the top ground surface (TGS) on a wooden plate. To enable the vertical movement and to secure the antennas from direct water contact a PVC cover-box was installed surrounding the antennas (Fig. 5.1). Optic fibres and a 12 V battery connected via a cable facilitated the remote energy supply and data transfer to the control unit of the system. The hydraulic hoist system was connected via a tube to a hydraulic pump in a distance of 6 m to the antennas. During a radar record, the antennas were lifted and sank several times with various speeds. We installed the whole system when the snow height above ground corresponded almost exactly to the height of the plastic box. Therefore it was possible to measure with the GPR system naturally layered snow with properties comparable to the surrounding snowpack. Figure 5.1 illustrates the test arrangement. For the comparison of the recorded reflections, we conducted manual snow pit measurements inside the marked and undisturbed test site. The largest distance from the location of the antennas to a snow pit was about 8 m. We discuss a selection of 9 radar measurements later on. The different distances d in Figure 5.1 are d_{tot} : the total height of the snowpack, $d_{box} \sim 45$ cm, $d_{GPR} = \Delta d_{air} + d_{snow}$ the actually measured distance to the surface, $d_{air} < 10$ cm in lifted position of the antennas, which was usually cut off from the data. The lift of the antennas was $d_{lift} = 14$ cm.

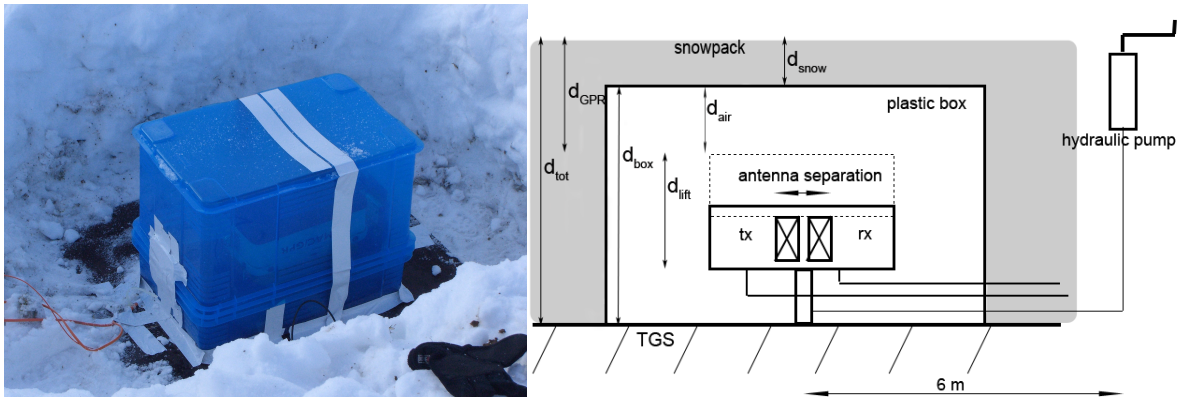

Figure 5.1.: The test arrangement of the field work. On the left a picture of the installation and on the right the sketch is displayed. See text for details.

5.2.2. Snow data acquisition

According to the guidelines of the International Classification of Seasonal Snow on the Ground (ICSSG) (e.g. Colbeck et al., 1990), conventional manual snow profiles with high resolution density measurements were conducted to interpret the radar data and to compare the resulting reflections with snowpack properties. We took at least two snow samples of 100 cm^3 of each recognized layer in the snow pit to determine the average layer density. Additionally, at the

end of almost each snow-pit measurement, we performed the compression test (van Herwijnen and Jamieson, 2007) for the determination of the snowpack stability and to identify weak layers. The stages of failure are given in values (CT-No.) corresponding to the number of hits. For conditions with recognized melt processes in the snowpack (snowpack temperature of 0°C), we made additional manual qualitative wetness determinations according to the ICSSG guidelines, described in detail e.g. by Heilig et al. (in press).

5.2.3. GPR-data processing

For a good comparison of all radar records obtained throughout the winter 2009 at different times and under different environmental conditions, we normalized the amplitude of all raw data sets using a constant factor. We applied the normalization function of the REFLEXW-program, in which one scaling factor is calculated from the quotient of the overall mean energy value of all profiles and the total energy value of the individual profile (Sandmeier, 1998). The energy values are determined within the given time range of each radar measurement. After the normalization, we processed the data as described in detail by Heilig et al. (in press). We applied a dewow filter for the removal of low frequency components from each trace in the profile, a linear gain function, bandpass filters and start time corrections depending on the particular data set. In all cases, we used a background removal for reflection ranges above the location of the direct wave (usually at a two-way travel time of about 2–7 ns). These areas were very much dominated by multiples of the direct wave and therefore not interpretable (e.g. example shown in Fig. 5.2, left part between 2.4–6.8 ns). The background removal filtered out the horizontally constant reflections in the travel time-trace number domain. Subsequently, processing steps were applied as described by Heilig et al. (in press). A static correction to the snow surface, which was uniquely detectable by the use of a target (Aluminum shovel at the surface, Fig. 5.2), was followed by a stack of traces and an average filter over one half cycle of the surface reflection in the end. The effect of the processing is clearly visible in Figure 5.2. Reflections with a vertical movement in the left part of the figure are still displayed after processing, while most of the signals, which occur originally horizontal in the raw data and originating from the system, are filtered out.

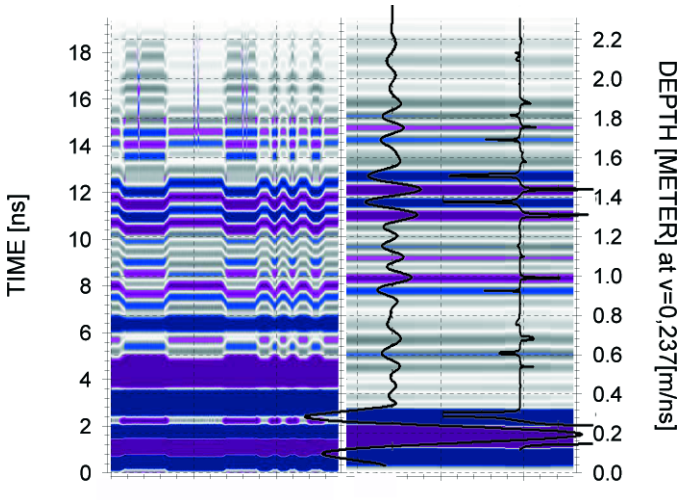

Figure 5.2.: Effect of the applied processing steps and the visualization procedure. The left part displays the status of the radargram prior the static correction. The right part shows the final conditions after the whole processing. The compaction of the signal via the visualization procedure is displayed by the two wiggles, the left one shows the mean trace of the right radargram and the right wiggle the compaction by the procedure described in section 5.2.4.

5.2.4. GPR-data visualization and magnitude retrieval

Pulse compression

Ideally, a source wavelet would comprise only two half-cycles and thus would be one wavelength long. Our source wavelet comprises more than two half-cycles. The resolution is therefore not limited by the wavelength, but by the length of our wavelet, making the overlap of wavelets reflected from different layer boundaries more likely. To improve the visualization of the GPR data, we examine various methods of pulse compression.

We first employed the deconvolution technique, a standard technique routinely applied to seismic and GPR data (e.g. Xia et al., 2004). Unfortunately, the application to our data sets did not provide significant improvements in signal compression. As deconvolution algorithms are usually written for the processing of data with higher signal to noise ratios (samples according to layer reflections in relation to samples recorded noise; see Fig. 5.2, left wiggle) we find that the application of deconvolution algorithms is not sufficient for the data sets presented here.

In a second approach we weigh the reflected signals with the source wavelet in the following manner, referred to as the P-visualization. This processing is applied to each of the nine analyzed data sets independently to obtain a normalized visualization of each measurement. After applying the processing steps described above, the final ten traces of each measurement are averaged

resulting in the mean trace $\vec{b} = (b_1, b_2, \ldots, b_N)$, a vector with N elements, i.e. the data samples. (In the following a subscript will refer to the respective element of a vector.) The number of elements N correspond to the number of samples of the recorded signal. As the reflected return signal in GPR systems is a convolved multiple of the emitted signal, despite of the phase structure and amplitude (Annan, 2002), we extract the first complete positive half cycle of the mean trace $\vec{b}$ and define it as the mother wavelet $\vec{m} = (m_1, m_2, \ldots m_I)$, a vector with $I < N$ elements (Perrin et al., 2000). This mother wavelet, assumed to be generated as part of the direct wave in air, is resampled to resemble a wavelet in snow, each sample at time t' in air is shifted to $t = t'c/\bar{v}$ in snow, where $\bar{v} = 0.237$ m/s is the mean wave speed in snow (see below) and c is the speed of light. We next define a series of $Q = N - I$ vectors $\vec{k}^q = (k_1^q, k_2^q, \ldots, k_I^q)$, $q = 1, \ldots, Q$, the I elements of which are the components of $\vec{m}$ element-wise weighted with a sub-vector $\vec{b}^q = (b_q, b_{q+1}, \ldots, b_{q+I-1})$ of the mean trace vector $\vec{b}$ with I elements. The i-th element of $\vec{k}^q$ is calculated from

$$k_i^q = \frac{m_i}{b_i^q}. \tag{5.1}$$

This division is performed Q times to cover all elements of $\vec{b}$. We next determine the standard deviation σ_q of each vector $\vec{k^q}$, yielding a vector $\vec{\sigma}$ with Q elements σ_q. Based on the mean trace vector $\vec{b}$, we define another subvector $\vec{b}^*$, defined as the part of $\vec{b}$ for the scan range above the direct wave. To exclude the influence of the direct wave for pulse compression, which dominates the signal, when comparing different measurements (Fig. 5.3), we will use the maximum $\bar{b}^* = \max|\vec{b}^*|$ for vector normalization. Finally, the element-wise operation

$$P_q = \frac{b_q}{\bar{b}^* \sigma_q}, \tag{5.2}$$

where b_q is the q-th element of $\vec{b}$ and again $q = 1, \ldots, Q$, yields the elements of a normalized trace vector $\vec{P}$ of length Q with compressed signal appearance. (The last I elements of $\vec{b}$ are not considered in this operation.) The traces $\vec{P}$ for each measurement are compared in Figure 5.3. Note that the processed traces are individually normalized in respect to the total energy content of the trace, so reflection amplitudes cannot be qualitatively compared among traces yet. This will be performed next.

Amplitude normalization for comparison of measurements

One means to characterize the temporal evolution of the snowpack is a time series of observed reflection magnitude of specific snow layers. For this comparison we started off with the individually normalized radar signals as described in section 5.2.3, but no further processing was applied to avoid artificial (processing-related) changes in reflection amplitudes. Subsequently, we used the maximum and minimum value of the amplitude of two half cycles of the mother

wavelet $\vec{m}$ to determine the scaling factor $\hat{m} = \max(\vec{m}) - \min(\vec{m})$.

For the comparison of the amplitudes of different measurements, we performed the static correction to the surface reflection for each normalized raw trace and calculated the mean of the static corrected traces of each measurement, $\vec{b}^{raw} = (b_1^{raw}, b_2^{raw}, \ldots, b_N^{raw})$. Furthermore, we included a simple correction for spherical divergence, finally yielding in $b^{\ddagger}$. The mean trace for each measurement is normalized according to

$$b_i^{\ddagger} = \frac{b_i^{raw} z_i}{\hat{m}}, \tag{5.3}$$

where z_i is the respective range of the retrieved sample in the space domain from the antenna.

The such normalized reflection amplitudes are displayed in Figure 5.4A and further discussed below.

5.2.5. Meteorological data set

An automatic weather station (AWS) was not available in the direct neighborhood of the radar antennas. The next AWS was in an air-line distance of about 2 km north-east and at 320 m lower altitude. For the time periods in between the measurements at Grünsee, we use the data of the AWS to compensate for the lack of data. The recorded temperature at the AWS (dark blue line) corresponds very well to the measurements at the test site (light blue line with markers Fig. 5.4B). The probed snow depth (green line with markers) is always above the measured snow height (red line Fig. 5.4B) of the ultrasonic snow-height sensor beside some large new snow events at the end of February, when we did not visit the station. Likely the snow height at the Grünsee was higher than at the AWS. The main reason for the on average lower snow height at the weather station is that it is located in a dense forrest. Nevertheless, the precipitation and settlement tendency of the seasonal snowpack is well represented by the AWS. The weather conditions at the the test site during the winter season 2009 were characterized by a high pressure period in January with almost no precipitation and cold temperatures with just sporadic peaks above melting point in a 2 hour average temperature (Fig. 5.4B). February and March were characterized by several large snow fall events, which resulted in an over-average snow height from mid of February until April. In combination with some embedded melt processes the snowpack stratigraphy was structured by various crusts and density differences. Figure 5.4B shows a comparison between probed snow depth and hand measured temperature at the test site and the at 10 minute intervals recorded snow height and temperature of the AWS.

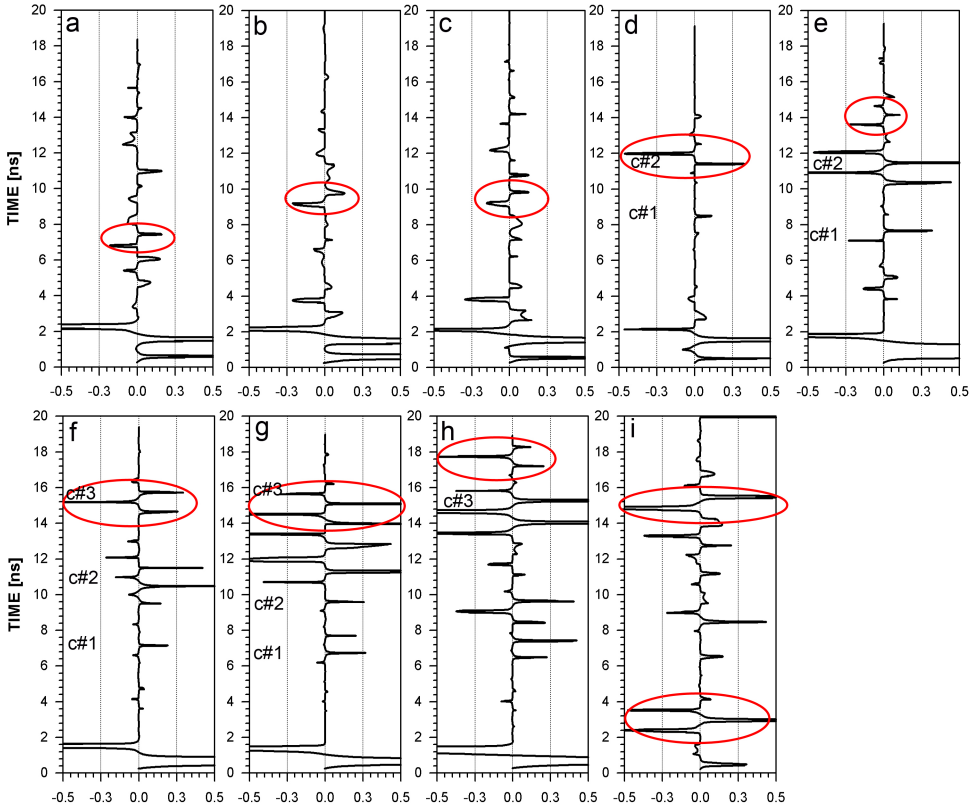

Figure 5.3.: P-visualization of all discussed radar measurements, eight for dry-snow (a–h) and one for wet-snow conditions. The notations are in accordance with Table 5.2.1. Ordinates: two-way travel time; abscissas: compressed amplitudes according to equation 5.2. Red ellipses indicate the snow surface and for measurement i the transition from air to snow below the snowpack as well.

5.3. Results and Discussion

5.3.1. Snow height evolution

Table 5.2.: Comparison of different snow height determinations. The probed snow depth is compared to radar-determined snow height d_{snow} either by using the mean wave speed in dry snow $\bar{v}$ = 0.237 m/s or the mean wave speed determined at each snow pit individually for each measurement day, v_{pit}.

Date	probed snow depth [cm]	radar snow height ($\bar{v}$) [cm]	radar snow height (v_{pit}) [cm]	v_{pit} [m/ns]
13.02.09	80	80.8	92.8	0.272
19.02.09	112	109.0	118.7	0.258
20.02.09	112	109.3	112.5	0.244
06.03.09	126	135.2	137.5	0.241
12.03.09	157	161.3	166.0	0.244
14.03.09	181.5	173.7	175.2	0.239
18.03.09	174	172.1	171.3	0.236
25.03.09	189	203.8	205.8	0.239

Using the P-visualization (Fig. 5.3, red ellipses), the development of the snow height determined from GPR is clearly displayed. Backscatter above the snow surface with an approximately similar amplitude to the surface reflection occurred only during strong precipitation events (Fig. 5.3a and c; Fig. A.1, 13.02.09, 20.02.09). The radargrams of both measurements influenced by the precipitation show horizontally non-persistent incoherent reflections above the snow surface. As the measurements were conducted in the time domain, the effect is comparable to weather radar applications, i.e. moving snow flakes generate backscatter during illumination by the radar beam. In comparison, other automatic snow-height sensors also receive a more noisy signal during snow-precipitation events (e.g. ultrasonic sensors, Bavay et al., 2009). In our data set the surface reflection is in all cases clearly detectable. No further data calibration is necessary. The radar-determined snow height using an average wave speed in dry snow, $\bar{v}$ = 0.237 m/ns (Heilig et al., in press) varies for all measurements in dry snow conditions in winter 2009 by less than 8% in comparison to the probed snow depth above the radar box (Tab. 5.2). In a 2.0 m high snowpack the miscalculated snow height is therefore ±16 cm. This error is, on the one hand, due to inhomogeneous vertical snowpack conditions, which result in variations in the wave speed between adjacent layers and, on the other hand, due to uncertainties in snow probing. It is very likely that the box (Fig. 5.1) was compressed by the snow masses and therefore had no plain surface as discovered after digging out the antennas in April. A difference in snow height of up to 10 cm above the box could occur due to the compression in the middle of the

box. While calculating a separate mean wave-speed value for each radar measurement, the difference to the probed snow depth increased up to 15% for the measurement of the 13.02.09 and less than 10% for all other measurements. A contributing factor to these specific variations is that the spatial variability of the snowpack conditions above the antennas and within the test site was larger than expected. This results in a remarkable variability in the characteristic of specific snow layers as layer thicknesses or layer locations. Even two measurements on adjacent days without melt processes but with low precipitation rates (Fig. 5.4B) and just about 3 m next to each other, result in different calculated average wave speed values (Tab. 5.2, 19.02.09, 20.02.09). The accuracy of the snow height determination using $\bar{v}$ for the conversion of the two-way travel time of the radar data, could have been distinctly higher, if the uncertainty in snow probing was lower. Our estimate is based on a maximum uncertainty of 10 cm in snow probing. Disregarding this error, the accuracy of the radar-measured snow height utilizing $\bar{v}$ is adequately accurate and slightly above the accuracy range of ultrasonic snow sensors ($\pm$3 cm, Egli and Jonas, 2009). In comparison to the measurements of Gubler and Hiller (1984), who determined the snow water equivalent with an inaccuracy of less than 5% in comparison to manually conducted measurements for dry snow densities between 200–400 kg/m^3, the here presented data is at about 7% slightly above this range, if the mismeasurement of the probed snow depth is not corrected. Taking this uncertainty into account the accuracy increases to differences of less than 5%, which is likely the accuracy limit, due to uncertainties in manual probing and allocating reflections to height (Gubler and Hiller, 1984). Recent work of Marshall et al. (2005) presents FMCW radar measurements with an uncertainty in SWE and snow depth of about 10%. For other climatic regions, such as e.g. maritime areas with distinctly higher average densities or on the opposite more continental areas with distinctly lower mean density values, respective $\bar{v}$ have to be determined. Of course the utilization of height-dependent wave speeds $v(h)$ are desirable, but seldomly easily obtained. Using a mean wave speed for a certain climatic region and time of the year is a justified approximation. If similar variabilities in density records of dry snow conditions to the values presented by Heilig et al. (in press) with a coefficient of variability of $CV = 6\%$ are observable, we assume that the accuracy range of snow height determination utilizing upward-looking GPR is adequately accurate for other climatic regions as well. The SWE in dry snow conditions can be determined in combination with an external snow height measurement directly. If the snow height is known a mean density for the radar measured snowpack above the antennas can be calculated and therefore the SWE be determined.

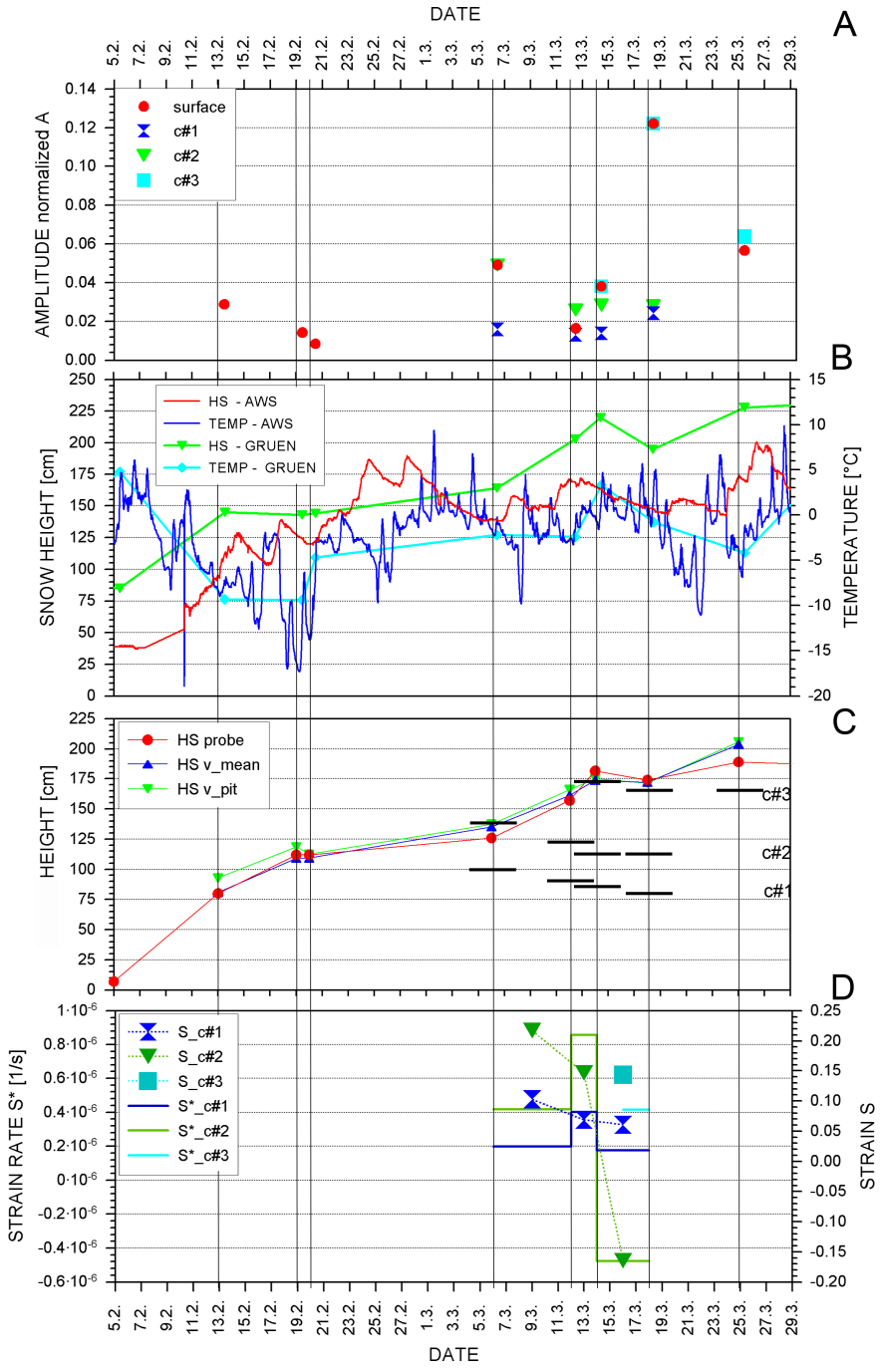

Figure 5.4.: A: values of the recorded reflection amplitude of the addressed snow layers and the snow surface. B: meteorological parameters manually recorded at the test site (GRUEN) in comparison to the measured snow height (HS) and temperature (TEMP) at the AWS. C: comparison of the three differently determined snow heights above the radar box: the probed HS (HS probe), HS calculated with $\bar{v}$ (HS v_mean) and HS calculated utilizing the density of the corresponding snow pits (HS v_pit). The black horizontal line segments indicate the position of the internal layers calculated with $\bar{v}$. D: the strain rates S^* (eq.5.5) of the respective layers (left ordinate) and the strain S (eq. 5.4), each determined for the respective measurement interval.

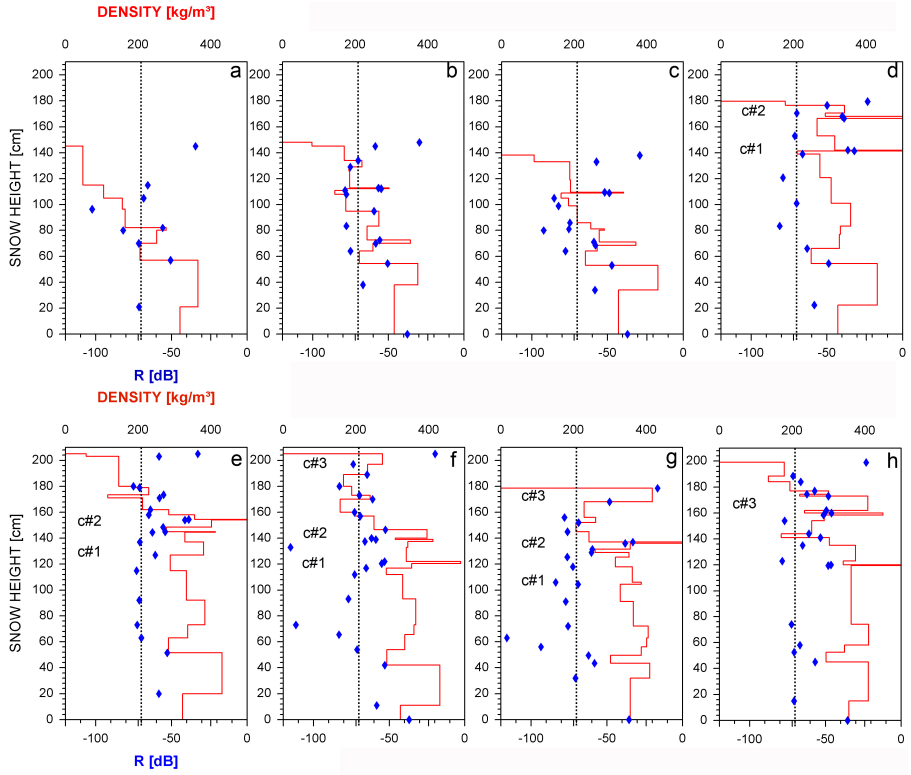

Figure 5.5.: Calculated effective reflectivity values R (blue diamonds) and measured densities (red lines) of the snow pits measured nearby the radar measurements.

5.3.2. Internal layers detected by GPR

Internal layers in the snowpack were recorded in all radargrams of this measurement period. In February, with average snowpacks of relatively low density, internal reflections are mainly caused by slight density changes. On the 13.02.09, (Fig. 5.5a) the density decrease at 118 cm height indicates the transition to the last new snow event. This event occurred during the previous 48 hours before the measurement and can be related to the reflection at 5–6 ns in two-way travel time τ (TWT) short below the surface in Figure 5.3a. Likely, the density decrease of the measurement b at about 92 cm height (Fig. 5.5b) resulted in another reflection at 7 ns in the radargram (Fig. 5.3b). Conditionally to the spatial snowpack variability, no direct one-to-one reflection relation to snowpack properties is possible. For the measurement c, the next day, probably the same density decrease is responsible for the similar reflection. The thin layer of higher density at 110 cm (Fig. 5.5c) is possibly the reason for the broad reflection at 8 ns (Fig. 5.3c). Due to snowfall with graupel during the radar measurements, this record also contains reflections above the snow surface (Fig. A.1).

In contrast, the internal reflections in March are very much dominated by strong crusts, which

were formed at the snow surface through starting melt processes at this low elevation and buried by further new snow events. Multiple internal layers in the snowpack are temporally traceable over several weeks. Since a noticeable snowpack above the antennas was recorded (13.02.09), the first meteorologically remarkable influence on the snowpack, besides of large new snow events, happened at the end of February. Figure 5.4B gives an overview of the temperature and snow-height conditions at the AWS-location for the measurement period. On 24.02.09 the snowpack at the weather station decreased by 20 cm in height in less than 2 days. The snow surface was additionally wetted by some rain initializing the next snow fall period with again more than 20 cm of new snow in less than 24 hours. This snowpack was compacted again and decreased in height by more than 50 cm towards the 06.03.09. Temperatures far above 0° C (up to 9.5° C, Fig. 5.4B) and a temperature decrease on the measuring day resulted in a strong melt crust at the snow surface, as obvious from the density increase in Figure 5.5d. The snowpack layers, which preliminarily decreased on the 26.02.09 resulted in another melt crust which was buried by the following snowfall event. These two melt crusts are visible in the P-visualization of the 06.03.09 (Fig. 5.3d) as well as in the manually recorded density profile (Fig. 5.5d). At $\tau = 8.2$ ns (Fig. 5.3d) the buried crust (c#1) is indicated by the positive peak and at about 11–12 ns a very strong amplitude with a positive – negative phase sequence (Fig. A.2) is visible which represents the snow-surface crust (c#2) that developed at that day. The absolute position of these events is also indicated in Figure 5.4C. Another strong precipitation event with more than 30 cm of new snow followed this measurement campaign. Both crusts are still visible in the measurements on the 12.03.09. Towards the 14.03.09, the snow height above the GPR antennas increased another 20 cm (Tab. 5.2; Fig. 5.3f), which was not measured by the AWS. Most likely a strong wind event, which was recorded by a nearby station on the evening of the 12.03.09 caused some snow accumulation at the test site. A strong increase in air temperature on 14.03.09 resulted in high radar reflection rates at the snow surface as visible in Fig. 5.3f. This snow surface formed the third crust (crust#3) during the day, recognizable in all later radargrams until the 25.03.09. Due to the higher temperatures in the middle of March (Fig. 5.4B) and therefore, likely melt processes, c#3 covers a large range of reflections in TWT at the snow surface as visible in Figure 5.3g. Likely, this large reflection range is caused by at least two strong reflections, one at the lower border of the crust and the other one at the upper border at the transition to air (Fig. 5.5g). At the following measurement (25.03.09) c#3 was buried by 40 cm of new snow the previous day. Due to the strong temperature differences ($\Delta T = 17$ K) in the period between the last measurement and this campaign (Fig. 5.4B) the internal crusts c#1 and c#2 were strongly influenced by melting and freezing processes and therefore levelled together to hardly distinguishable layers. The measurement in the beginning of April was more influenced by melt processes. We recorded an isothermal snowpack, with wetness intrusions down to 96 cm in the profile. The strong reflection amplitude at about $\tau = 8.6$ ns (corresponding to this depth) confirms this observation (Fig. 5.3i). Further wetness and density differences were recorded as

reflections.

5.3.3. Snowpack stability

We next discuss stability properties, although a temporal observation of typical weak layers in regard of avalanche release cannot be presented within this data set. A reflection at a layer boundary, which failed in the stability test was recorded at the 13.02.09, where the failure happened on an early stage (CT 9) below some recently fallen loose new snow. On 06.03.09 the stability test resulted in a crack at a high rank (CT 24) slightly below the surface within the recorded crust c#2 . Other typical weak layers, such as buried surface hoar (Schweizer and Wiesinger, 2001; Hägeli and McClung, 2003), were not observed above the antennas in this winter season. It remains the question if such layers or layer boundaries can be observed with the utilized radar system. However, Schweizer and Wiesinger (2001) state that only in 50% of skier-triggered avalanches a weak layer was discovered. In the majority of events, snowpack failures are described as interface failure. Interfaces with a distinct change in hardness and density are likely recordable by radar systems. Additionally, we are able to determine the amounts of loads of new snow over former surfaces, which are an important contributing factor for the evolution of self-released avalanches (see for details chapter 1.3; Schweizer and Wiesinger, 2001).

5.3.4. Snow wetness

In general, dry snow conditions were prevailling during the field measurements. However, significant wetness influence on the radar measurements is observable on 14.03.09 (Fig. 5.6). The first radar record was obtained in the morning with already positive air temperatures but not observeable melting at the snow surface. The second measurement was conducted in the afternoon with remarkable melt processes, but limited to the snow surface. Figure 5.6 clearly reflects these circumstances. The snow surface has a completely different reflection signature in the afternoon, while the lower parts are equal concerning the reflection and phase structures. Additionally, one can determine very accurately the depth of the melt intrusion on that day, which is an important gain of knowledge for the prediction of wet snow avalanches. Our results indicate that radar measurements from beneath the snowpack are a sufficient technique to record melt intrusions with depth and observe these intrusions temporally. The digging of a snow pit, however, does not provide a comparable information. Recording infiltrating water in snow pits is difficult, because the pit acts as a drainage and distorts the flow path. Due to its destructive nature, it is also not possible to make comparisons from day to day, or only statistically, because there is a large spatial variability (Machado, 2000). Furthermore, the pit wall is exposed to ambient air temperature and solar irradiance and thereby altering the depth of the melt influence. Radar measurements from above the surface, however, are strongly influenced by the melt layer, making

a clear detection of the melt front very difficult, because a transition dry – wet is easier detectable than wet – dry. This information can only be provided by upward-looking radar systems.

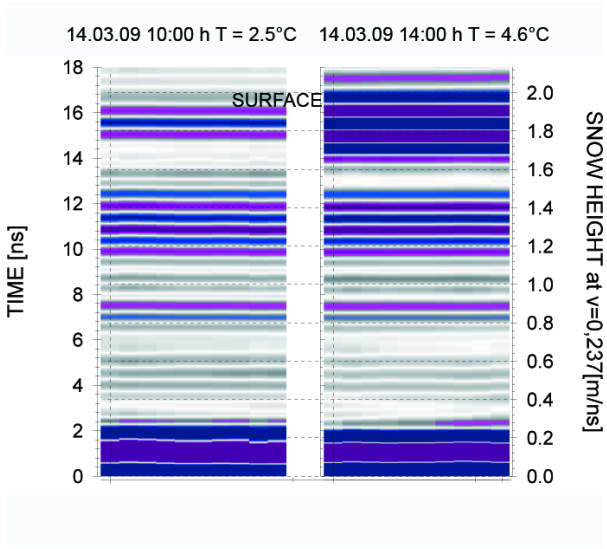

Figure 5.6.: Influence of infiltrating wetness in the snowpack on two radar measurements recorded the same day at different time periods, which are indicated above together with the prevailling air temperature.

5.3.5. Settling - Compaction of the snowpack

Especially the continuous destruction-free observation of the same snow column over time enables insights into the characteristics of settlement and involved processes. To investigate the related features we define as $z_n(t_i)$ the position of reflector c_n ($n = 0, 1, 2, 3$) at time t_i (with $n = 0$ being the constant snow-ground interface). The thickness of layer n between two reflectors n and the one below, $n-1$,

$$d_n(t_i) = z_n(t_i) - z_{n-1}(t_i) = \frac{1}{2}\left(\frac{\tau_n(t_i)}{\bar{v}_n(t_i)} - \frac{\tau_{n-1}(t_i)}{\bar{v}_{n-1}(t_i)}\right)$$

changes in the period t_i to t_{i+1} by

$$\Delta d_n|_{t_i}^{t_{i+1}} = d_n(t_{i+1}) - d_n(t_i) = \frac{1}{2}(\tau_n(t_{i+1})v_n(t_{i+1}) - \tau_n(t_i)v_n(t_i)),$$

where $\tau_n(t_i)$ is the two-way travel time of the n-th reflector at time t_i and $\bar{v}_n(t_i)$ the mean wave speed over the whole column from the antenna to the reflector at time t_i. To simplify, we use a temporally and vertically constant $\bar{v} = 0.237$ m/ns. We normalize the absolute thickness change Δd_n by the mean layer thickness

$$\bar{d}_n|_{t_i}^{t_{i+1}} = \frac{1}{2}(d_n(t_{i+1}) + d_n(t_i))$$

in the respective time period to derive the relative change in thickness of layer n, which yields the dimensionless strain

$$S_n|_{t_i}^{t_{i+1}} = \frac{\Delta d_n|_{t_i}^{t_{i+1}}}{\bar{d}_n|_{t_i}^{t_{i+1}}} \tag{5.4}$$

observed in the time interval t_i to t_{i+1}. From this the strain rate follows as

$$S_n^*|_{t_i}^{t_{i+1}} = \frac{S_n|_{t_i}^{t_{i+1}}}{t_{i+1} - t_i} \tag{5.5}$$

with dimension 1/time, for which we will use the units 1/s, i.e. per second. Note that as we have only a limited number of observations at times t_i, we can only use the difference quotient, but cannot approximate the differential quotients of the actual strain rate.

Table 5.3 displays the change in position above ground of specific layer reflectors in TWT and Figure 5.4 shows the strain, strain rates (Fig. 5.4D) and the radar measured location (TWT-depth conversion by $\bar{v}$) of the layers in comparison to the snow surface (Fig. 5.4C). The radar-measured change in snow height of these layers is due to two reasons, which can have an opposing effect on travel time. First, an altered TWT is caused by the physical change of the reflector location due to settlement of the snowpack. Second, due to densification or melt water intrusions the wave speed is reduced and therefore the TWT of the observed reflection increases. For example, a compaction of the underlaying 1.0 m thick snowpack of $\Delta\rho = +100$ kg/m^3 decreases the wave speed by about 6–7% for reasonable density values (100–500 kg/m^3) in snow, resulting in an increased TWT. The apparent strain rates of specific layers can become negative if the TWT of the radar waves changes variably for various reflectors in the snow cover. This is the case for the reflectors c_2 and c_1 at the time range between 14.03.–18.03.09 (Tab.5.3; Fig.5.4). While the snow layer between the antennas and c#1 is decreasing by about 4% in TWT, c#2 is recorded as being constant in time. As the reflector c_1 is situated below c_2, and the TWT of c_1 decreases, we would therefore expect a density increase of about 50 kg/m^3 in the layer between c_1 and c_2 to reduce the wave speed to result in a constant TWT of c_2 in the measurements with a time period of four days. This density increase between c#1 and c#2 was not observed in the snow pits (Fig. 5.5f, g). Therefore, we expect melt water intrusions to reduce the wave speed as a consequence of the relative warm temperatures the days before the 18.03.09 (Fig. 5.4B).

Obviously, the highest strain rates were present in the period from the 12.03.–14.03.09 (Fig. 5.4D). This is due to the strong new snow load the days before the 12.03.09 and the increasing temperatures in this time period (Fig. 5.4B). At this time of the winter season the lower parts of the snowpack still participated remarkably in the settlement, which resulted in an increase in density below c#1 (Fig. 5.5f, g). Additionally, for snow conditions without melt water percolation the strain rates are usually higher for layers closer to the snow surface, due to on average lower densities and a stronger influence of meteorological parameters at the upper parts of

the snow cover (e.g. Fig. 5.6). With specific layers as tracers, it seems possible to determine and quantify the strain rates of the snowpack in relation to prevailling snow and weather parameter, given that wave speed is either constant or adequately measured. If compaction or moisture intrusions are not uniformly vertically distributed, wave-speed values have to be considered for each layer individually.

Table 5.3.: Location of the three temporal traceable internal reflectors and their spacings in the time domain of ($\triangle\tau|_{n_i}^{n_{i+1}}(t_i)$), the number of days between the measurements as well as the average (mean) and the upper quartile (Q3) of the temperature within the time period between the measurements.

Date time t_i	c_1 $\tau_1(t_i)$ [ns]	c_2 $\tau_2(t_i)$ [ns]	spacing $\Delta\tau|_{c_1}^{c_2}(t_i)$ [ns]	c_3 $\tau_3(t_i)$ [ns]	spacing $\Delta\tau|_{c_2}^{c_3}(t_i)$ [ns]	days	mean/Q3 temperature [°C]
06.03. 10:20	8.5	11.87	3.37				
12.03. 10:30	7.67	10.38	2.71			6	-2.05/-1
14.03. 10:00	7.16	9.5	2.34	14.66	5.16	2	-0.10/+0.4
18.03. 10:00	6.74	9.5	2.76	13.97	4.47	4	+0.97/+2
25.03. 10:30				13.97		7	-2.86/-0.1

5.4. Interpretation - Physical origin of reflections

The gathered physical information of the presented radar records are the occurrence and the location of a reflection in the snowpack, the reflection's magnitude and its phase structure. The physical origin defines the radar-signal response yielding these information. In dry snow conditions density variation is the sole parameter influencing the dielectric permittivity (Kovacs et al., 1995; Mätzler, 1996). Therefore, the reflectivity can be determined utilizing the magnitude of density variation at a two-media transition. Marshall et al. (2007) applied an equation in which the layer thickness and the used frequency contribute to the determination of the effective reflectivity R_i (eq. 5.6),

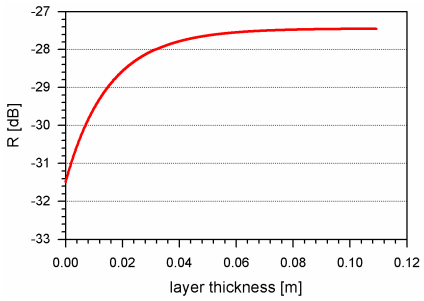

Figure 5.7.: The influence of layer thickness on the calculated effective reflectivity (R_i).

$$R_i = |\Gamma_i|^2, \tag{5.6}$$

$$\Gamma_i = \frac{r_i + \Gamma_{i+1} e^{-2jk_i d_i}}{1 + r_i \Gamma_{i+1} e^{-2jk_i d_i}}, \tag{5.7}$$

with k_i the wave number, d_i the layer thickness and Γ_{i+1} the reflection response of the boundary situated above boundary Γ_i. This approximation was applied to the data of the snow density and is shown in Figure 5.5. Heilig et al. (in press) present the theoretical backgrounds in further detail. The calculated effective reflectivity of an embedded ice layer ($\rho = 918$ kg/m^3) in a homogeneous snowpack ($\rho = 200$ kg/m^3) is displayed as a function of layer thickness in Fig. 5.7. The given densities are in accordance with the values of Marshall et al. (2007). As the frequency is not modulated and the layer thickness is in the exponent of the equation (5.7), the calculated R_i becomes an exponential function. Therefore, a thickness of the embedded ice layer of about $d > 5$ cm results in the highest effective reflectivity. Layers with a larger thickness do not increase the reflectivity and for thicknesses below 2 cm the reflectivity is remarkably decreasing but, for this input data, still appears as reflection as being considerably larger than $R_i = -70$ dB. This seems to be sufficient for reflections to be detectable. Heilig et al. (in press) assume that an effective reflectivity of about $R_i = -70$ dB or larger results in a distinct reflection in the radargram, if the layer thickness is adequately developed ($d_i \geq \lambda_s/10$; Olhoeft, 1998) and no interference occurs. The data presented in Figure 5.5 confirm this assumption, conditionally on the spatial variability of the snowpack, which was larger than expected for a plain measurement field. As the antennas together with the cover-box were arranged in a snowpack at approximately 50 cm snow height, all snow parameters beneath these 50 cm are not recorded. Additionally, the strong influence of the direct waves prevented singularly evaluable reflections of the first 20 cm above the plastic box. Considering only density and reflectivity values above 80–90 cm in the snow pits, the calculated effective reflectivity values of about $R_i \geq -70$ dB can be correlated to recorded reflections. Exceptions are the two small dense layers in Figure 5.5b and c with a density gradient at the layer transition of about $\Delta\rho = 120$ kg/m^3 (b) and $\Delta\rho = 170$ kg/m^3 (c), which were with $d_i = 0.5$ cm likely too thin for such low permittivity differences in comparison to

embedded ice layers. All other reflectivity values larger than $R_i = -70$ dB have a corresponding reflection in the radar measurements, although they are often not separable. Obviously, it is not possible to separate reflections, which interfere with each other, because they are situated too close together. In Figure 5.5, especially in parts e, f, g and h, where various adjacent reflectivity values (blue diamonds) are above the threshold, the corresponding reflections in Figure 5.3 and A.2, A.3 appear usually as numerous peaks and several consecutive reflection half cycles. The larger bandwidth of a FMCW system would probably improve the ability to distinguish among the layer transitions (see appendix C).

Regarding the phase sequences, we can first state that all reflections correspond to dielectric permittivity changes. In dry snow conditions, positive or negative density gradients influence the appearance in phase sequences. The direct wave or mother wavelet, as the first signal observable in all raw radargrams, has a negative – positive phase sequence (– +) for the here utilized radar system. A phase reversal occurs in dry snow conditions, when the density gradient is positive in radar-wave direction (from the ground to the snow surface). Therefore the strong negative density gradients in measurement a and b (Fig. 5.5) at about 118 cm (a) and about 92 cm snow height (b) are obtained with a negative – positive phase sequence. All snow surface reflections before measurement d have a (– +)-sequence, too, and appear to be in agreement with the prevailling conditions of a permittivity decrease from snow to air (Fig. 5.3). Strong positive density gradients in combination with a calculated effective reflectivity value of $R \geq -70$ dB, on the contrary, result in a phase reversal with a (+ –)-sequence. This is observable for all crusts within the snowpack and at the surface, apart from crust c#1 for some measurements (Fig. 5.3 e.g: d, f, g). The circumstances, that some c#1-reflections do not result in a phase reversal are not contradictory to the physical principles. Likely, the reflections of the density decreases slightly below the crust interfere with the crust reflection, which causes the observed phase structure. Especially the measurement e (Fig. 5.5) shows a remarkable decrease in density below the crust and thus an almost comparable negative phase amplitude in relation to the positive oscillation. The smaller, with a lower gradient developed density decreases in the measurements f and g (Fig. 5.5) appear in a distinctly less developed negative phase and by this support this interpretation.

Especially the phase reversal of the near surface signal for the two measurements in mid March (e, f) is a distinct example for the influence of temporal changes of the dielectric permittivity on the phase sequence. In part e, the low-density new snow below the surface has a phase sequence in correspondence to the mother wavelet, while in part f the sequence appears inversely (Fig. 5.3). A crust evolution at the surface altered the reflection response and a moisture intrusion later in the afternoon increased this phase appearance (Fig. 5.6).

Regarding the normalized amplitude, a quantitative comparison is not possible. In this study, the values should only be regarded as qualitative indicators, as a real normalization is not possible so

far. The antennas were buried in the snowpack for over two months, with the consequence that influences of different temperatures and humidity occurrences within the plastic box can not be completely neglected. However, the maximum amplitude values of specific reflections confirm qualitatively the previous observations. Apart from the first measurement (13.02.09), where the surface amplitude is still influenced by the direct wave and therefore shows a far too high amplitude, all surface reflection magnitudes of loose snow at the surface are situated distinctly below surface-crust reflections (Fig. 5.4A). Especially the new-snow layer of the 12.03.09, above the surface of the previous radar record, approves this. The magnitude of internal reflections appear always in the same graduation (c#1 < c#2 < c#3).

5.5. Conclusion

We could show that it is possible to observe the temporal evolution of the snowpack using upward-looking GPR technique from beneath the snow cover. The results are encouraging in several aspects, technically and scientifically. Regarding the difficulties concerning the antenna coverage of an uneven surface, the accuracy of the snow-height determination of the radar measurements is in good agreement with the probed snow depth. We achieved an accuracy slightly below the one of ultrasonic snow height sensors. In contrast to the sonic sensors, the used radar is feasible of recording internal layers and following their temporal evolution. In the determination of SWE values, this study is in good agreement to previous works using FMCW radar systems. The utilized system is a suitable technique to measure automatically the infiltration of liquid water with depth due to melt processes at the surface. These measurements could be a supplemental contribution to the predictability of wet snow-avalanche events. By the use of internal layers as tracers, we determined different strain rates for layers, which are closer to the surface than for deeper layers. The phase sequences in relation to the effective reflectivities enable the relation of snow layers to reflections. For the case of a highly resolved temporal observation of the snowpack with the utilized pulsed radar systems, it might be possible to improve the predictability of avalanches (e.g. wet snow avalanches or avalanches triggered by large accumulation rates) and to gather spatial information of internal layering in areas, which are difficult and dangerous to access. In combination with regularly recorded snow pits, a more detailed conclusion on the evolution of internal layers with time is possible and thereby, a better validation of snowpack simulation models achievable.

Bibliography

Annan, A., 2002. Gpr - History, Trends, and Future Developments. Subsurface Sensing Technologies and Applications 3 (4), 253–266.

Bavay, M., Lehning, M., Jonas, T., Löwe, H., 2009. Simulations of future snow cover and discharge in Alpine headwater catchments. Hydrological Processes 23, 95–108.

Colbeck, S., Akitaya, E., Armstrong, R., Gubler, H., Lafeuille, J., Lied, K., McClung, D., Morris, E., 1990. The international classification for seasonal snow on the ground. Tech. rep., International Commission of Snow and Ice of International Association of Scientific Hydrology / prep. by Working group on Snow Classification.

Comm. Glaciology, 2009. Mass balance Vernagtferner. [access date: 31.07.09].
URL `http://www.lrz-muenchen.de/~a2901ad/webserver/webdata/massbal/index.html`

Egli, L., 2008. Spatial variability of new snow amounts derived from a dense network of Alpine automatic stations. Annals of Glaciology 49, 51–55.

Egli, L., Jonas, T., 2009. Hysteretic dynamics of seasonal snow depth distribution in the Swiss Alps. Geophysical Research Letters 36.

Escher-Vetter, H., Kuhn, M., Weber, M., 2009. Four decades of winter mass balance of Vernagtferner and Hintereisferner, Austria: Methodology and results. Annals of Glaciology 50, 87–95.

Gubler, H., 1981. An inexpensive remote snow-depth gauge based on ultrasonic wave reflection from the snow surface. Journal of Glaciology 27 (95), 157–163.

Gubler, H., Hiller, M., 1984. The use of microwave FMCW radar in snow and avalanche research. Cold Regions Science and Technology 9, 109–119.

Heilig, A., Schneebeli, M., Eisen, O., in press. Upward-looking Ground-Penetrating Radar for monitoring snowpack stratigraphy. Cold Regions Science and Technology.

Hägeli, P., McClung, D., 2003. Avalanche characteristics of a transitional snow climate – Columbia Mountains, British Columbia, Canada. Cold Regions Science and Technology 37, 255–27.

König, M., Sturm, M., 1998. Mapping snow distribution in the Alaskan Arctic using aerial photography and topographic relationships. Water Resources Research 34 (12), 3471–3483.

Kovacs, A., Gow, A., Morey, R., 1995. The in-situ dielectric constant of polar firn revisited. Cold Regions Science and Technology 23, 245–256.

Kronholm, K., Schweizer, J., 2003. Snow stability variation on small slopes. Cold Regions Science and Technology 37, 453–465.

Lehning, M., Bartelt, P., Brown, R., Russi, T., Stöckli, U., Zimmerli, M., 1999. Snowpack model calculations for avalanche warning based upon a new network of weather and snow stations. Cold Regions Science and Technology 30, 145–157.

Lehning, M., Völksch, I., Gustafsson, D., Nguyen, T., Stähli, M., Zappa, M., 2006. ALPINE3D: a detailed model of mountain surface processes and its application to snow hydrology. Hydrological Processes 20, 2111–2128.

Machado, A., 2000. Spatial and temporal variability of meltwater pathways in a continental subalpine snowpack. Master's thesis, University of Colorado, Boulder, Colorado, USA.

Marshall, H., Koh, G., 2008. FMCW radars for snow research. Cold Regions Science and Technology 52, 118–131.

Marshall, H., Koh, G., Forster, R., 2005. Estimating alpine snowpack properties using FMCW radar. Annals of Glaciology 40, 157–162.

Marshall, H., Schneebeli, M., Koh, G., 2007. Snow stratigraphy measurements with high-frequency FMCW radar: Comparison with snow micro-penetrometer. Cold Regions Science and Technology 47 (1-2), 108–117.

McClung, D., Schaerer, P., 2006. The Avalanche Handbook, 3rd Edition. The Mountaineers, Seattle, USA.

Mätzler, C., 1996. Microwave permittivity of dry snow. IEEE Transactions on Geoscience and Remote Sensing 34 (2), 573–581.

Olhoeft, G., 1998. Electrical, magnetic and geometric properties that determine ground penetrating radar performance. In: Proceedings of GPR '98. 7th International Conference on Ground Penetrating Radar. pp. 177–182.

Perrin, S., Bibaut, A., Duflos, E., Vanheeghe, P., 2000. Use of Wavelets for Ground-Penetrating Radar Signal Analysis and Multisensor Fusion in the Frame of Landmines Detection. Systems, Man and Cybernetics, 2000 IEEE International Conference on 4, 2940–2945.

Pozdnoukhov, A., Purves, R., Kanevski, M., 2008. Applying machine learning methods to avalanche forecasting. Annals of Glaciology 49, 107–119.

Sandmeier, K., 1998. Reflexw version 4.1 manual.
URL http://www.sandmeier-geo.de/Download/reflexwmanual.pdf

Schneebeli, M., Laternser, M., 2004. A Probabilistic Model to Evaluate the Optimal Density of Stations Measuring Snowfall. Journal of Applied Meteorology 43, 711–719.

Schweizer, J., Wiesinger, T., 2001. Snow profile interpretation for stability evaluation. Cold Regions Science and Technology 33, 179–188.

Turcotte, R., Fortin, L.-G., Fortin, V., Fortin, J.-P., Villeneuve, J.-P., 2007. Operational analysis of the spatial distribution and the temporal evolution of the snowpack water equivalent in southern Québec, Canada. Nordic Hydrology 38 (3), 211–234.

van Herwijnen, A., Jamieson, B., 2007. Fracture character in compression tests. Cold Regions Science and Technology 47, 60–68.

Xia, J., Franseen, E., Miller, R., Weis, T., 2004. Application of deterministic deconvolution of ground-penetrating radar data in a study of carbonate strata. Journal of Applied Geophysics 56 (3), 213–229.

6. Conclusion and Outlook

This thesis demonstrates the capabilities of impulse radar systems for the development of further instrumentations to modernize and improve current methods in avalanche search and prediction techniques. The fundamental questions concerning feasibility and basic system components towards a further operational application are answered. The relevant system requirements are analyzed via various field campaigns ranging from measurements from beneath the snowpack up to about 12 m above the snow surface.

Concerning the location of avalanche victims, this thesis shows that an implementation of impulse radar systems on a helicopter basis is feasible. Experiences of other studies, which applied GPR systems in a ground-based matter, showed that it is only possible with an airborne location operation to improve significantly the survival rate of buried avalanche victims not equipped with location devices. Due to the blocky surface conditions and the normally enormous spatial dimension of an avalanche debris, no ground-based radar application is able to shorten search duration. Based on the results of the various field campaigns, this study presents relevant results for the detectable range of a single antenna concept, which is 3–5 m for a flight-height range from 6 to 12 m. The introduced location algorithm works sufficiently for all kind of dry snow conditions. The utilized GPR system is also tested on its reflection magnitude and penetration performance in various snow conditions. An increasing flight height reduces the reflection magnitude of the snow surface and thereby, of a buried victim remarkably. This thesis confirms empirical results of other works, which assumed the decrease in reflection magnitude to be almost linear of a defined reflector in an increasing distance. The field results together with the modelling in wet snow avalanche conditions, lead me to conclude that an application of electromagnetic wave based sensor systems is not promising. Due to various changes in moisture content in an avalanche debris (vertically and horizontally), supplementally to permittivity alternations, multiple changes in electrical conductivity occur. Hence, a reflection hyperbola from the buried victim is usually not sufficiently developed, due to various scattering and distraction at permittivity and conductivity changes. Furthermore, the orientation of the victim in respect to the antenna polarization is influencing the reflection magnitude of a victim, which decreases of about 30 % if the victim is orientated parallel to the antenna polarization. Therefore, a search flight with a flight height of about 10 m above ground, should be based on a defined grid with less than 5 m mesh width, according to the results of the detectable range measurements.

In summary, the present work investigated possibilities and limitations of impulse radar systems for an automatic airborne avalanche victim location. This study has not the pretension to present a ready-to-use instrument, but based on this work, it is now possible to adapt the system components of hard- and software to helicopters. Nevertheless, the software algorithm must be adjusted to less comfortable flight conditions in comparison to chairlifts. More turbulences cause more unsteadiness in the radar records, which influence the snowpack discrimination part of the algorithm. These adaptions must be performed by a future manufacturer of this system in close collaboration with operators and the software developer.

Concerning the snowpack sensor system, a feasibility study was performed. This study presents the direction, in which further research in GPR application in snowpack recording should be persecuted. The basic instrumentation, as frequency usage for dry and wet snow conditions and the test arrangement for a remote operation of impulse radar antennas over months is presented. This thesis demonstrates that specific characteristics of internal reflections (e.g. the phase structure) are in correspondence to physical snowpack properties as density gradient or moisture differences. The determined effective reflectivity of snowpack conditions lead to the assumption that below a certain threshold of $R = -70$ dB, a reflection in the radargram is hardly detectable with current instruments. On the contrary, one can assume that, if a reflection appears in the radargram, the physical properties of the layer boundaries in the snowpack, such as density gradient and layer thickness must lead to a calculated reflectivity above the threshold. Frequently GPR records in comparison to regularly snow pits in an environment, representative for the radar measurements, enable further statements on the reliability of the recorded snowpack conditions by radar. Repetition of such measurements on a daily basis may allow for quasi real-time and destruction free monitoring of the development of snowpack stratigraphy and concurrent information to estimate avalanche danger. These measurements should be conducted with zero-offset antennas (transmitter and receiver in a fixed small distance) and with multi-offsets arrangements (transmitter and receiver are disarranged to each other on certain distances) to determine different wave speeds for various layers in the snowpack. A comparison to other electromagnetic wave transmitters, such as stepped frequency or frequency modulated continuous wave system (FMCW) can reveal the respective potential in accuracy and resolution of each system in direct comparison. As radar system components for stepped frequency and FMCW antennas are now often attached in cellular phones, the prices for such components may decrease, while the availability increases, which leads to the assumption that such antenna systems can be alternatives to GPR technology in the future.

This study provides an initial step for prospective autonomous monitoring of snow stratigraphy also in potentially unstable slopes without risks for the investigators. Further research, basing on the here presented results, investigates, employs and advances the application of remotely operated upward-looking radar systems to non-destructively image and characterize the local

physical properties of the snowpack, and assimilation thereof into an existing model of snowpack evolution.

Appendix

A. Radargrams of the time series 2009

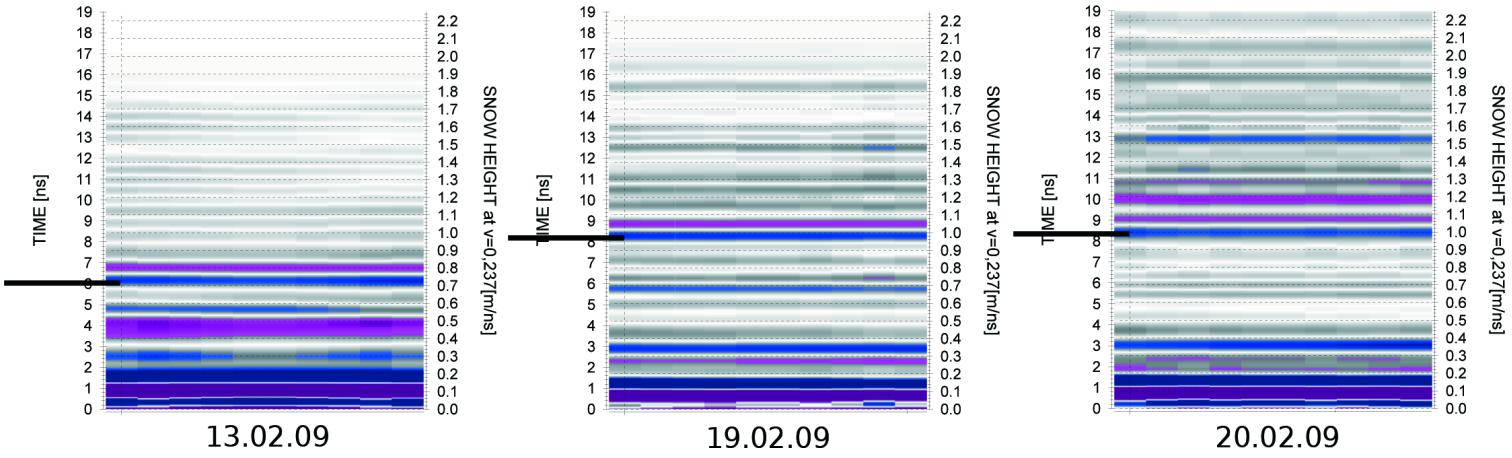

Figure A.1.: Time series from the 13.02.–20.02.09 at the Grünsee - location. The horizontal black bars indicate the snow surface. The snow height values are calculated utilizing $\bar{v} = 0.237$ m/ns.

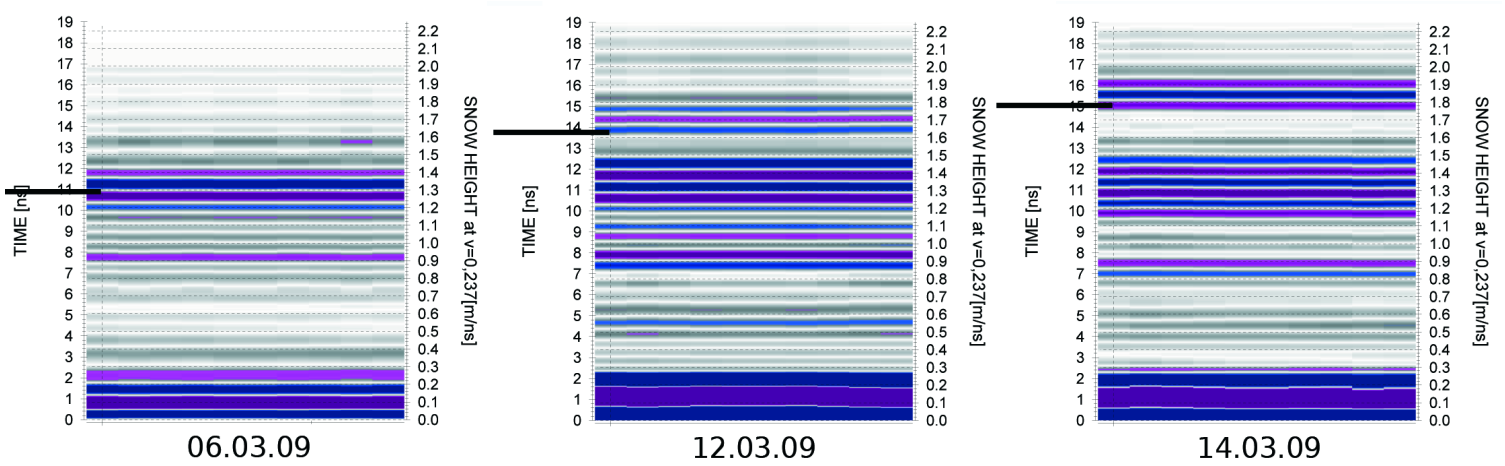

Figure A.2.: Time series from the 06.03.–14.03.09 at the Grünsee - location. The horizontal black bars indicate the snow surface. The snow height values are calculated utilizing $\bar{v} = 0.237$ m/ns.

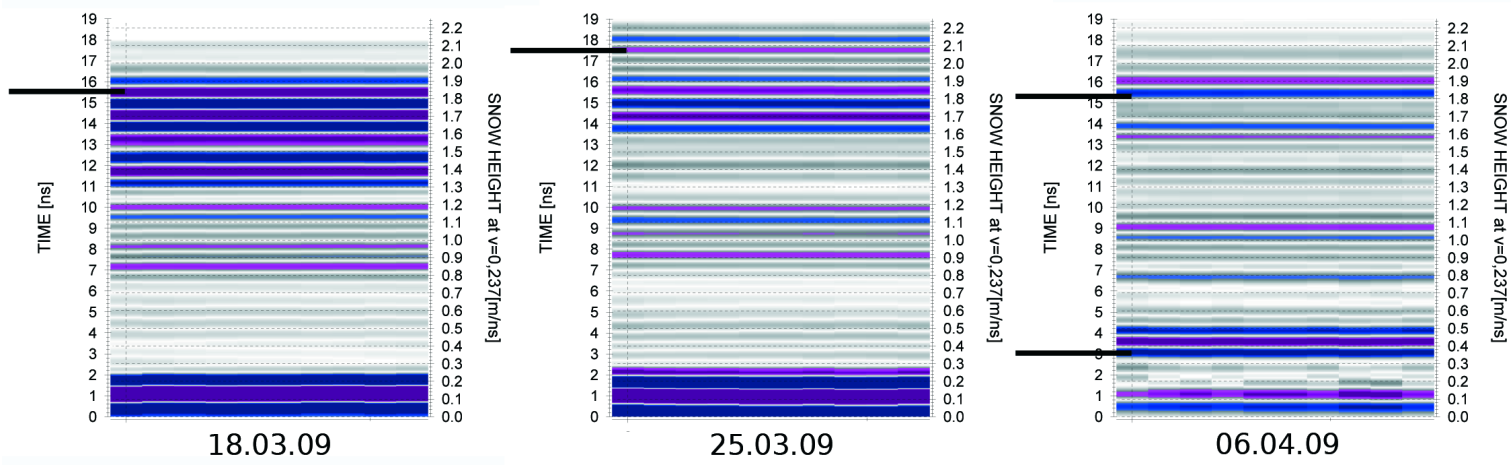

Figure A.3.: Time series from the 18.03.–06.04.09 at the Grünsee - location. The horizontal black bars indicate the snow surface and additionally at the 06.04.09 the transition from air-snow beneath the snowpack. The snow height values are calculated utilizing $\bar{v} = 0.237$ m/ns.

B. Next level for snowpack monitoring in real-time using Ground-Penetrating Radar (GPR) technology [1]

Achim Heilig, Michael Schober, Martin Schneebeli and Wolfgang Fellin

This part of the appendix is published as non peer-reviewed article in the conference proceedings for the *ISSW International Snow Science Workshop 2008*. The workshop took place from the 21. – 27.09.2008 in Whistler, BC, Canada. The here presented work is the basis, on which Paper 3 was extended towards a peer-reviewed publication accepted for publication in a special issue of the journal *Cold Regions Science and Technology*.

Abstract

Currently available snowpack monitoring methods are limited due to spatial resolution or to adequate weather and secure avalanche conditions. Snow pack monitoring is impossible, if the method is destructive as snow probing and thereby, the use for avalanche forecasts limited. Ultrasonic snow height sensors are not feasible for an application in snow deposition areas along ridges or in avalanche paths. For the validation and improvement of snowpack simulation models, it is of high importance to measure snowpack conditions with a high spatial resolution in real-time. We developed a measuring concept for the application of Ground Penetrating Radar (GPR) systems from below the snowpack. With vertically moving GPR-antennas it is possible to record reflections, which can be related to snow height and internal layering with adequate density

[1] published in similar form as: Heilig, A., Schober, M., Schneebeli, M., Fellin, W. 2008. Next level for snowpack monitoring in real-time using Ground-Penetrating Radar (GPR) technology, In: C. Campbell, S. Conger and P. Haegeli (Editors), Proceedings ISSW 2008, International Snow Science Workshop, Whistler, Canada, 21-27 September 2008, pp. 111-117.

steps and layer thickness. Field data sets from three winters in the Austrian Alps resulted in an average value for the velocity of propagation of pulsed radar waves in dry snow with a coefficient of variation (CV) of about 6%. Additionally we conducted some preliminary measurements in a wet spring snowpack to analyze the feasibility of the system. In contrast to Frequency Modulated Continuous Waves (FMCW) radar using X- and Ku- band frequencies, the snow-air-interface was detectable and thereby the snow height could be estimated. The applied sensor system is able to determine snow height, snow accumulation and erosion rates in combination with a known dielectric permittivity value of dry snow. In combination with nearby traditional snow height measurement systems, the snow water equivalent can be derived very accurately and with high temporal resolution.

B.1. Introduction

The automatic measurement of snow depth is currently limited to flat areas which are not exposed to avalanches. Direct snow depth determinations in avalanche paths are impossible, or very expensive to instrument with radars (Gubler and Weilenmann, 1986) or with synthetic aperture radars (Martinez-Vazquez et al., 2005). The possibilities for field observations are limited due to manpower or avalanche danger. For the local or regional avalanche warning services, at areas critical to arrive, additional information would be an immense support for the evaluation of the current avalanche danger. Currently, in case of doubt, an usage of explosives is made to verify and reduce the avalanche danger. This technique requires helicopters or special on purpose fabricated railways to get to the points of interests and provides no internal information about the current snow conditions. Additionally, it is very expensive to determine the avalanche danger with explosives and helicopters. Otherwise, the regional avalanche danger level is estimated by manual snow pits, which require a huge effort and result in rare point measurements. For short-term predictions and localized danger evaluations these field analysis are not adequate. Especially for the information about the formation of snow depositions along ridges or within avalanche paths an automated snowpack information system will be useful. A sensor system buried in the ground and operating independently of the current snow and weather conditions will transmit the recordable snow conditions to the responsible avalanche warning centers in real-time. Although spatial resolution will be coarse, the measurement can be taken at all critical locations. The previous research work on sensor systems for the non-destructive analysis of the snow stratigraphy (Gubler, 1981; Gubler and Hiller, 1984; Koh et al., 1996; Schneebeli et al., 1998; Waldner et al., 2001; Harper and Bradford, 2003; Marshall et al., 2004) lead us to conclude that radar is the the most reliable technique to monitor snowpack properties. Marshall et al. (2007) received convincing results with the application of FMCW radar in resolving snowpack stratigraphy from above the surface. The problem of FMCW radar is that, up to now, the systems

are custom-made and single-unit productions. Additionally FMCW radar needs a calibration measurement to eliminate artifacts before the snowpack record (Marshall et al., 2007). This will be very difficult to realize from below the snowpack. In contrast to FMCW, GPR is produced by several manufacturers and has a wide field of application.

The aims of the present study are: (i) to develop a measuring arrangement for the application of GPR from beneath the snowpack, (ii) to analyze the possibilities of GPR systems in quantifying snow stratigraphy and (iii) to determine the differences in the electromagnetic response for different snowpack properties. One additional aim of this research is the determination of an approximate value for the velocity of propagation of pulsed radar waves in dry snow conditions. This approximate value might simplify further interpretations of radar measurements in a way that snow height could be calculated from the radar data remotely.

B.2. Methods

B.2.1. Instrumentation

GPR-system

We used a commercially available RIS One GPR instrument (IDS, Ingegneria dei Sistemi, Pisa, Italy) with 900 MHz antennas for the ground based application beneath the snowpack. In order to generate a modulated signal in pulsed radar, the antennas must be moved. A modulation is needed to distinguish reflections caused by the snow stratigraphy from internal antenna signals. Otherwise, the system has to be operated throughout the whole winter to record a modulated snowpack. The energy consumption and the huge amount of data argue against an all-time usage of the system. A short time data request at specific times during the day would minimize this problem. By this, the practical implementation then needs an antenna moving horizontally or vertically in place.

Snow-data

A conventional snow profile (e.g.Colbeck et al., 1990) with density determinations was made to compare with the radar measurements. Additional snow profiles were recorded with a high resolution penetrometer (SnowMicroPen SMP) (Schneebeli et al., 1999). The SMP is a unique instrument to gather highly resolved depth profiles of penetration resistance (250 measurement values per millimeter). Density was estimated from penetration resistance according to Keller et al. (2004) as described in Heilig et al. (2008).

B.2.2. Theory

Kovacs et al. (1995) and Mätzler (1996) state that in dry snow dielectric permittivity is solely a function of density. Kovacs slightly improved the fit of Robin et al. (1969) to

$$\varepsilon_r^{'} = (1 + 0.845\rho)^2 \tag{B.1}$$

with ρ the density or "specific gravity" of firn or ice. Mätzler, however, applied several fitting formulas on known ice volume fractions in various snowpacks and compared the results to the effective medium formula of Polder and van Santen (1946). He concludes that an influence of a liquid layer is not detectable in dry snow conditions. In his opinion the Looyenga formula (Looyenga, 1965) with the empirical fitting parameters of $\varepsilon_h = 0.9974$ for the host material (air) and $\varepsilon_{so} = 3.215$ for the solid parts (ice) with b $= \frac{1}{3}$ provided good results and the parameter are very close to the actual values

$$\varepsilon_r^b = (1 - \upsilon) \cdot \varepsilon_h^b + \upsilon \cdot \varepsilon_{so}^b \tag{B.2}$$

υ describes the ice volume fraction, the quotient of snow-density through ice-density.

Both equations differ by less than 2% (Tab. B.1) in resulting dielectric permittivity applying the density records measured of the last three winters at the test site in the Austrian Alps (Fig. B.1).

Table B.1.: Comparison of the two different dielectric permittivity determinations of density (Kovacs et al., 1995; Mätzler, 1996). The calculated permittivity values basing on equation (B.1) and equation (B.2) were divided and the average and median values of the manual density records of the referring winter season were displayed in percent values. The sample size (N) of the respective winter is displayed as well in the table.

	N	mean $\varepsilon_{Kov}/\varepsilon_{Maet}$ [%]	median $\varepsilon_{Kov}/\varepsilon_{Maet}$ [%]
06	50	1.8	1.9
07	57	1.9	1.9
08	14	1.9	2.0

As the stratigraphic resolution and therefore, the influence of the snow on the radargram depends on the dielectric permittivity, we analyzed various data sets on changes in the calculated values. The permittivity was derived from manual density measurements and density estimations from the SMP data using both equations (eq. B.1,B.2)

To calculate the speed of electromagnetic waves in snow, we applied the following equation

(Jaedicke, 2003; Daniels, 2004)

$$v_s = \frac{v_a}{\sqrt{\varepsilon_r}} \tag{B.3}$$

with v_s the velocity in snow and v_a the velocity in air, the speed of light.

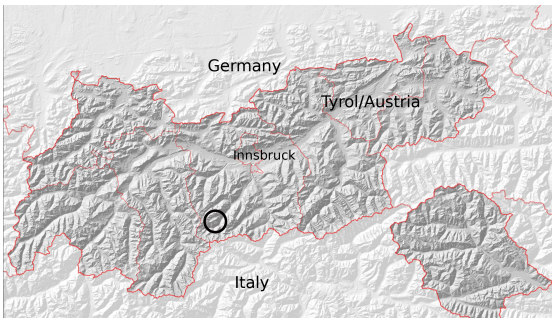

Figure B.1.: Map of the test site. The black circle marks the location of the field tests.

B.2.3. Test arrangement

Since the frequency of GPR antennas is not modulated the interpretability of short term radar records is distinct improved by moving the antenna. Measuring from below the snowpack requires either horizontal or vertical movement. The horizontally moved antenna did not provide evaluable results for a movement distance of about 1 m length. Therefore, we arranged an experiment set-up with a vertically moved antenna (Fig. B.2). We applied different test arrangements and varied the movement distance as well as the speed and manner. We used a lever and alternatively a pneumatic system. The variation of the movement ranged between 0.1 m to 0.3 m. The lever system resulted in a fast and continuous movement, while the pneumatic system resulted in a very slow and jerky uplift.

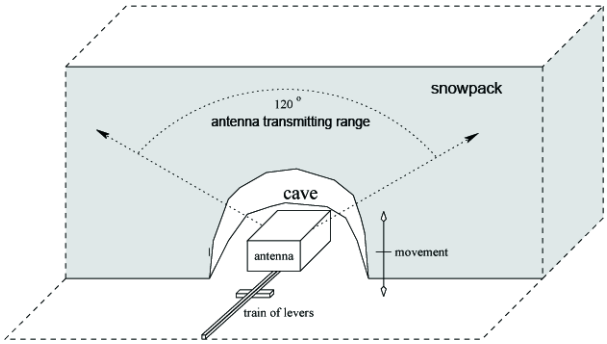

Figure B.2.: Sketch of the test arrangement for measurements with a vertically moved antenna by the use of a lever.

B.3. Results

B.3.1. Radar records from below the snowpack

The results of the vertical measuring set-up were interpretable and several interfaces could be distinguished. The artifacts, resulting from internal antenna signals of the GPR system, could be removed easily via this movement (Fig. B.3, B.5). We applied various movement heights with the lever system. The longer the uplift, the more of a circular movement the antenna will describe. With an uplift of $d = 0.1$ m the antenna will be turned by $\alpha_{0.1} = 5.7°$, with an uplift of $d = 0.3$ m, α will increase to $\alpha_{0.3} = 17.5°$. A 5° turn of the antenna is negligible in our opinion. In the following, we describe measurements with the 0.1 m movement to keep the circular movement-error negligible. Another error occurs by the conversion of two-way travel time values in depth values. We used the velocity of propagation of radar waves in snow, but measured across two medias, air and snow. Therefore, the conversion of the transition air-snow above the snow cave is not correct. Nevertheless we disregarded this error as the focus lies on the correct reproduction of the snow depth and the snow stratigraphy above the cave, which is not influenced by this error. In a future application the monitoring system will be installed in the ground probably in a plastics box, with the top of the box at the ground surface. Therefore, the snowpack can be measured without this conversion error.

B.3.2. Stratigraphic resolution with GPR systems

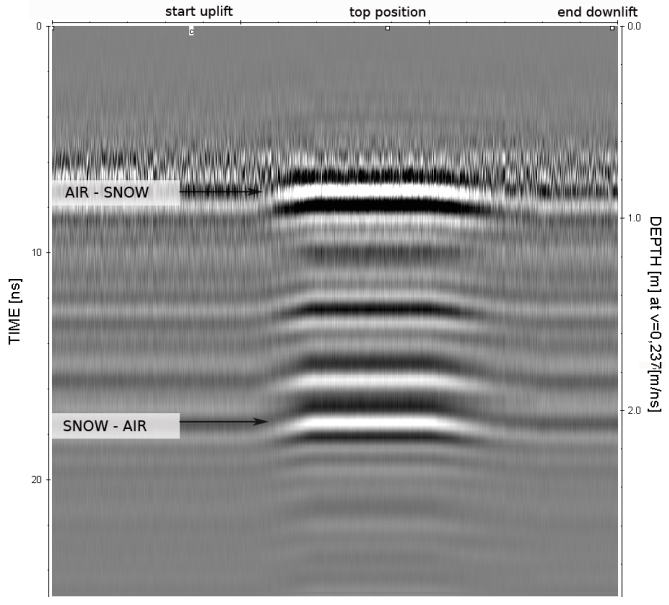

Figure B.3.: Radargram of measurements with a 0.1 m vertically moved antenna by a lever.

In January 2008 we performed field measurements on the Stubai Glacier in the Austrian Alps on about 2850 m a.s.l. (Fig. B.1). The results of a measurement with an uplift of 0.1 m are shown in Figure B.3. At least four reflections are distinctly developed. Named are the transitions from the snow cave to the snowpack (AIR - SNOW) and at the snow surface (SNOW - AIR). The antenna movement is reproduced by a slight ascent of the reflections at the start of the uplift and correspondingly by a slight descent towards the end of the down lift. The depth conversion of the two-way travel time is calculated for the mean velocity of propagation of the radar waves in snow. Therefore, the reflection ascent and descent values at the transition air – snow do not agree to the 0.1 m uplift. In contrast, the internal uplift reflections agree very well to the length of the vertical movement.

The internal reflections in Figure B.3 correspond with pronounced density and hardness steps in the snow profile (Fig. B.4). We marked the internal layer and the media transitions by black lines and turned the radargram by 180° to assimilate it to the profile. The radargram was scaled to fit the layering, but obviously the relative differences between both transitions and the internal reflections match well with the profile. By using $\upsilon = 0.237$ m/ns the calculated snow depth in Figure B.3 corresponds well to the $d = 1.0$ m from the cave to the snow surface in the snow profile (Fig. B.4), considering the fact that we were not able to shape the cave adequately perpendicular to the pit wall and uncertainties of 10 cm are possible.

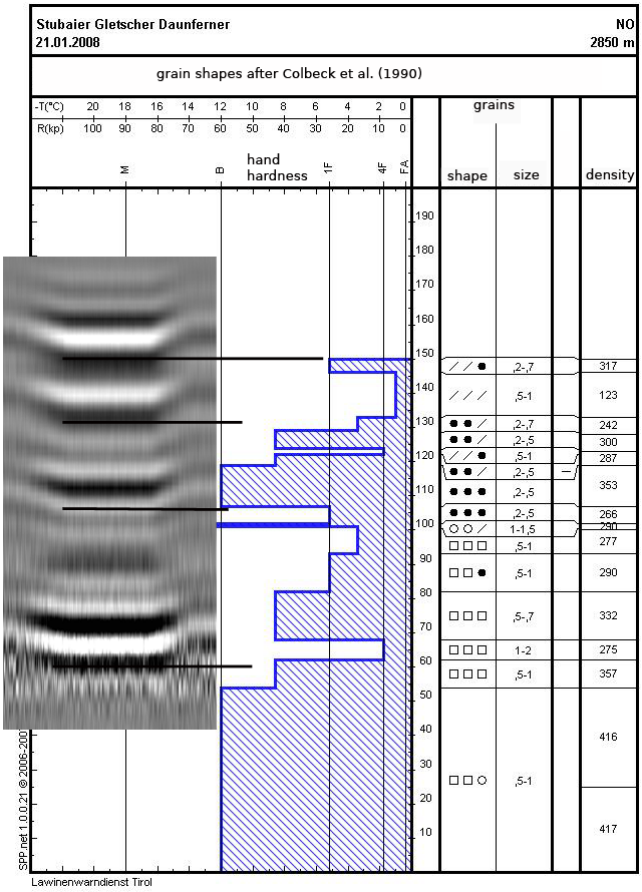

Figure B.4.: Direct comparison of the radar data and the conventional snow profile. The transition from air to snow in the cave was situated at about 0.6 m in the hand-profile. The reflections are linked to the corresponding layers or transitions by the black bars.

The density measurements of the conventional snow profile fit very exactly to the radar records (Fig. B.4) . The snow profile was dug to the glacier ice, while the radar records started at about 60 cm in the profile. Distinctive layers were recognizable in the snowpack with several various pronounced density steps. According to Mätzler (1996); Harper and Bradford (2003) and others, in dry snow conditions contrasts in dielectric permittivity are the only snow parameter causing reflections in a radargram. The permittivity however is weakly sensitive to small changes in density (Heilig et al., 2008), therefore, an adequate density difference is required to cause reflections in the radargram. Additionally, the vertical resolution of GPR depends on the wavelength and the velocity of propagation in the medium (Jaedicke, 2003; Daniels, 2004). With an applied system frequency of 900 MHz and a mean velocity of propagation in dry snow of $\bar{v} = 0.237$ m/ns (Tab. B.2), the radar theoretically resolves vertical stratigraphy down to about 12 cm layer thickness. This is based on the assumption of Daniels (2004) that the vertical resolution is ap-

proximately half of the wavelength ($\lambda/2$) for small divergence angles (angle here is approx. 0°). The reflections in Figure B.3, B.4 and B.5 confirm these theoretical approximations. The density step at 107 cm (Fig. B.5) with a layer thickness of 12 cm in the snow profile is clearly represented in the radar record at the corresponding depth. Furthermore, the strong density decrease above 133 cm can be related to the respective reflection in the radar records. Other density steps resulting in lower reflectivity values are not distinguishable in the radargram. Likely, because of the location adjacent to the dominating media transitions, constructive interference at 146 cm and destructive interference at 62 cm prevented the evolution of these reflections in the radargram.

In Figure B.5 it is possible to allocate the density steps at 107 cm and above 133 cm to internal reflections in the radargram. Both layers adjacent to the density steps have a sufficient thickness larger than the resolution limit and the contrasts in density are adequate to cause reflections. The next sharp density change is situated too close to the snow surface and probably interfere in reflections with the transition from snow to air and is thereby not distinguishable as a single reflection.

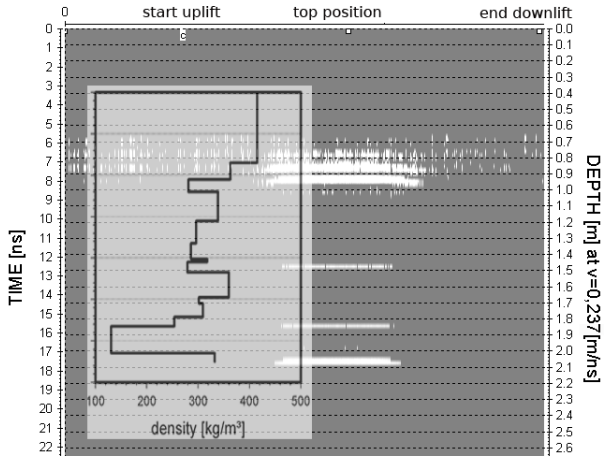

Figure B.5.: Density profile in comparison to the processed radargram. The cave position in the density profile is linked to the first radar reflection.

B.3.3. Differences in electromagnetic responses for different antenna positions

Different test arrangements were used to measure the interactions between snow and electromagnetic waves between winter 2006–2008. The data of these three winters were analyzed for differences in electromagnetic response for different antenna positions. A GPR antenna was used from above the snow surface up to 12 m as well as from beneath the snow surface. We calculated snow depths via the mean velocity of propagation for each radar scan and compared these depths with the results of snow probings. The agreement of both methods was good utilizing the resulting mean value in Table B.2. The velocity of propagation was calculated from directly

Table B.2.: Converted dielectric permittivity values (ε) for density measurements conducted between 2006 and 2008 for dry snow conditions. The permittivity has been calculated with equation (B.1) after Kovacs et al. (1995) and the velocity of propagation values (v) were calculated with (eq B.3). N is the sample size.

year	ε mean	ε stdv	CV	v mean [m·ns^{-1}]	v stdv	CV	N
06	1.6552	0.2298	14 %	0.235	0.017	7 %	50
07	1.5889	0.1674	10.5 %	0.239	0.013	5.5 %	57
08	1.5839	0.5839	8.5 %	0.239	0.011	5 %	14
mean	1.6162	0.1946	12 %	0.237	0.015	6 %	121

measured density and density estimated from penetration resistance (Tab. B.2).

The average value of the different velocity determinations is $\mu = \bar{v} = 0.237$ m/ns, the standard deviation of these 121 measurements is $\sigma = 0.015$ and the resulting coefficient of variation with $CV = \frac{\sigma}{\mu}$ is $CV = 6\%$. The accuracy of the snow height determination by using the mean value was adequate in every radargram (see also Fig. B.3, B.4, B.5). Furthermore, preliminary test measurements from above the snow surface in May 2006 with moisture in the snowpack penetrated a more than 2 m thick snowpack. It is not possible to apply a calculated average velocity of propagation value for moist snowpacks. If layers with different water contents exist, a specific velocity value has to be calculated for each layer individually. Due to the lack of adequate wetness determination for each single layer and due to the fact that the permittivity is no longer solely a function of density, it is more complex to calculate an average value for wet snow conditions. Nevertheless, it is still possible to monitor the interfaces with the applied GPR system.

B.4. Discussion

The results of field measurements for the development of an automatic snow sensor based on GPR technology are encouraging. First of all, two different arrangements for the field tests showed that the only solution for a practical GPR sensor system is a vertically moving antenna. We could show that for dry snow conditions an average velocity of propagation can be calculated. Even if the density variation is underestimated the mean velocity over the whole snowpack in natural dry snow conditions varied only about 6% as the analysis of density data for three winters showed. This fact shows that independently of a manual snow probe measurement the snow height determination with GPR instruments is adequately accurate for a remote snowpack monitoring. Especially, if considering that exact reflection determination in depth values is quite improper in a radargram, because of the difficult appointment of signal's first arrival (Daniels, 2004). However, this is still an acceptable result for most practical applications, especially

taking into account that the true values are very variable due to spatial variability. The presented average values were only determined for one region in the Austrian Alps (Fig. B.1). Geographical and meteorological conditions as the distance to the sea (salt or dust concentration) and the average air humidity can influence the average velocity of propagation.

The derived stratigraphic resolution of the radar data corresponds to the theoretical values. An adequate step in the gradient of density as well as in layer thickness can be reproduced in the radargrams. The question arises, if this vertical resolution is appropriate for the intended application. FMCW systems are probably more capable to resolve the stratigraphic layering in the snowpack and to determine their spatial variability but are not feasible in conditions with moisture in the snowpack for most frequency ranges (Marshall et al., 2007). However, the relatively cheap and established GPR technology will be more realizable and affordable for automatic snowpack monitoring. Additionally, a higher layer resolution is possible by increasing the applied antenna frequency. The spatial resolution of snow monitoring via GPR is not comparable to repeated laser scanning but the capability is completely independent of the meteorological conditions, which is an immense advantage compared to laser systems. Additionally, by increasing the number of sensors beneath the snowpack, it is possible to improve the interpolation among the measured points. In contrast to ultrasonic systems, these sensors can be installed at every slope aspect and angle. These circumstances allow placing the instrument at the most interesting and critical locations. If the average density of the snowpack can be estimated by nearby traditional measurements, snow water equivalent can be determined accurately and with high temporal resolution.

In wet snow conditions with a completely temperate snowpack the used GPR system was detecting the snow-air interface in a very attenuated way (Heilig et al., in press). Internal reflections were caused by water layers and not by density or hardness steps. Furthermore, in all spring measurements performed from above the snow surface, the snow and ground-interfaces could be detected in the radargrams (Heilig et al., 2008).

The development and deployment of such an automated snowpack monitoring system requires still a lot of work. Up to now, the problems of power supply, remote operation, remote data transmission have not been fully discussed in a further application. Nevertheless, these problems occurred already in other implementations as automatic weather stations or satellite techniques and should not be the obstacle for further investigations in this research.

B.5. Conclusion

This feasibility study demonstrated that it is possible to derive snow depth and major snow stratigraphic features from beneath the snowpack with a GPR system. Furthermore, an average

value for the mean velocity of propagation of the whole snow cover could be determined to calculate snow depths in high winter conditions independently of a manual snow profile.

Acknowledgment

Financial support for this research was provided by the Centre of Natural Hazard Management (alpS), PIEPS GmbH, WSL Swiss Federal Institute for Snow and Avalanche Research SLF and RHM (Risk and Hazardmanagement). IDS Ingegneria dei Sistemi kindly supported us with the radar system. For assistance in the field we thank S. Link, S. Unterader and S. Leimgruber. We would also like to thank H.-M. Schuler and K.J. Sandmeier for discussions that helped to improve the paper.

Bibliography

Colbeck, S., Akitaya, E., Armstrong, R., Gubler, H., Lafeuille, J., Lied, K., McClung, D., Morris, E., 1990. The international classification for seasonal snow on the ground. Tech. rep., International Commission of Snow and Ice of International Association of Scientific Hydrology / prep. by Working group on Snow Classification.

Daniels, D., 2004. Ground Penetrating Radar, 2nd Edition. The Institution of Electrical Engineers, London, UK.

Gubler, H., 1981. An inexpensive remote snow-depth gauge based on ultrasonic wave reflection from the snow surface. Journal of Glaciology 27 (95), 157–163.

Gubler, H., Hiller, M., 1984. The use of microwave FMCW radar in snow and avalanche research. Cold Regions Science and Technology 9, 109–119.

Gubler, H., Weilenmann, P., 1986. Seasonal snow cover monitoring using FMCW radar. In: ISSW International Snow Science Workshop 1986. pp. 87–97.

Harper, J., Bradford, J., 2003. Snow stratigraphy over a uniform depositional surface: spatial variability and measurement tools. Cold Regions Science and Technology 37, 289–298.

Heilig, A., Schneebeli, M., Eisen, O., in press. Upward-looking ground-penetrating radar for monitoring snowpack stratigraphy. Cold Regions Science and Technology.

Heilig, A., Schneebeli, M., Fellin, W., 2008. Feasibility study of a system for airborne detection of avalanche victims with ground penetrating radar and a possible automatic location algorithm. Cold Regions Science and Technology 51 (2-3), 178–190.

Jaedicke, C., 2003. Snow mass quantification and avalanche victim search by ground penetrating radar. Surveys in Geophysics 24, 431–445.

Keller, T., Pielmeier, C., Rixen, C., Gadient, F., Gustafsson, D., Stähli, M., 2004. Impact of artificial snow and ski-slope grooming on snowpack properties and soil thermal regime in a sub-alpine ski area. Annals of Glaciology 38, 314–318.

Koh, G., Yankielun, N., Baptista, A., 1996. Snow cover characterization using multiband fmcw radars. Hydrological Processes 10, 1609–1617.

Kovacs, A., Gow, A., Morey, R., 1995. The in-situ dielectric constant of polar firn revisited. Cold Regions Science and Technology 23, 245–256.

Looyenga, H., 1965. Dielectric constant of heterogeneous mixtures. Physica 21, 401–406.

Marshall, H., Koh, G., Forster, R., 2004. Ground-based frequency-modulated continuous wave radar measurements in wet and dry snowpacks, Colorado, USA: an analysis and summary of the 2002/03 NASA CLPX data. Hydrological Processes 18, 3609–3622.

Marshall, H., Schneebeli, M., Koh, G., 2007. Snow stratigraphy measurements with high-frequency FMCW radar: Comparison with snow micro-penetrometer. Cold Regions Science and Technology 47 (1-2), 108–117.

Martinez-Vazquez, A., Fortuny-Guasch, J., Gruber, U., 2005. Monitoring of the snow cover with a ground-based synthetic aperture radar. In: EARSeL eProceedings 4,. Vol. 2.
URL `http://www.eproceedings.org/static/vol04_2/04_2_martinez1.html`

Mätzler, C., 1996. Microwave permittivity of dry snow. IEEE Transactions on Geoscience and Remote Sensing 34 (2), 573–581.

Polder, D., van Santen, J., 1946. The effective permeability of mixtures of solids. Physica 12 (5), 257–271.

Robin, G. d., Evans, S., Bailey, C., 1969. Interpretation of radio echo sounding in polar ice sheets. Phil. Trans. R. Soc., Ser. A 265 (116), 437–505.

Schneebeli, M., Coléou, C., Touvier, F., Lesaffre, B., 1998. Measurement of density and wetness in snow using time-domain reflectometry. Annals of Glaciology 26, 69–72.

Schneebeli, M., Pielmeier, C., Johnson, J., 1999. Measuring snow microstructure and hardness using a high resolution penetrometer. Cold Regions Science and Technology 26, 101–114.

Waldner, P., Huebner, C., Schneebeli, M., Brandelik, A., Rau, F., 2001. Continuous measurements of liquid water contents and density in snow using tdr. In: Dowding, C. (Ed.), Proceedings 2. International Symposium and Workshop on Time Domain Reflectometry for Innovative Geotechnical Applications. pp. 446–556.

C. Non-destructive quantification of snowpack properties [1]

Achim Heilig, Hans Peter Marshall, Olaf Eisen, Martin Schneebeli

This part of the appendix will be published as non-peer-reviewed paper in the conference proceedings for the *ISSW International Snow Science Workshop 2009*. The workshop will take place from the 27.09. – 02.10.2009 in Davos, Switzerland. This article is a short review of the two different radar systems – FMCW and GPR systems, which are used for the record of snowpack properties to date.

Abstract

A temporal observation of the stratigraphy of seasonal snowpacks is only possible with non-invasive methods. Electromagnetic waves, specifically radar waves, proved to be the most appropriate technique to estimate internal snow parameters and media transitions non-destructively. Thereby, it is possible to estimate quantitatively snowpack stratigraphy and observe the snowpack evolution with time. Radar systems work as an active wave transmitter, which records reflection intensities with travel-time. Either the system modulates the signal on a defined frequency range, such as frequency modulated continuous wave systems (FMCW) or a short impulse is radiated at a center frequency and bandwidth. The stratigraphic resolution and the penetration depth of both systems depends on the system parameters. The frequency determines the penetration depth and sensitivity and the bandwidth determines the vertical resolution. In previous studies FMCW X- and Ku-band frequencies failed to penetrate a moist snowpack, but provided convincing results in resolving the snowpack stratigraphy. Pulsed 900 MHz antennas, as well as L- and C-band FMCW systems penetrated a wet snowpack up to one meter and measured adequate gradients in snow density. Current research in pulsed and modulated systems

[1] submitted, the 10.08.09 to the proceedings of the ISSW 2009, 27.09. – 02.10.2009, Davos Switzerland.

show that electromagnetic wave systems are convincing methods to quantitatively measure snow stratigraphy non-destructively.

C.1. Introduction

The determination of snowpack properties, such as stratigraphy and snow height, and changes thereof are essential features for compiling avalanche warning bulletins, preferably on a daily basis. For data assimilation in snowpack models the accuracy and spatial resolution depends on the input data. To date, the spatial resolution of these models is dependent on the spatial distribution of automatic snow height stations (Bavay et al., 2009). Schneebeli and Laternser (2004) noticed, that large daily new snow events are often unobserved by automatic snow height stations. Concerning the manual data acquisition, especially in slope and ridge regions, the data volume is limited by accessability and man-power. For avalanche warning services, further spatio-temporal snowpack data on both plain and slope areas are an important support for the regional risk and hazard management.

A spatio-temporal observation of snowpack properties is only possible, if the method is quickly applicable and non-destructive. Furthermore, temporal observations of internal snowpack conditions are constrained to non-invasive measurements. For spatial observations of properties, time consuming methods like probing or digging snow pits are not sufficient. In-situ observing and remotely operated radar systems seem most promising for operational implementation. To date, two different system types were successfully applied in snow and avalanche research, namely impulse radar, such as ground-penetrating radar (GPR), or frequency modulated continuous wave (FMCW) systems (Marshall and Koh, 2008).

In this study we compare two possibilities to measure snowpack conditions with radar systems and discuss their applicability in the quantification of specific parameters such as snow depth and layer determination.

C.2. Methodology

GPR-system

The use of impulse radars with high frequencies (2–7 GHz) to measure snow stratigraphy in an mountain snowpack, was firstly described more than 35 years ago by Vickers and Rose (1973). Recent works in Scandinavia and in alpine regions used impulse radar systems, such as ground-penetrating radar to determine the snow-water equivalent (SWE) (Marchand et al., 2001), snow depth and snow accumulation variability (Harper and Bradford, 2003; Machguth et al., 2006) as

well as to detect avalanche victims (Heilig et al., 2008).

Here, we used a GPR instrument with shielded antennas with a nominal frequency of about 800–900 MHz. Further processing and interpretation steps focus on distinguishing between snow stratigraphic reflections and noise or static signals caused by the test arrangement and antenna design. If the antennas are stationary, all signals appear in horizontally constant responses. Therefore, the antenna noise in pulsed radar systems partly masks the reflections caused by the snow stratigraphy, which makes it difficult to detect the snow signals. In order to remove this effect, the antennas are moved vertically resulting in a signal pattern in which instrumentally caused signals are recorded horizontally constant and reflections generated by stratigraphic parameters correspond to the vertical movement.

FMCW-system

FMCW applications in snow and avalanche research have comparable long history (e.g. Gubler and Hiller, 1984). Marshall and Koh (2008) review the research done on the use of FMCW radar for snow analysis. The example results from an FMCW radar system shown below are based on measurements made and reported in Marshall et al. (2007). This system operates in the X- and Ku-band frequencies, specifically 8–18 GHz. Since the snowpack was dry, the highest frequency and largest bandwidth was used for this study to maximize vertical resolution and sensitivity to stratigraphy, since penetration was not an issue. One advantage of FMCW radar is that a very large bandwidth can be used; in contrast, impulse radar systems typically are limited to a bandwith that is close to the center frequency. In a wet snowpack, L- and C-band FMCW systems are typically used (e.g. Yankielun et al., 2004; Koh and Jordan, 1995).

Like impulse radar, FMCW radar systems have instrumental noise, which must be removed before analysis. As with the impulse system, the antennas are typically moved vertically to differentiate the snowpack signals from instrumental noise (Fig. 2, Marshall et al., 2007). FMCW radar systems allow horn antennas to be used, which can have significantly more directionality than dipole antennas. This makes it possible to point the antennas at the sky, and use this signal to accurately remove instrumentation-related signals with a filtering algorithm (Fig. 3, Marshall et al., 2007). The instrumentation noise can change with temperature, therefore these "sky calibration" measurements are typically made periodically to do the best possible job of removing unwanted noise.

C.2.1. Test arrangement

The radar data of the present study conducted with GPR systems were recorded from beneath the snowpack. In order to enable a measurement system applicable in slopes with a predominant

avalanche hazard, we constructed a sensor system, which is not prone to avalanche destruction. For the interpretability of the gathered GPR records, we arranged an experimental set-up with vertically moved antennas. Fixed GPR antennas were installed from January 2009 until the beginning of April 2009 at a test site in the Bavarian Alps at 1420 m a.s.l.. The antennas were remotely lifted by a hydraulic hoist system and completely buried in the snowpack. Conventional snowpack measurements in a snow pit were performed about 5–7 m away from the place of the radar records in a flat field, to leave the snow above the antennas undisturbed.

The test site of the FMCW measurements was located in the Swiss alps slightly higher in elevation at 1560 m a.s.l.. The test arrangement for the FMCW measurements consisted of vertical moved antennas as well. Contrary to the GPR measurements, these records were conducted from above the snow surface, and covered a distance of 10 meters. After the FMCW profile was recorded, the standard snowpit measurements and Near Infrared photography was used to record in-situ snow properties at one location which the radar measured, and at 5 different locations profiles were made with the SMP.

C.2.2. Theoretical basics

In dry snow conditions, as recorded in the here presented examples, the sole snowpack parameter to cause reflections of the emitted electromagnetic waves is a change in density (Kovacs et al., 1995). The responses of the emitted signals are recorded in two-way travel time. Radar systems measure the time of an emitted electromagnetic wave travelling to a position, which causes reflection and back to the receiver. An reflection with a larger travel time is further away of the signal source, the transmitter. In dry snow conditions respective average wave-speed values were determined for both pulsed and continuous wave signals using a mean density value $\bar{\rho}$ of the snow pits and equation (C.1) for low loss medias

$$v = \frac{c}{\sqrt{\varepsilon_r}}. \tag{C.1}$$

ε_r is the relative dielectric permittivity, which is for dry snow conditions only a function of density and calculated by

$$\varepsilon_r = (1 + 0.845\rho)^2,$$

the approximation by Kovacs et al. (1995) with ρ given in cm^3/g. Using eq. (C.1) for the determination of the snow height of the penetrated snow cover results in an accuracy of 2–10% for both applied radar techniques, calculating with a mean value of the density (Marshall et al., 2005; Heilig et al., submitted).

C.3. Results

Example radar profiles with both pulsed systems and frequency modulated systems are presented together with the corresponding snowpack properties in Figure C.1. The left side of the Figure shows the GPR profile and the right side the FMCW profile. The snow-pit data and the SMP profile are each related to the recorded radar signals. It is important to note that the radargram on the left side in Figure C.1 consists of recorded and processed reflections and on the right side are only displayed the propability density function (PDF) of the location of major peaks recorded with the FMCW system during a measurement when the system was moved vertically. These peaks correspond to persistent high reflection values and are therefore comparable to the bright reflections recorded with the GPR system. Nevertheless, we measured two different snowpacks and do not compare the capabilities of each system directly.

The conditions of both observed snowpacks are comparable. While the thickness of the scanned snow covers was almost double for the GPR measurement, the mean density, the density distribution and the layer thicknesses were very similar between both measurements (Fig. C.1). Both radar systems showed a clear reflection response at the snow surface. Furthermore, various internal layers are recorded by the two radar systems. The GPR radargram (Fig. C.1; left side) shows three remarkable separable reflections (B, C, D). The first reflection in radar wave direction occurs at the density increase at a snow height of 73 cm (D), the second reflection consits of an interference of the density decrease at 115 cm and the strong increase at 127 cm (C) and the third reflection is again another interference of two single signal responses at very varying snow layers. The strong crust at 154 cm in the profile likely caused the first bright reflection peak and the following strong decrease in combination with another increase at the second crust interfered to reflections A and B. This varying snow stratigraphy is below the vertical resolution limit and therefore can not be recorded as single reflections.

The FMCW system produced a reflection at the snow surface, and at the first layer transition recorded in the snowpit (A) (Fig. C.1). Reflection B is not related to a manually identified layer boundary, however the much higher resolution of the SMP shows an increase and subsequent decrease at this location. Reflection C occurs at the second major stratigraphic boundary, identified in the snowpit and SMP. Several persistent ice layers were found deep in the snowpack, which were detected by all 3 methods.

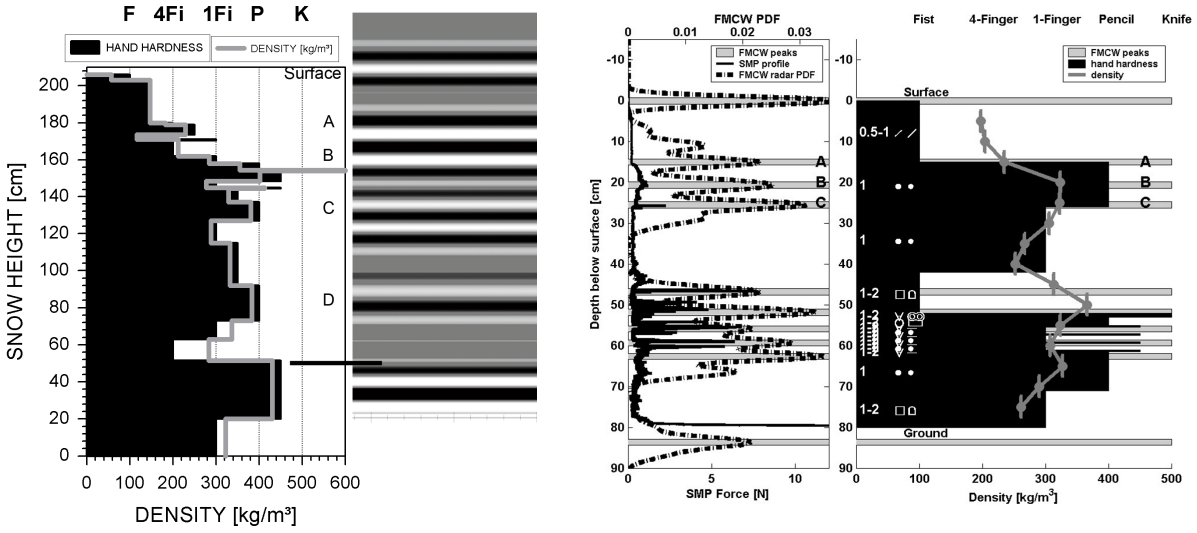

Figure C.1.: Snowpack conditions recorded with radar systems in comparison to measurements of the density and hand hardness. Left the relation of GPR records to density and hand hardness is displayed and right visualizes the relation of the calculated probability density function (PDF) of FMCW measured reflections to density and hand hardness as well. Furthermore, recorded SMP signals are compared to the location of major radar reflections. Both figures show snow depth relative to the location of the antennas - on the left it is a distance in snow above the antennas, and on the right it is the depth below the snow surface.

C.4. Discussion & Conclusion

This study shows that with ground-pentrating radar systems as well as with continuous wave systems, relevant dry snowpack conditions are recordable in a non-invasive way. The determination of the snow height is adequately accurate with both systems. Additionally, internal layers could be recorded and related to changes in density and peaks in penetration resistance. This enables two different applications. First, radar systems are capable to determine the spatial variability in occurrence, persistence and location of specific layers of a slope much faster than previously by snow pits. Second, while utilizing radar systems from beneath the snowpack, it is possible to quantify the temporal evolution of the snow cover at one point and determine compaction and accumulation rates. As these measurements can be conducted at large ranges of slope angles and in avalanche endangered slopes, such kind of information can be very supportive for avalanche warning centers.

Whether to use GPR or FMCW systems has to be decided according to the intended operation. The ability to distinguish between two adjacent layers is distinctly higher by the use of FMCW systems with such a large bandwidth. This can be a decisive argument for the application to

determine the spatial variability. Moreover, there is no commercial manufacturer of FMCW-systems in the frequency range suitable for applications from beneath the snowpack. If it is intended to place several radar antennas on different slopes to determine the snowpack evolution, the application of commercially available GPR systems is probably more reasonable, while the layer resolution is still accurate. Commercial GPR systems are made in large quantities by manufacturers for many different applications, therefore user support is provided, while FMCW radars currently must be built by researchers as they are not available for purchase.

Electromagnetic waves penetrate the snow cover non-destructively, which enables a much faster investigation of larger areas concerning the temporal observation of the evolution of specific layers and the snow height at specific locations. This gain of knowledge can be used to improve the spatial representativeness of measurements and for validating the calculated temporal changes of snowpack simulation models. Furthermore, more data for a better understanding of the spatial variability in large slopes can be achieved by the fast and non-invasive scan of a whole slope.

Bibliography

Bavay, M., Lehning, M., Jonas, T., Löwe, H., 2009. Simulations of future snow cover and discharge in alpine headwater catchments. Hydrological Processes 23, 95–108.

Gubler, H., Hiller, M., 1984. The use of microwave FMCW radar in snow and avalanche research. Cold Regions Science and Technology 9, 109–119.

Harper, J., Bradford, J., 2003. Snow stratigraphy over a uniform depositional surface: spatial variability and measurement tools. Cold Regions Science and Technology 37, 289–298.

Heilig, A., Eisen, O., Schneebeli, M., submitted. Temporal Observations of a Seasonal Snowpack using Upward-Looking GPR. Hydrological Processes.

Heilig, A., Schneebeli, M., Fellin, W., 2008. Feasibility study of a system for airborne detection of avalanche victims with ground penetrating radar and a possible automatic location algorithm. Cold Regions Science and Technology 51 (2-3), 178–190.

Koh, G., Jordan, R., 1995. Sub-surface melting in a seasonal snow cover. Journal of Glaciology 41 (139), 474–482.

Kovacs, A., Gow, A., Morey, R., 1995. The in-situ dielectric constant of polar firn revisited. Cold Regions Science and Technology 23, 245–256.

Machguth, H., Eisen, O., Paul, F., Hoelzle, M., 2006. Strong spatial variability of snow accumulation observed with helicopter-borne GPR on two adjacent Alpine glaciers. Geophysical Research Letters 33 (13).

Marchand, W.-D., Bruland, O., Killingtveit, A., 2001. Improved measurements and analysis of spatial snow cover by combining a ground based radar system with a differential global positioning system receiver. Nordic Hydrology 32 (3), 181–194.

Marshall, H., Koh, G., 2008. FMCW radars for snow research. Cold Regions Science and Technology 52, 118–131.

Marshall, H., Koh, G., Forster, R., 2005. Estimating alpine snowpack properties using FMCW radar. Annals of Glaciology 40, 157–162.

Marshall, H., Schneebeli, M., Koh, G., 2007. Snow stratigraphy measurements with high-frequency FMCW radar: Comparison with snow micro-penetrometer. Cold Regions Science and Technology 47 (1-2), 108–117.

Schneebeli, M., Laternser, M., 2004. A probabilistic model to evaluate the optimal density of stations measuring snowfall. Journal of Applied Meteorology 43, 711–719.

Vickers, R., Rose, G., 1973. High resolution measurements of snowpack stratigraphy using a short pulse radar. In: Proceedings of the Eighth International Symposium on Remote Sensing of the Environment. pp. 261–277.

Yankielun, N., Rosenthal, W., Davis, R., 2004. Alpine snow depth measurements from aerial FMCW radar. Cold Regions Science and Technology 40 (1,2), 123–134.

Declaration of Authorship

I certify that the work presented here is, to the best of my knowledge and belief, original and the result of my own investigations, except as acknowledged, and has not been submitted, either in part or whole, for a degree at this or any other University.

09/01/09

Achim Heilig